Chapter 2
Reduction of Metal Ions in Polymer Matrices as a Condensation Method of Nanocomposite Synthesis

It would be not an exaggeration to say that development of the methods of synthesis of nanoparticles governs the mainstream of the science concerning nanomaterials [1]. This is, first of all, discovery of carbon nanotubes [2], synthesis of highly organized quantum dots [3], controlled morphology of CdSe nanocrystals [4], etc. New fields of application and unique properties of materials are related, more to a possibility of control of size and shape of particles in nanometer scale than to a change in their sizes [5]. Presently it is expressed in existence of a huge library of nanoparticles including a wide range of compositions, structures, sizes, and this is also true for synthetic methods used for development of nanomaterials. Among successfully developed approaches there are vapor-gas syntheses for production of one-dimensional structures [6, 7]. There are extensive solution methods including such approaches as co-deposition, sol-gel synthesis, microemulsion method, hydrothermal and solvothermal processes, template synthesis, etc. [8–12].

It is known that liquid-phase methods of production of nanoparticles make it possible to control effectively sizes and morphology of particles [13–19]. Many processes of metal ion reduction widely used in synthesis of metal colloids relate to liquid phase reactions [20–22].

2.1 Formation of Metal Nanoparticles During Chemical Reduction

Contemporary ideas about formation of nanoparticles are based on the main principles proposed by J. Turkevich, which include stepwise mechanism of nucleation, growth and agglomeration [23].

On the whole, synthesis of nanoparticles with a certain diameter having almost monodisperse distribution in size and low degree of agglomeration is limited by two

A.D. Pomogailo, G.I. Dzhardimalieva, *Nanostructured Materials Preparation via Condensation Ways*, DOI 10.1007/978-90-481-2567-8_2

principal boundary conditions: precision control over the nucleation stage and seeds growth; efficient impending of the agglomeration process [13, 24–26].

According to LaMer model [27] nucleation is endothermic process. Break of bonds in the initial compound, removal of a solvate shell is energy consuming. At the same time, the processes of seeds growth and agglomeration accompanied by a decrease in enthalpy of the system owing to the bond energy of a lattice are exothermic, i.e. formation of a blocked solid is always energetically beneficial as compared to nanoparticle formation with a typically extensive surface, unsaturated bonds, non-occupied coordination sites. We shall consider each stage separately.

2.1.1 Nucleation

In a typical chemical synthesis of metal nanoparticles a compound metal-precursor reduces with formation of zero-valent metal atoms, building blocks of metal nanoparticles. During fast reduction concentration of atoms reaches the supersaturation point, and from this moment spontaneous homogenous nucleation begins, which is characterized by high-energy barrier (Fig. 2.1). As supersaturation decreases, nucleation ceases, and the formed seeds go on growing. Due to short time of the nucleation the obtained particles have narrow size distribution. At high supersaturation an additional mechanism of a decrease in dispersion of particles is possible [28, 29]. The essence of the conception of "explosive nucleation" [27] is in inducing of an individual nucleation process and excluding of additional nucleation from the further growth process. This method as a method of synthetic strategy is often called "separation of nucleation and growth" [29, 30].

Thermodynamic model of homogenous nucleation is considered in detail in [11].

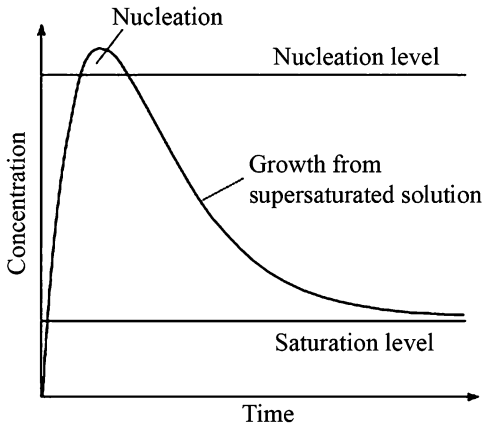

Fig. 2.1 Diagram of the change of precursor concentration under nanoparticle growth [13]

Gibbs free energy of spherical crystals with r radius formed from solution with S supersaturation is defined by the equation:

$$\Delta G = 4\pi r^2\gamma + \frac{4}{3}\pi r^3 \Delta G_v \tag{2.1}$$

in which γ is the surface free energy per unit area and $\Delta G_\nu = -RT\ln S/V_\mathrm{m}$ (V_m is molar volume of the blocked crystal) is a change in free energy between a monomer in a solution and unit volume of the blocked crystal. The r, at which ΔG is maximum, is called critical radius r_c. This is a minimal radius of a seed, which can grow spontaneously in supersaturated solution.

When $d\Delta G/dr = 0$,

$$r_c = \frac{-2\gamma}{\Delta G_2} = \frac{2\gamma V_m}{RT\ln S} \tag{2.2}$$

One of the necessary conditions for supersaturation during homogenous nucleation follows from Eq. 2.2. The S value should be quite high to provide the critical radius r_c smaller than the germ size of a crystal from which a seed forms during homogenous nucleation. Size of these germs should be no less than 1 nm, which is compatible with sizes of inorganic molecular crystals. One can get the equation for critical Gibbs free energy ΔG_c via combination of Eqs. 2.1, 2.2 necessary for formation of stable seeds:

$$\Delta G_c = \frac{16\pi\gamma^3}{3(\Delta G_v)^3} = \frac{16\pi\gamma^3 V_m^2}{3(RT\ln S)^2} \tag{2.3}$$

For the reduction reactions an important moment is a problem concerning particles, which aggregate in seeds, and then grow to a nanoparticle: whether they are reduced or unreduced. An example of formation of Pt^{II}–Pt^{I} и Pt^{I}–Pt^{I} dimers formed from the products of hydrolysis of $[PtCl_4]^{2+}$, which is a typical precursor of synthesis of Pt nanocrystals shows that the precursor compound can transform directly in the seeds form or associate with a growing nanocrystal without reducing to zero-valent state [31, 32]. According to the numerical analysis performed by molecular dynamic method, dimers and trimers have higher electron affinity than the initial precursor. It is assumed that reduction will go predominantly by transition of electron from a reducing agent to these dimer and trimer intermediates on the way to clusters and seeds [33].

At that, association of complexes to a cluster or a respective removal of a ligand from the cluster can significantly accelerate growth of metal nanocrystal. Such acceleration is usually regarded as autocatalytic process which is found in many systems (Fig. 2.2) [24–26, 34–36].

It should be noted that the considered mechanism of reduction is preferable under special experimental conditions, for example, when intermediately strong reducing agents are used and/or concentration of a precursor is high, and in this case reduction of the latter to atomic state is not critical. The surface of a cluster or

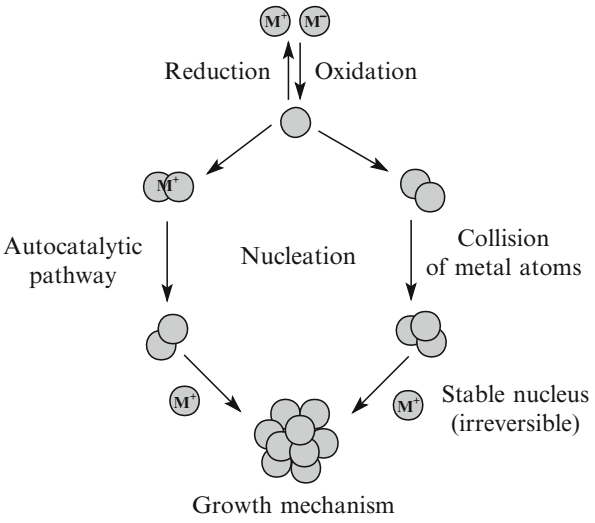

Fig. 2.2 Mechanism of nucleation and growth of nanoparticles [36]

nanocluster is surrounded by positively charged metal ions coordinated with molecules of a ligand or solvent.

Reduction also may be preceded by formation of a complex with a reducing agent. For example, characteristic band in UV-vis spectrum of two-valence copper in Cu^{2+}- polyvinylpyrrolidone [37] disappears at addition of hydrazine-hydrate, and instead of it absorption band appears in the region of 700 nm, which points to formation of $Cu[(N_2H_4)_2]^{2+}$ complex (Fig. 2.3) [38].

Thus, unstable small clusters of atoms or ions formed at the initial stage of reduction of metal ions are the sources of formation of metal nanoparticles. For their studies most often methods of pulse radiolysis [39], electrospray mass spectrometry [40, 41], electrospray photoelectron spectroscopy [42], absorption and emission spectroscopic methods are used.

As many research teams have shown, Ag clusters demonstrate different optical spectra depending on a number of Ag atoms contained in a cluster [39, 43–45].

Atoms of Ag_0 produced during reduction undergo subsequently some transformations with cluster formation [46–50]:

$$Ag_2^{+} \rightarrow Ag_3^{2+} \rightarrow Ag_4^{2+} \rightarrow Ag_8^{2+}$$

or

$$\begin{aligned}
&Ag^{+} + \mathrm{Red} \leftrightarrow\ Ag_1 + \mathrm{Red}^{+};\\
&Ag_1 + Ag^{+} \leftrightarrow Ag_2^{+};\\
&Ag_2^{+} + \mathrm{Red} \leftrightarrow Ag_2 + \mathrm{Red}^{+}\\
&\ldots\ldots\ldots\ldots\ldots\ldots\ldots\ldots\ldots\\
&Ag_n + Ag_m = Ag_{m+n}
\end{aligned}$$

Red is the reduction agent

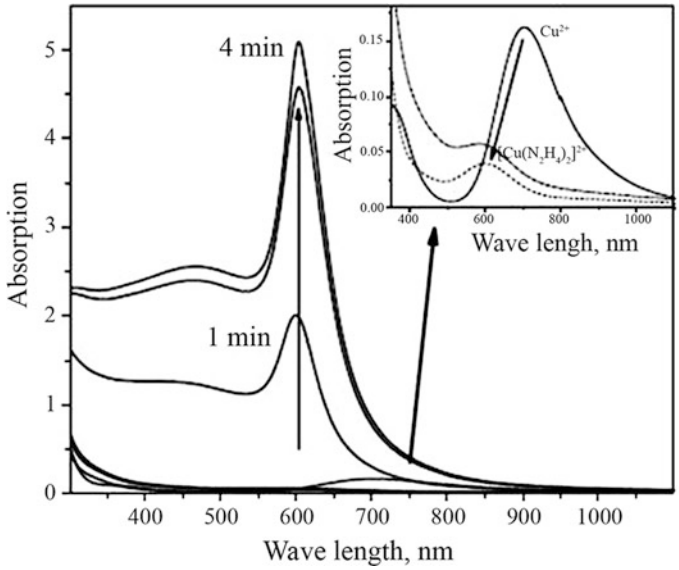

Fig. 2.3 The change of UV-vis-near IR spectra during Cu(II) reduction in DMF at 333 K. In the insert: evolution of the Cu^{2+} band absorption under addition of hydrazine hydrate at 333 K [38]

Particles of Ag_1 and clusters consisting of a small number of atoms are unstable (redox-potential of atomic silver $E^{o}_{Ag_1/Ag^+} = -1.8\text{V}$ (is referred to by [51]) instead of $E^{o}_{Ag/Ag^+} = +0.799\text{V}$ for metal silver). As metal clusters grow, their stability increases. For example, Ag_8^{2+} cluster is quite stable, it lifetime is measured by 10 min. Optical band corresponding to it in the absorption spectrum differs from the bands typical for Ag (360 nm) and Ag_2^{+} (310 nm) dimers and disappears as Ag_8^{2+} cluster transforms in silver sol (Fig. 2.4) [39].

Theoretical calculations and experiment [52] have shown that critical size for gold clusters is 2 nm (theoretical calculation gives 1.7 nm). For these particles there is no mode of collective plasmon resonance (Fig. 2.5), i.e. Au_{25}(glutathione)$_{18}$ clusters show one-electron absorption peaks, while 4-nm nanoparticles are plasmon, and transition from cluster to fcc crystal state takes place just about 2-nm size.

Probably, it can be assumed that the analogous types of clusters can be included as intermediates during formation of a metal phase seeds, whose main characteristic features are presence of physical interphase and ability to reduction of absorbed metal ion, i.e. ability of the seeds to growth.

2.1.2 Growth

As long as a seed forms, it begins to grow due to adding of atoms. Theoretical consideration of the "diffusion growth" model (referred to by [11]) has shown that growth rate of particles is inverse to their radius, because a number of atoms

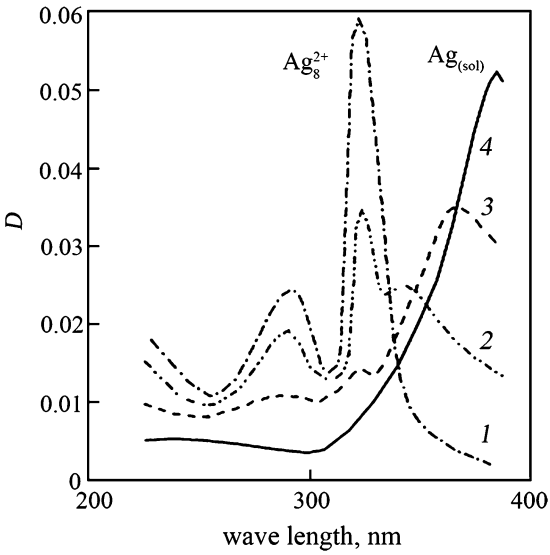

Fig. 2.4 Absorption spectra of the silver salt solution after an electron beam exposure (Ag_8^{2+} cluster transformations in a silver sol). The solution of $1 \times 10.4\,M$ $AgClO_4 + 0{,}1\,M$ 2-propanol. Irradiation duration: 6 s (*1*), 1 min (*2*), 5 min (*3*), 15 min (*4*) [39]

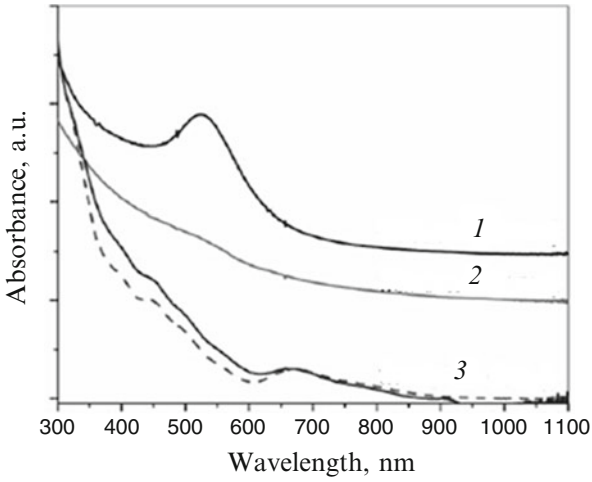

Fig. 2.5 UV spectra of the different sized Au nanoparticles, (*1*) first precipitate (ca. 4 nm) redissolved in water; (*2*) second precipitate (ca. 2 nm) redissolved in water, and (*3*) the *left* supernatant (for comparison, the spectrum of pure $Au_{25}(SG)_{18}$ (*dashed line*) is also shown) [52]

diffusing to the surface of a particle increases in proportion to its squared radius, and the particle volume increases as cube of its radius. Taking this into account, it is shown that for the ensemble of spherical particles a change in radius distribution σ^2 decreases during the growth.

$$\frac{d(\sigma)^2}{dt} = 2V_m D(C_{bulk} - C_s)\left[1 - \overline{r}\,\overline{\left(\frac{1}{r}\right)}\right] \tag{2.4}$$

where $\bar{r}$ and $(\overline{1/r})$ are average values of r and $1/r$, respectively, C_{bulk}, C_{s} are concentrations in solution and on the particle surface, respectively.

In other words, particle size distribution narrows, independently on the initial distribution while all particles grow and no additional nucleation appears. This self-regulating mechanism of size distribution is often called "focusing effect" [29].

On the whole, particle growth is controlled by competition of two processes: a decrease in bulk energy, which advances growth (absorption) and an increase in the surface energy associated with particle dissolution. With account for kinetics of the growth process and its dependence on a particle size, opposite to the "focusing" effect can be obtained: the smaller particle radius, the more difficult its growth, but easier dissolution for higher chemical potential. Two mechanisms of control of particle size distribution are formulated from the results of theoretical studies and numerical simulation [53, 54]: (i) "focusing effect" which is kinetically governed process, when growth is diffusion-controlled and supersaturation is quite high; (ii) Ostwald ripening, which appears at low supersaturation, i.e. under conditions when not all particles remain able to grow and those, whose radii are below critical r_{c}, dissolve, concentration of the particles decreases slowly. Atoms formed during dissolution diffuse to coarser particles and absorb on their surface. On the whole, Ostwald ripening broadens standard deviation to the particle size distribution, i.e. it causes an increase in polydispersion, and the average size of nanoparticle grows.

On the contrary, under conditions of excess stabilizing ligands, so called digestive ripening, growth of nanoparticles is accompanied by narrowing of the size distribution. Single crystalline Ag particles were subjected to such ripening in presence of dodecylamine, the particle size decreased from 12.4 ± 5.1 to 6.1 ± 0.5 nm [55]. Depending on the origin of ligands, particle sizes may not only decrease, but also increase, and the final size, as has been mentioned above, is determined by dynamic ratio of the dissolution rate of metal atoms from particles of some size to the re-absorption rate on particles of other sizes [56, 57].

There are some synthetic methods for separation of the nucleation and growth processes. In so-called "seed-mediated growth" nucleation is physically differs from growth via using of preliminary obtained nanocrystals for a nucleus seed. Actually, in this case heterogeneous nucleation impedes formation of additional nuclei, which would be the case at homogenous nucleation. Pre-seeds are introduced in a reaction matter, and as a precursor is added, the formed atoms absorb on the surface of the formed nucleus. At that, concentration of the precursor remains rather low to prevent homogenous nucleation. This strategy can be used to obtain homogenous particles [58–60] and heterogeneous structures of core-shell type [61, 62]. The considered method makes it possible to finely regulate particle size; however, a necessary condition is monodispersion of the initial seed particles.

The "hot injection" method [3, 63–66] realizes homogeneous nucleation. At fast addition of excess precursor in hot solution of surfactant "explosion" nucleation proceeds. During the nucleation concentration of atoms in the solution decreases dramatically and the nucleation rate decreases.

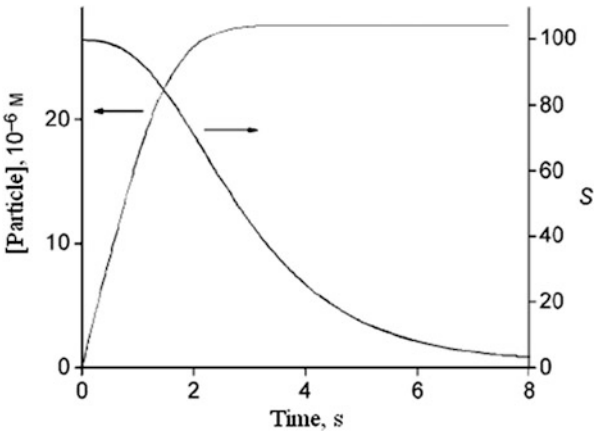

Fig. 2.6 The results from numerical simulations of nucleation and growth of nanocrystals. The particle concentration and supersaturation as a function of time. Values of simulation parameters: $S = 100$, $T = 523$ K, $\gamma = 0.11$ J m^{-2}, $A = 10^7$ s^{-1}, $D = 10^{-15}$ m^2 s^{-1}, and $\Delta t = 10^{-2}$ s. [11]

Numerical simulation of homogeneous nucleation [11] during "hot injection" with account for a number of nuclei formed at each time step provides:

$$\frac{dN}{dt} = A\exp\left[-\frac{\Delta G_c}{kT}\right] = A\exp\left[\frac{16\pi\gamma^3 V_m^2}{3k^3T^3N_A^2(\ln S)^2}\right] \tag{2.5}$$

(here a rate of increment in number of particles N is defined as the nucleation rate), it shows that inducing of high supersaturation causes fast consumption of a monomer which, respectively, stops nucleation, thus, the nucleation process can be separated from growth (Fig. 2.6). The results of this modeling are consistent with experimental data of a change in concentration of CdSe nanocrystals as a time function during their synthesis [67].

Finally, standard methods of control over direction of reactions and equilibriums in colloid chemistry are electrostatic and steric stabilization of the particle surface just after nucleation stage [20, 68, 69] (Fig. 2.7).

Electrostatic stabilization can be reached by specific ion sorption (H^+, OH^-, SO_4^{2-}, NO_3^-, $RCOO^-$, RSO_3^-, R_4N^+, etc.) by the surface of nanoparticles. Such agents as citrate ions make a double ionic layer on the surface of a nanoparticle which generates repulsive Coulomb forces (Fig. 2.8).

On the contrary, addition of salts containing weakly coordinated organic or inorganic anions such as sodium dodecyl sulfate or sodium p-toluene sulfonate, lithium trifluoromethanesulfonate, or lithium perchlorate causes a decrease in thickness of the double electric layer and thus favors coagulation of nanoparticles [70].

Steric stabilization is realized by absorption of long-chained organic molecules (for example, oleyl amines, oleic acid, trioctylphosphine oxide), polymers and biomolecules. Growth and agglomeration of nanoparticles can also be controlled by separation of reaction spaces, for example, via considerable dilution, and continuous removal of formed nanoparticles in microfluid flow-through setups [71]. The principle of limiting of cluster growth to coarse particles using the effect of their low solubility in organic solvents is shown for Au_n(glutathione)$_m$- [72] and Ag_7- clusters [73, 74].

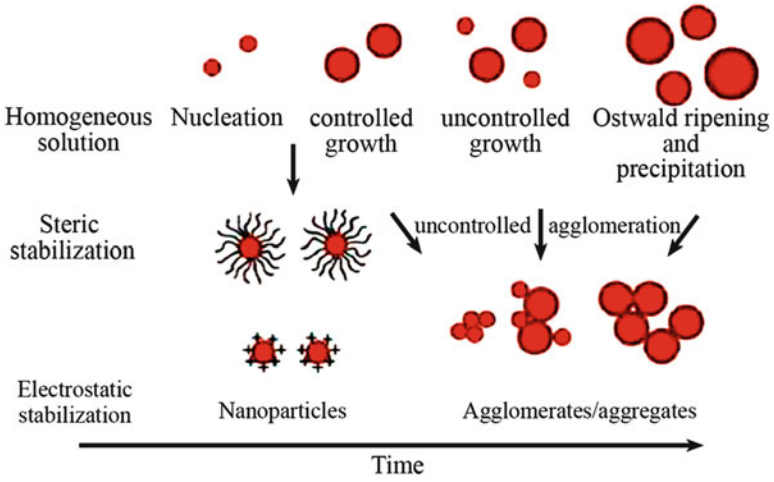

Fig. 2.7 Growth and stabilization of nanoparticles [13]

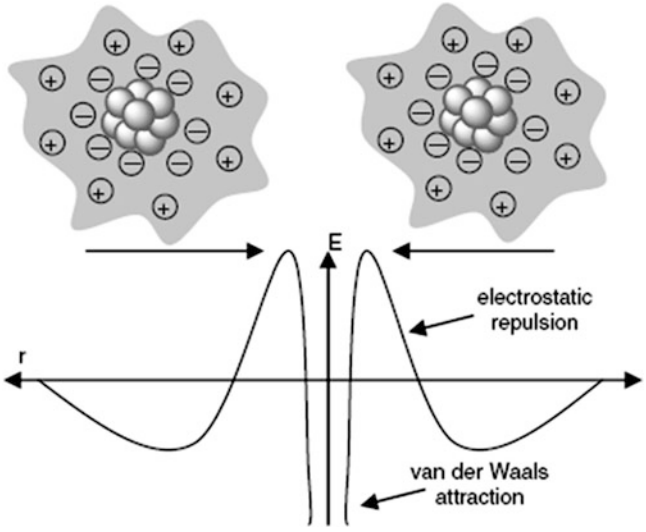

Fig. 2.8 Electrostatic stabilization of nanoparticles

There is one more important problem, whose solution is inextricably associated with understanding of the mechanism of nucleation and growth of nanoparticles, this is control over shape of the particles. Synthetic strategy of production of nanoparticles with a specific morphology, various mechanistic aspects of formation of 1D, 2D, and 3D structures of nanocomposite materials attract keen attention of researchers and are widely discussed in literature [75]. In the recent review [76] concerning detailed analysis of reaction ways of fabrication nanoparticles of

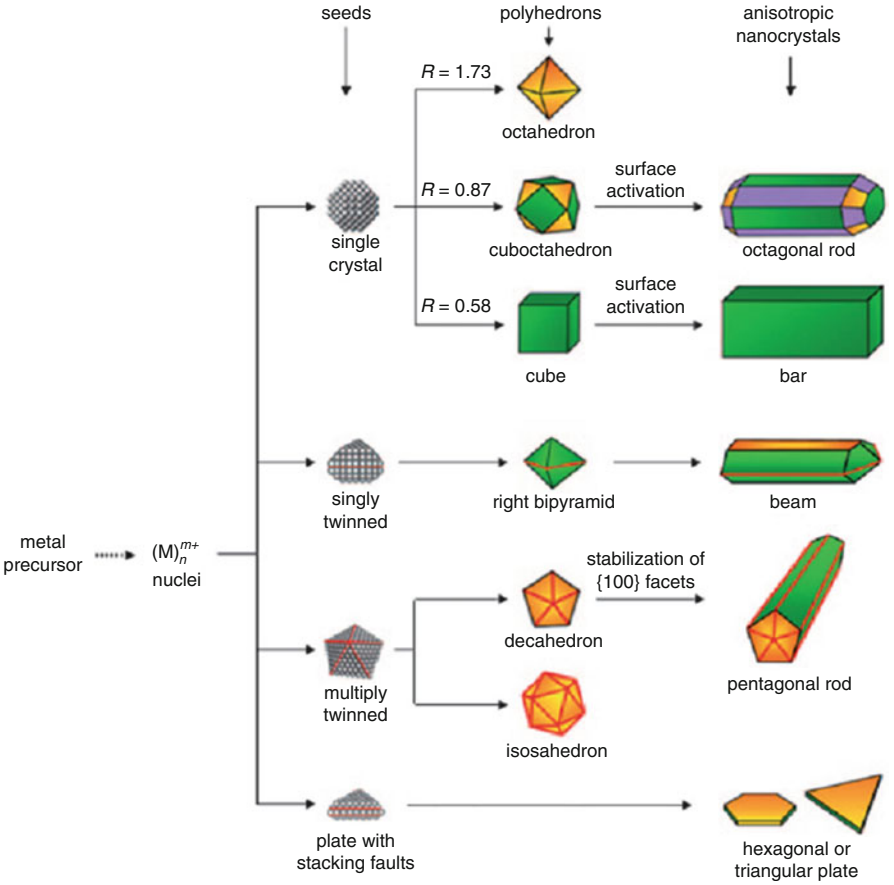

Fig. 2.9 Reaction pathways that lead to fcc metal nanocrystals having different shapes. The parameter R is defined as the ratio between the growth rates along the {100} and {111} directions [76]

different shapes it has been shown that the key role in this would play internal structure of the formed seeds and binding affinity of a stabilizing agent. Structure of the seeds can be ether single or multiple twinned crystals (Fig. 2.9).

Actually, these structures can co-exist during synthesis of one or other nanoparticle. The essence of the problem is fine regulation of growth of seed populations for producing metal nanoparticles with desired shape and morphology. The possibilities for its realization are provided by thermodynamic factors and by kinetic conditions of reactions. This can be achieved by significant decrease in the reduction rate of a precursor [77, 78], action of weak reducing agents [79–81], cooperation of the reduction reaction with oxidizing etching [82], Ostwald ripening [83, 84], etc.

It is known, for example, that Ag_3^+ and Ag_3 clusters in the basic state have a triangle structure with D_{3h} symmetry [85, 86]. Both these clusters have higher

electron affinity than Ag^+, which make them prevailing sites for further growth to a nanoparticle. It has been shown that an average edge length of the Ag nanoplate increases as the initial concentration of trimer silver clusters decreases during $AgNO_3$ reduction by polyvinylpyrrolidone [87].

The effective way for shape control of the particles is usage of selective chemically absorbing (capping) agents. This can be ligands, formed as side products during decomposition or reduction of a precursor, or various compounds (low-molecular ions, surfactants, polymers, biomolecules, etc.) specially added to a reaction solution and simultaneously playing a stabilizing role [7, 88–90]. Via chemical binding with the surface of a metal particle a capping agent can change free energy of various planes and therefore their relative growth velocities. For example, polyvinylpyrrolidone as a capping agent is bound most strongly via oxygen atoms with {100} face of Ag and Pd atoms [91], thus providing metal atom bonding to surfaces of other faces. The similar behavior shows citrate ion [92–94]. Moreover, reduction of $HAuCl_4$ using ammonium citrate in presence of Fe^{3+}, Ni^{2+}, Cu^{2+}, Zn^{2+} и Al^{3+} ions causes formation of polygonal gold nanoparticles by ion-inducing mechanism [95]. It is reported that Ag^+ ions can have the same effect [96, 97]. It is suggested that metal ions present in the reacting media are bound predominantly with {111} face of metal atoms, as with the most stable, and prevent growth in this direction.

2.2 Chemical Methods of Reduction

The method of liquid phase chemical reduction discovered by Faraday [98] more than 150 years ago is most widely used technique for production of metal nanoparticles. Another substantial step in development of this approach is connected with J. Turkevich, who for the first time implemented reproducible synthesis of Au (20 nm) nanoparticles by the reaction of citrate reduction of $[AuCl_4]^-$ [23, 99, 100]:

$$x\mathrm{M}^{n+} + \mathrm{n}x\mathrm{e}^- + \text{stabilizer} \rightarrow \mathrm{M}^0{}_\mathrm{n}(\text{cluster}) \tag{2.6}$$

Among the known reduction methods there are: the “diborane” method of production of $Au_{55}(PPh_3)_{12}Cl_6$ (1.4 nm) nanoclusters stabilized with phosphine ligands; nanoclusters of transition metals stabilized by polyoxoanion and tetrabutyl ammonium; alcohol reduction, so called polyol process [101–104], with the polyvinylpyrrolidone [105, 106], polyvinyl alcohol, etc. used as stabilizers, and reduction of metal salts with formic acid, CO, sodium formate, formaldehyde, and benzaldehyde [107]. In metal nanocolloids silanes, tetrakis hydroxymethyl phosphonium chloride (THPC), hydrazine, hydroxylamine are used as reducing agents. The method of borate reduction is based on the sodium/lithiumborohydrate or tetraalkylammonium hydrotriorganoborates systems, which provide extensive possibilities for production of nanocrystals by chemical reduction of transition metal salts [108, 109].

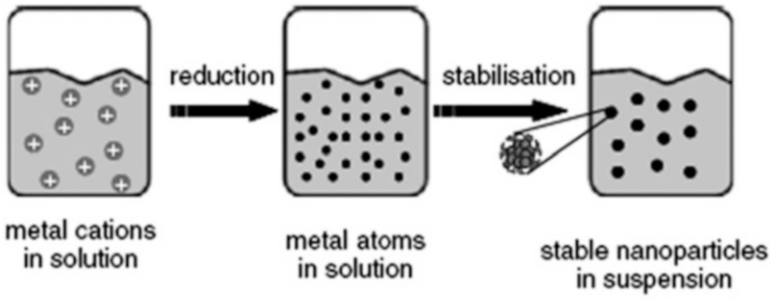

Fig. 2.10 Formation of nanoparticles in the chemical reduction

The chemical reduction method is based on mixing of a reducing agent with a metal-precursor salt in presence of stabilizing agents (ligands, polymers, surfactants) (Fig. 2.10).

Role of the latter is confined to preventing of undesirable particle agglomeration and formation of metal powder. Formation of stable and re-dispersing nanoparticles depends on properties of a stabilizing agent [107].

On the whole, the chemical reduction methods provide a possibility of precision control over growth of nanoparticles, efficient passivation of surface states of nanoparticles, quite narrow distribution of obtained nanoparticles by sizes and control over their morphology [110, 111].

2.2.1 General Characteristics of Low Molecular Reducing Agents

Reducing agents are used to reduce Fe from ores (C, H_2, aqua and natural gases, CO, propane, butane), during production of nonferrous and rare metals in metal heat treatment (C, Si, Al, Na, Ca, Mg, La), during precipitation (cementation) of nonferrous metals from aqua solutions and their salts (Fe, Zn); during production of metals and their lower oxides and halogenides, and during chemical deposition of metals, nitrides and carbides from gas phase (H_2, NH_3, CH_4, etc.); during decomposition of chemical processes in solutions ($SnCl_2$, $FeSO_4$, H_2SO_3, N_2H_4, NH_2OH, HCOOH, H_2S, etc.); in organic synthesis (H_2, Na, Zn, $LiAlH_4$, $NaBH_4$, B_2H_6, etc.). These substances can also comprise the main group of reducing agents during formation of nanoparticles. The most often used ones are described below.

2.2.1.1 Sodium Borohydrite ($NaBH_4$)

It is widely used in organic synthesis as a reducing agent. It is used to reduce carbonyl compounds to alcohols, imines to secondary amines, nitro compounds,

etc. In aqua solutions it is hydrolyzed to Na_3BO_3 and H_2, hydrolysis is accelerated in acid and slows down in alkaline solutions, hydrolysis of sodium borohydrite is catalyzed by salts of transition metals. Oxidation–reduction potential of sodium borohydride in acid and alkaline media is 0.43 and −1.37 V, respectively. One of the schemes of reduction reactions of metal ions M_{2+} can be expressed by equation $2\,M^{2+} + BH^{4-} + 4H_2O \rightarrow 2\,M^0 + B(OH)^{4-} + 2H_2 + 4H^+$, and for alkaline medium by the expression $2\,M^{2+} + BH^{4-} + 4OH^- \rightarrow 2\,M^0 + B(OH)^{4-} + 2H_2$.

2.2.1.2 Lithium Aluminum Hydride ($LiAlH_4$)

It is a strong reducing agent used inn organic synthesis. It is more powerful than other often used agents, for example, sodium borohydride due to weaker Al-H bonds as compared to B-H bonds. It reduces complex ethers, carboxylic acids, and ketone to alcohols, nitro compounds to amines. The temperature of thermal decomposition is −150 °C.

2.2.1.3 Hydrazine Hydrate ($N_2H_4 \cdot H_2O$)

It is a colorless, slow, steaming in air liquid with a specific faint odor. Its density is 1.03 g/cm^3. Melting point is 118.5 °C at 740 mm of mercury and 47 °C at 2 mm of mercury. It solidifies below −40 °C. The reaction agent is mixed with water and ethyl alcohol, does not solve in diethyl ether, chloroform and benzene. Hydrazine hydrate has a pronounced alkali reaction; its dissociation constant (as a base) is $K_1 = 8{,}5 \cdot 10^{-7}$, $K_2 = 8{,}4 \cdot 10^{-16}$ at 25 °C. Hydrazine and hydrazine-hydrate, hydrazine-sulfate, hydrazine-chloride are widely used as reducing agents of gold, silver, platinum metals from diluted solution and their salts. In organic synthesis hydrazine is used for reduction of a carbonyl group of aldehydes and ketones.

2.2.1.4 Dodecylamine

Dodecylamine. (1-dodecanamine, laurylamine) $C_{12}H_{25}NH_2$, molar weight is 185,34; colorless liquid; melting point is 28,35 °C, boiling point is 247–249 °C, 134–135 °C at 15 mm of mercury; is dissolved in organic solutions, low dissolved in water forming hydrates and liquid crystalline phases. It has low basicity (pK_a 2,68, 25 °C).

2.2.1.5 Sodium Citrate

In the citrate method of formation of nanoparticles citrate ion, which is obtained during water solution of three-substituted sodium salt of citric acid, serves both as a reducing agent and a stabilizer:

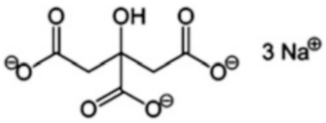

At heating of the solution and oxidizing of citrate ion acetonedicarboxylic and itaconic acids form, they absorb on the particle surfaces and control the particle growth.

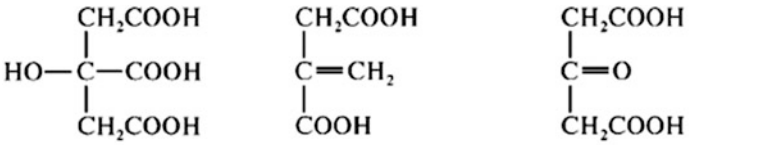

In water solutions at $t < 60$ °C citric acid and citrates oxidize with formation of 3-ketaglutaric acid as intermediate product, and then followed by formation of formaldehyde and formic acid, which are also reducing agents:

$$C_3H_4(OH)(COOH)_3 \xrightarrow{-CO_2} C_2H_4(CO)(COOH)_2 \rightarrow \xrightarrow{-3,5CO_2} HCOH + {}^1/_2HCOOH.$$

Citrate ions absorbed on the surface of colloid particles give them negative charge and thus prevent their aggregation.

2.2.1.6 Ethylene Glycol (HO-CH2-CH2-OH)

Using of ethylene glycol and other alcohols as reducing agents are the basis for polyolic processes of fabrication of nanoparticles. It is assumed [112] that formation of metal nanoparticles in ethylene glycol follows the scheme:

$$HOCH_2CH_2OH \rightarrow CH_3CHO + H_2O$$
$$2CH_3CHO + M(OH)_2 \rightarrow CH_3 - CO - CO - CH_3 + 2H_2O + M$$

The formed nanoparticles are stable in alkali solutions, which supposed their stabilizing by absorption of ethylene glycol and OH^- -type anions [101]. According to the refined mechanism [113], hydroxide ions can take part in acetate ions formation, which are responsible for stabilization of nanoparticles in ethylene glycol, as it has been shown for organic sols of ruthenium:

$$HOCH_2CH_2OH \rightarrow CH_3CHO + H_2O$$
$$3CH_3CHO + 2Ru^{3+} + 9OH^- \rightarrow 3CH_3COO^- + 2Ru + 2H_2O$$

or platinum:

$$HOCH_2CH_2OH \rightarrow CH_3CHO + H_2O$$

$$2CH_3CHO + (PtCl_6)^{2-} + 6OH^- \rightarrow 2CH_3COO^- + Pt + 6Cl^- + 4H_2O$$

2.2.1.7 Ascorbic Acid

Ascorbic acid is a strong reducing agent: enol groups easily oxidize to keto groups. In aqua solution there is a possibility of ascorbic acid self-oxidizing.

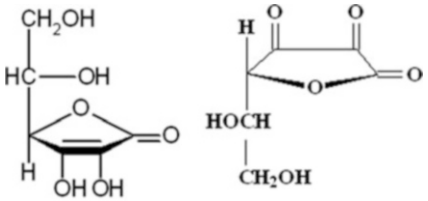

I II

2.2.1.8 L-Ascorbic Acid

L-Ascorbic acid (γ-lacton 2,3-diketo-L-gulonic acid; formula I) has molecular weight 176.12; consists of colorless crystals, the melting point is 190–192 °C (with account for decomposition). Specific optical rotation for D-line of sodium at the temperature 20 °C is $[\alpha]_D^{20} + 23^\circ$ (for the concentration 1.6 g per 100 mL of water); high dissolubility in water (22.4 %), lower dissolubility in alcohol (4.6 %), low dissolubility in glycerol and acetone; pKa 4.17 and 11.57; λ_{max} 245 (pH <7) и 265 nm (pH >7).

2.2.1.9 Dehydroascorbic Acid

Dehydroascorbic acid (γ-lacton 2,3-diketo-L-gulonic acid; formula II) has molecular weight 174.12; consists of colorless crystals, the melting point is 237–240 °C (with account for decomposition). Specific optical rotation for D-line of sodium at the temperature 20 °C is $[\alpha]_D^{20} + 55$, water dissoluble.

In aqua solutions, especially in alkali media, it is reversibly oxidized fast to dehydroascorbic acid (oxidation-reduction potential is +0.058 V), and then irreversibly to 2,3 diketo-gulonic, and then to oxalic acid.

2.2.1.10 Aminoboranes

Aminoboranes are classical examples of adducts of acids and Lewis bases. Most aliphatic aminoboranes are solid crystal matters stable in air and resistant to moisture.

Primary and secondary aminoboranes are thermally stable up to 80 °C. They are soluble in protonic and aprotonic media. On the whole, reduction ability depends on a nature of a complex-forming amine. In the case of alkyl-aminoboranes strength of a reducing agent decreases as a portion of alkyl substituent in the nitrogen compound increases: $H_3N \cdot BH_3 > H_2MeN \cdot BH_3 > HMe_2N \cdot BH_3 > Me_3N \cdot BH_3$ [114]. The reducing ability of aryl-aminoboranes depends on basicity of amines: the lower pK_a of amine, the stronger its reducing properties. In the recent years aminoboranes have being widely used in synthesis of metal nanoparticles, including the processes in aqua and non-aqua media, and in solid state. The main achievements in synthesis of nanocomposites with participation of aminoboranes, their efficiency and advantages as compared with classic reducing agents are analyzed in a recent review [115] and summarized in the Table 2.1.

2.2.2 The Main Factors Controlling the Reduction Process

2.2.2.1 Reducing Ability

A relative reducing ability of two or more substances is found by comparison of changes in Gibbs energy ΔG_p^0 in reactions of these substances with the same oxidizing agent, and in the case of reactions with participation of elementary substances, by energy of formation ΔG_{form}^0 of the oxidation products of the elementary substance. The higher ΔG_p^0, or the modulus value ΔG_{form}^0, active reducing agent is a substance. Often, to compare reducing ability of substances, standard electrode potential E^0 is used. The higher E^0 modulus of half-reaction of reduction with some substance, the stronger reducing properties of this substance (Table 2.2).

Some typical reducing agents have more negative potentials, than the redox-potential of $2H^+/H_2$ pair. As a rule, the most active among them capable of reducing not only noble, but also base metals, have $E \sim -0.5$—1.3 V. These reducing agent include hypophosphite, hydrazine, formaldehyde, borohydride, alkyl substituted aminoboranes, etc. If there is a great difference between redox-potential of a reducing agent and a reduced metal ΔE, finely dispersed product of reduction forms fast. The oxidation potential of reducing agents depends on pH: the higher pH, the greater shift of the potential to negative values. In order to obtain wide range of potentials, in which reduction processes can take place, solutions with high pH, containing ligands forming quite strong complexes with ions of a reduced metal, are usually used.

Apart from being a sign of probability of a reaction, a velocity of chemical reaction can be predicted by ΔE^0. A possibility of controlling redox-potential of the reacting components and the reaction on the whole is important for control of properties of the formed metal particles. Electrochemical potential of the majority of metal systems can be changed by their complexation or deposition; the value of the effect will depend on the constant of stability or solubility of final products. For example, at formation of complexes with increasing constants of stability (K_f), the

Table 2.1 Synthesis of nanoparticles in organic and aqueous medium using amine-borane complexes [115]

Nanoparticles	Metal-containing precursor	Stabilizing agent	Reduction agent	Particle size, nm
In organic medium				
Au	$[Au(PPh_3)Cl]$	Dodecanthiol	$tBuH_2N \cdot BH_3$	6
Au	$HAuCl_4 \cdot 3H_2O$	Oleylamine	$tBuH_2N \cdot BH_3$	1–10
PtPb nanorods	$Pt(OAc)_2$, $Pb(OAc)_2$	Hexadecanthiol, Hexadecylamine, Adamantic acid	$tBuH_2N \cdot BH_3$	length $= 45 \pm 12$, width $= 5.9 \pm 2.8$, aspect ratio $= 8.2 \pm 2.8$
Pd	$Pd(OAc)_2$	Oleylamine	$nBu_3N \cdot BH_3$	4
Ni	$Ni(OAc)_2$	Oleylamine	$nBu_3N \cdot BH_3$	3
		Oleyic acid		
Fe@Rh	$Fe[N(SiMe_3)_2]_2$, $[Rh(allyl)_3]$	Tetramethyl-piperidine	$iPr_2HN \cdot BH_3$	1.7 ± 0.8
In aqueous media				
Fe	FeSO4	–	$H_3N \cdot BH_3$	~60 (aggregates)
Cu, Ag, Au	$CuSO_4 \cdot 3H_2O$, $AgNO_3$, $HAuCl_4 \cdot 3H_2O$	Poly(vinylpyrrolidone)	$H_3N \cdot BH_3$	Cu0: 4.3, Ag0: 4.7, Au0: 5.1
Co–Co_2B, Ni–Ni_3B,Co–Ni–B	$CoCl_2$, $NiCl_2$, or their mixture	–	$H_3N \cdot BH_3$	4–8
Ni	$NiCl_2$	Starch	$H_3N \cdot BH_3$/ $NaBH_4$	10
Pd	$Pd(OAc)_2$	Poly(vinylpyrrolidone)	$H_3N \cdot BH_3$	3.2 ± 0.5
Ru, Pd	$RuCl_3$, K_2PdCl_4	Poly(4-styrenesulfonic acid co-maleic acid) sodium salt	$H_3N \cdot BH_3$	Ru0: 1.9 ± 0.7 Pd0: 3.2 ± 1.5
Rh	$RhCl_3$	Sodium laurate	$Me_2HN \cdot BH_3$	5.2 ± 2.7
Ru	$RuCl_3$	Sodium laurate	$Me_2HN \cdot BH_3$	2.6 ± 1.2
Rh	$RhCl_3$	Sodium zeolite Y	$H_3N \cdot BH_3$	–

(continued)

Table 2.1 (continued)

Nanoparticles	Metal-containing precursor	Stabilizing agent	Reduction agent	Particle size, nm
Ni	[Ni(4,4′-bipy)(1,3,5-benzenetricarboxylate)]	MOFs (metal-organic frameworks)	$H_3N \cdot BH_3$	~100
Ni	$NiCl_2$	Poly(vinylpyrrolidone)	$H_3N \cdot BH_3$/ $NaBH_4$	–
Au–Ni@SiO2	[Au(этилендиамин)$_3$Cl], [Ni$(NH_3)_6Cl_2$], Si$(OC_2H_5)_4$	–	[$H_3N \cdot BH_3$/ $NaBH_4$]	3–4
Au@Co	$HAuCl_4$, $CoCl_2$	Poly(vinylpyrrolidone)	$H_3N \cdot BH_3$	~7
Amorphous Co	$CoCl_2$	–	$H_3N \cdot BH_3$/ $NaBH_4$	–

Table 2.2 Redox potentials of reduction agents in aqueous solutions (Referred by [51])

Electrode reactions	E, V
$H_2PO_2^- + 3OH^- = HPO_3^{2-} + 2H_2O + 2e$	E = −0.31–0.09 pH
$HPO_3^{2-} + 3OH^- = PO_4^{3-} + 2H_2O + 2e$	E = +0.14–0.09 pH
$H_2PO_2^- + H_2O = H_2PO_3^- + 2H^+ + 2e$	E = −0.504–0.069 pH
$H_3PO_2 + H_2O = H_2PO_3^- + 3H^+ + 2e$	E = −0.446–0.09 pH
$H_2PO_2^- + H_2O = HPO_3^{2-} + 3H^+ + 2e$	E = −0.323–0.09 pH
$H_3PO_3 + H_2O = H_3PO_4 + 2H^+ + 2e$	E = −0.276–0.06 pH
$H_2PO_2^- + 2H^+ + e = 2H_2O + P$	E = −0.248–0.12 pH
$HCHO + 3OH^- = HCOO^- + 2H_2O + 2e$	E = +0.19–0.09 pH
$HCHO + H_2O = HCOOH + 2H^+ + 2e$	E = +0.056–0.06 pH
$2HCHO + 4OH^- = 2HCOO^- + H_2 + 2e$	E = +0.25–0.09 pH
$BH_4 + 8OH^- = BO_2^- + 6H_2O + 8e$	E = −0.45–0.06 pH
$BH_4 + 8OH^- = H_2BO_3^- + 5H_2O + 8e$	E = −0.40–0.06 pH
$N_2H_4 + 4OH^- = N_2 + 4H_2O + 4e$	E = −0.31–0.06 pH
$N_2H_4 + 2OH^- = 2NH_2OH + 2e$	E = +1.57–0.06 pH
$N_2H_5^+ = N_2 + 25H^+ + 4e$	E = −0.23–0.075 pH
$NH_2OH + 7OH^- = NO_3^- + 5H_2O + 6e$	E = +0.683–0.07 pH
$2NH_2OH + 4OH^- = N_2O + 5H_2O + 64e$	E = −0.21–0.06 pH
$H_2 = 2H^+ + 2e$	E = 0.000–0.06 pH
$S_2O_4^{2-} + 4OH^- = 2SO_3^{2-} + 2H_2O + 2e$	E = +0.56–0.12 pH
$SO_3^{2-} + 2OH^- = SO_4^{2-} + H_2O + 2e$	E = −0.09–0.06 pH
$S_2O_3^{2-} + 6OH^- = 2SO_3^{2-} + 2H_2O + 4e$	E = +0.69–0.09 pH
$HSnO_2^- + H_2O + 3OH^- = Sn(OH)_6^{2-}$	E = +0.33–0.09 pH
$Ti^{3+} = Ti^{4+} + e$	E = −0.04
$Sn^{2+} = Sn^{4+} + 2e$	E = +0.151
$Cr^{2+} = Cr^{3+} + e$	E = +0.41
$Fe^{2+} = Fe^{3+} + e$	E = +0.771
$V^{2+} = V^{3+} + e$	E = −0.25
$R_2NHBH_3 + 3H_2O = R_2H_2N^+ + H_3BO_3 + 5H^+ + 6e$	$E = E_0$–0.05 pH

value of standard redox-potential E^0 of the Ag^+/Ag^0 system can decrease from +0.799 V to +0.23 V, when relatively unstable complex $Ag(SO_3)_2^{3-}$ ($pK_f = 8.68$) forms, to −0.290 V in the case of rather stable $Ag(CN)_2^-$ species ($pK_f = 19.85$) [116]. This tendency is also typical of the case when Ag^+ ions form deposits with decreasing solubility of the products. Thus, in AgCl ($K_{sp} = 1.82 \cdot 10^{-10}$) redox-potential Ag^+/Ag^0 decreases to +0.222 V, whereas deposition of far less soluble Ag_2S ($K_{sp} = 6.3 \cdot 10^{-50}$) causes a decrease in E^0 to −0.69 V.

Another characteristic, which allows efficient control of ΔE^0 is pH of a medium. An effect of pH of the medium can be illustrated using for example a redox system containing hydrazine-hydrate [116]:

$$N_2H_4 \cdot H_2O + 4OH^- \rightleftharpoons N_2 + 5H_2O + 4e^- \tag{2.7}$$

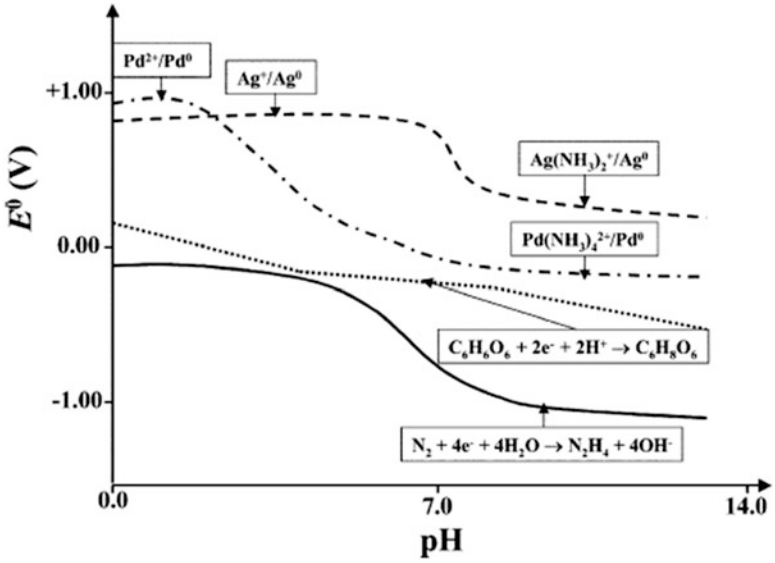

Fig. 2.11 The changes in the standard redox potential of Pd^{2+}, Ag^{+}, ascorbic acid, and hydrazine species with pH [116]

The value E^0 of this process decreases non-linearly from 21.16 in alkali medium to 20.21 V in acid medium, which proves that reducing ability of hydrazine hydrate decreases as OH^- concentration in a solution decreases. In the case when in reaction system a complex with a metal ion forms, the effect of general redox-reaction on E^0 becomes more complicated. It is known, for example, that ammonia forms a great number of complexes with ions of many transition metals of various stabilities. Figure 2.11 shows E^0/pH diagram, which reflects a complicated dependence of redox-potential on pH of a media in a system containing different alike complexes.

For reducing $Pd(NO_3)_2$ the different tetralkyl-ammonium carboxylates with general formula $(n\text{-}C_8H_{17})_4N^+(R'CO_2^-)$ (where $R' = CH_3$, Cl_2CH, $CH_3CH(OH)$, $HOCH_2$, $(CH_3)_3C$) can be used. A choice of the respective reducing agent allows control over size of forming Pd particles in the range 2.2–5.4 nm (Table 2.3) [117].

Carboxylates with electron-donor substituents (as in the case of pivalate) advance formation of nanoparticles of smaller size, while for the reducing agents with electron-acceptor groups (as in the case of trichloroacetate) the opposite effect appears which correlates with values of their oxidation potentials. The lower is $E_{p\,(Ox)}$, the stronger is reducing agent, the finer are particles. For example, $NaBH_4$ is a stronger reducing agent than hydrogen, and its using brings to formation of Pt particles of smaller sizes [118]. The same was observed during deposition of platinum on the surface of carbon nanotubes under action of $NaBH_4$ or ethylene glycol [70].

Similar laws are typical of many colloid systems.

Monodisperse Ag nanoparticles were used as templates for producing bimetal Ag-Au alloys in the substitution reaction between silver particles and $HAuCl_4$ [55]. Taking into account that a standard reduction potential of $AuCl_4^-$/Au (1.0 V

Table 2.3 The influence of the redox potential of a reduction agent on the size of palladium nanoparticles [117]

Reduction agent (n-$C_8H_{17})_4N^+(R'CO_2^-$)	$E_{p(Ox)}$, V	pK_a	d, nm
$R' = Cl_2CH$, dichloroacetate	1.44	1.5	5.4
$R' = CH_3CH(OH)$, lactate	1.16	3.1	2.8
$R' = HOCH_2$, glycolate	1.17	3.8	2.9
$R' = CH_3$, acetate	1.07	4.8	2.0
$R' = (CH_3)_3C$, pivalate	1.08	5.0	2.2

vs. standard hydrogen electrode, SHE) is higher than for Ag^+/Ag (0.80 V), atoms of a silver nanoparticle oxidize to Ag^+ during mixing with $AuCl_4^-$ in the solution. The substitution reduction reaction can be written as:

$$3Ag\,(s) + AuCl_4^- \rightarrow Au\,(s) + Ag^+ + 4Cl^- \tag{2.8}$$

The formed gold atoms are absorbed by the surface of nanoparticles.

Significant interest for the reduction reactions is in polyoxymetalates (POMs), anion oxide structures (Keggin and Dawson structures) with their unique ability to demonstrate widely varied and finely controlled redox-potentials depending on structure and a degree of reduction. Some these POMs, including one-electron reduced Keggin POMs $SiW_{12}O_{40}^{4-}$ b $H_2W_{12}O_{40}^{6-}$ ($SiW_{12}O_{40}^{5-}$ and $H_2W_{12}O_{40}^{7-}$), univalent and bivalent Dawson phosphotungstates $P_2W_{18}O_{62}^{6-}$ ($P_2W_{18}O_{62}^{7-}$ and $P_2W_{18}O_{62}^{8-}$) and bi and tetravalent reduced Dawson phosphomolybdates $P_2Mo_{18}O_{62}^{6-}$ ($P_2Mo_{18}O_{62}^{8-}$ и $P_2Mo_{18}O_{62}^{10-}$) were tested in the reaction of reduction of Ag^+ to Ag^0 nanoparticles [119]:

$$POM(e^-) + Ag^+ \rightarrow POM + Ag^0{}_{colloid} \tag{2.9}$$

As is seen from Fig. 2.12, the value $\log k$[1] for the reaction (2.9) is linearly dependent on the redox-potential corresponding to respective POMs, and the more electronegative redox-potentials, the higher electron transport of electron to Ag^+.

2.2.2.2 The Effect of the Origin of a Reducing Agent

As it was discussed above, origin of a reduction agent can have a significant effect on anisotropy of formed nanoparticles. Often for producing anisotropic structures reducing agents of intermediate force are used. As $AgNO_3$ is reduced in presence of $NaBH_4$, nanoparticles with truncate octahedral structures form, in the case of 1, 2-hexadecandiol nanoparticles of icosahedron shape form (Fig. 2.13) [55].

[1] k is constant of the reaction velocity in per min, because this reaction is of the first order by POM and zero order by Ag+, k has been obtained from the ratio of the initial rate of re-oxidation of POM measured by a decrease in characteristic absorption at 730 nm to the initial POM concentration.

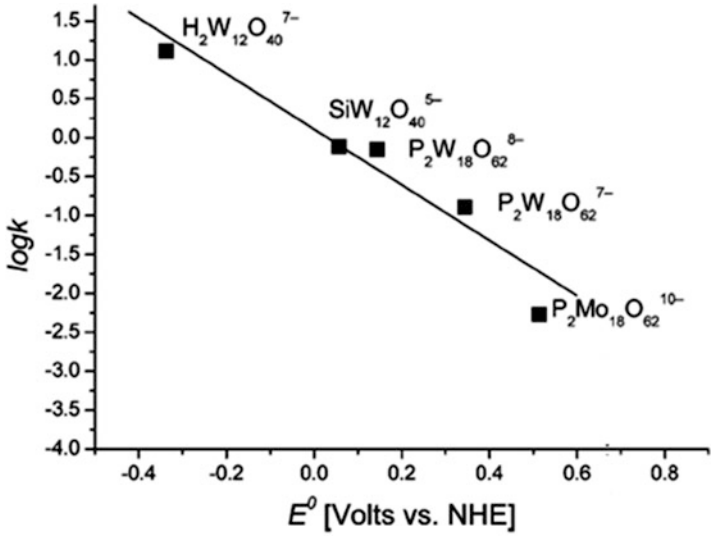

Fig. 2.12 Linear function of log*k* vs. the reduction potential of various reduced POMs for the reduction of Ag^+. [POMs] 1.0×10^{-4} M, [Ag^+] 0.5×10^{-4} M [119]

Moreover, formation of unusual structures, like Au truncate decahedrons favors formation of AgCl-oleyl-amine due to C=C bonds of NH_2 group [120]. Decahedrons had two types of truncation: parallel and perpendicular to the fivefold symmetry axis (Fig. 2.14).

There is an interesting approach called "in situ seeding method" based on introduction into a medium already containing intermediately strong reducing agent a small amount of a strong reducing agent. The aim of the latter is to initiate homogenous nucleation, and the further growth goes due to a weak reducing agent. This method is used to obtain golden nanoparticles shaped as rods/wires, rectangular, cube, and tetrapodlike, and also silver plates and discs [121]. Similarly, the mixture $NaBH_4$-ascorbic acid allows efficient control over nucleation and growth processes and fabrication of various anisotropic particles to grams weight [65, 122]. At higher concentration of borohydride faster nucleation is induced and the formed particles have small size (<5 nm) and spherical shape. If content of borohydride is low, nanoparticles have wide distribution of sizes and shapes; for intermediate nucleation rate nanoparticles become anisotropic and narrow-dispersed. It is interesting to notice that under conditions of seed-mediated growth the process of nanoparticles formation can be realized under medium conditions. It has been shown, for example, that Au seeds enhance reduction effect of ascorbic acid, which, as is known, is unable to reduce $HAuCl_4$ at room temperature [123].

2.2.2.3 The Effect of the Reducing Agent Concentration

A great excess of the reducing agent allows control over sizes of Cu nanoparticles [124, 125] and their shape [126–128].

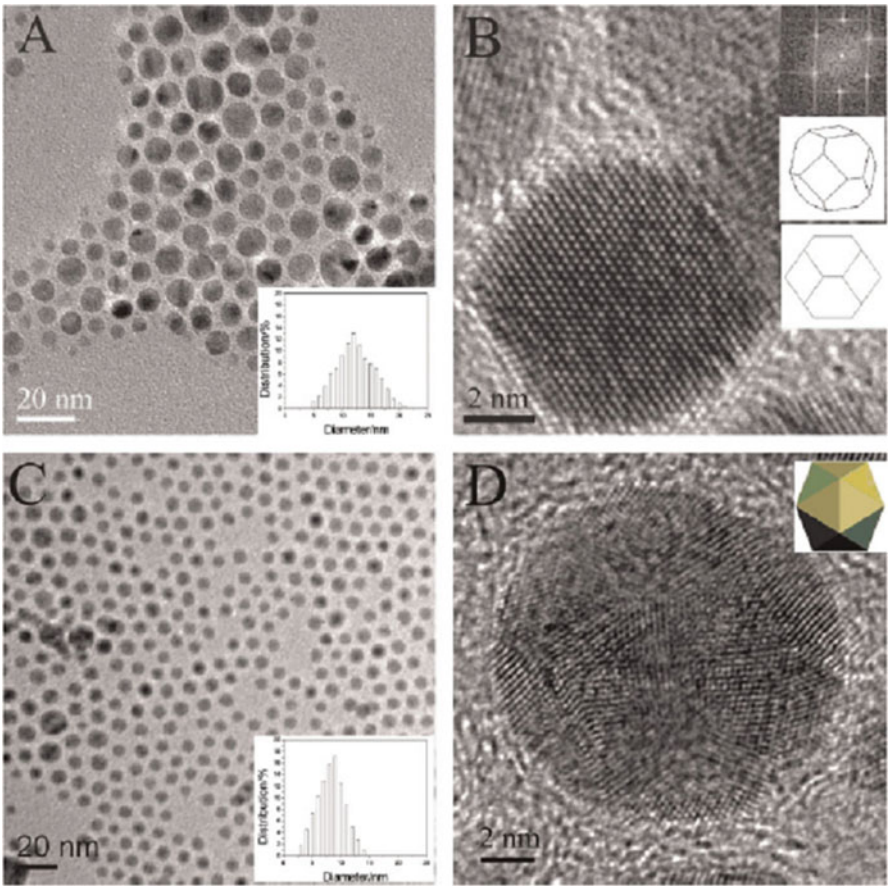

Fig. 2.13 TEM (**a**) and HRTEM (**b**) images and histogram of the Ag nanoparticles prepared by $NaBH_4$ reduction; TEM (**c**) and HRTEM (**d**) images and histogram of the Ag nanoparticles prepared by polyol synthesis; the *inset* shows the schematic illustration of an icosahedron [55]

Variation of the ratio $[N_2H_4]/[AOT]$ (AOT – di(2-ethyl-hexyl)sulfosuccinate Na) from 4.7 to 11.8 leads to increase in sizes of silver nanodiscs and to increase in their polydispersion [129]. Hydrazine hydrate molecules, probably absorb on crystallographic faces, like AOT do, and thus they carry on kinetic control over growth of nanoparticles [88, 130, 131].

The effect of citrate [132] or ferric ammonium citrate (FAC) [95] concentration on golden particle sizes is stronger than on their morphology. And, as is shown for the latter case, average edge length (158 ± 49 nm) of a polygonal nanoparticle at the molar ratio $[FAC]/[HAuCl_4] = 1.0$ far exceeds those found for the molar ratios of the reducing agent and $HAuCl_4$ 0.5 (100 ± 22 nm) and 1.5 (124 ± 24 nm), respectively.

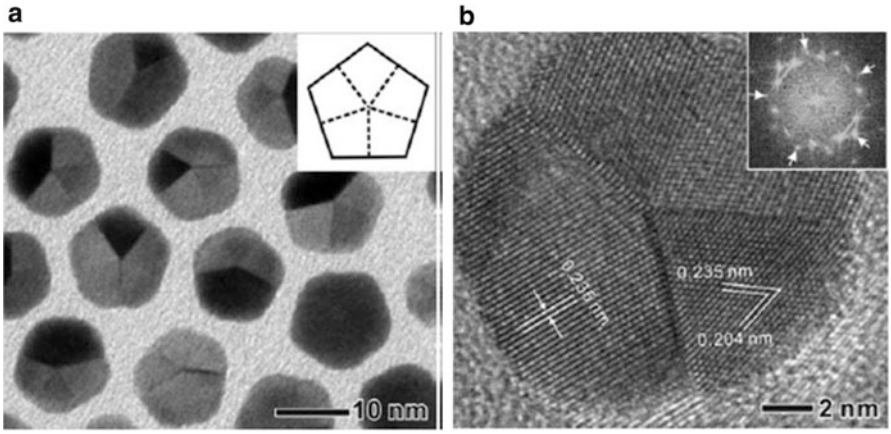

Fig. 2.14 (**a**) TEM image of truncated Au decahedrons. The *inset* shows a two-dimensional schematic drawing of the truncated decahedron. The *dashed lines* indicate the twin boundaries. (**b**) High resolution TEM image taken from an individual truncated Au decahedron recorded along the {011} zone axis and the corresponding FFT pattern (*inset*). In the pattern, the *spots* indicated by *arrows* can be indexed as the {200} reflections from the five single-crystal domains [120]

A change in concentration of the reducing agent $SiW_{12}O_{40}^{5-}$ from 1.0×10^{-4} M to 8.3×10^{-4} M causes an increase in the re-oxidation rate by Ag^{+} ions from $SiW_{12}O_{40}^{5-}$ to $SiW_{12}O_{40}^{4-}$(Fig. 2.15) [119].

An increase in concentration of the reducing agent is reflected in consequent formation of nanoparticles of smaller sizes (Table 2.4). At the lowest concentration $[SiW_{12}O_{40}^{5-}]_0$, 1.0×10^{-4} M the coarsest nanoparticles (>55 nm with wide distribution have been obtained).

2.2.2.4 The Effect of Temperature

At room temperature such reducing agents as citric acid, easily oxidized solvents (alcohols, DMF) and polymers (for example, polyvinyl alcohol) show weak reducing properties with respect to many metal-containing precursors. However, they are able to reduce most metal ions at high temperatures [133–136]. Depending on redox-potentials of a metal compound and a reducing agent, the required temperature of reaction can vary significantly.

In heterophase reactions the reducing regimes have a significant effect both on a degree of reduction and on dispersion of formed nanopowders. Cobalt nanopowders were synthesized by low temperature hydrogen reduction of cobalt hydroxide obtained via interaction of solid salts of cobalt with alkali solution [137]. Increase in temperature from 150 to 320 °C causes increase in a degree of reduction of cobalt hydroxide from 5 to 100 vol.% (Table 2.5).

However, specific surface of the powders decreases from 35.1 to 4.96 m^2/g. During reduction of the metal to 60 %, abrupt decrease in dispersion of the reducing products appears due to sintering of metal particles (Fig. 2.16).

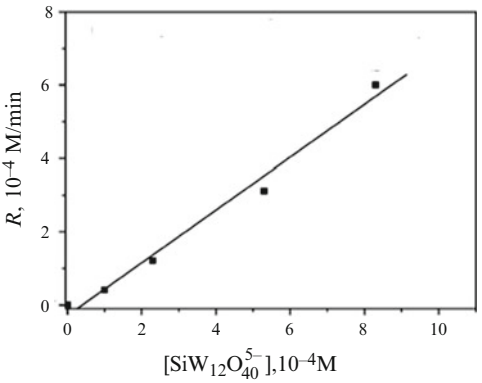

Fig. 2.15 Effect of the initial concentration of $SiW_{12}O_{40}^{5-}$ on the initial rate of reoxidation of $SiW_{12}O_{40}^{5-}$ by Ag^+; reduced POM [obtained by illumination of a deaerated solution of $SiW_{12}O_{40}^{4-}$ (1.0 mM), and propan-2-ol (1.0 M)], Ag^+ (0.84×10^{-4} M) [119]

Table 2.4 Average size of silver nanoparticles obtained upon reduction of Ag^+ (0.84×10^{-4} M) by various concentrations of $SiW_{12}O_{40}^{5-}$ [119]

$[SiW_{12}O_{40}^{5-}]_0$, M	Diameter, nm	r.s.d.,%
8.3×10^{-4}	28.2	±19.0
5.3×10^{-4}	38.0	± 21.4
2.3×10^{-4}	44.0	±10.6
1.0×10^{-4}	–	–

Note. *r.s.d.* relative standard deviation

Table 2.5 Characterization of Co nanopowders [137]

Reaction temperature, °C	Phase composition, vol.%	Reduction degree, %	Specific surface, m^2/g
150	$Co(OH)_2$-88.5; Co_3O_4-8.85; Co – 2.65; CoOOH-3.39; CoO-0.85; Co-4.24	4	35.1 ± 0.06
200	Co_3O_4-25.87; CoO-12.26; CoOOH-3.42; Co-59.25	59	61.04 ± 0.81
250	Co_3O_4-21.12; CoO-21.12; Co-57.76	58	6.06 ± 0.02
320	Co	100	4.96 ± 0.03
380	Co	100	4.38 ± 0.02
420	Co	100	3.39 ± 0.02

An increase in sizes of Pd nanoparticles (from 1.24 to 3.94) in the temperature interval from 15 to 60 °C during electrochemical reduction of Pd(II) nitrate is associated with some events, including high velocities of a stabilizer desorption from surface of nanoparticles at high temperatures [138]. It is interesting that the temperature-dependent change in conformation of poly(N-isopropyl acryl amide) has an effect on shape of platinum nanoparticles formed during reduction of K_2PtCl_4 by hydrogen [139].

On the whole, temperature is important parameter for regulation of the processes of heterogenous/homogenous nucleation and nucleation/growth. An illustrative

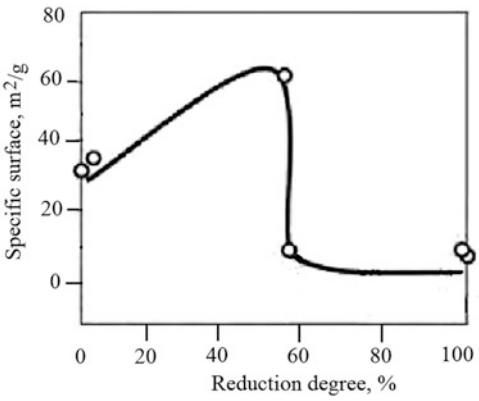

Fig. 2.16 The dependence of the specific surface of Co nanopowder on the degree of conversion during the reduction of cobalt (II) hydroxide by H_2 (the rate of flow 40 L/h) [137]

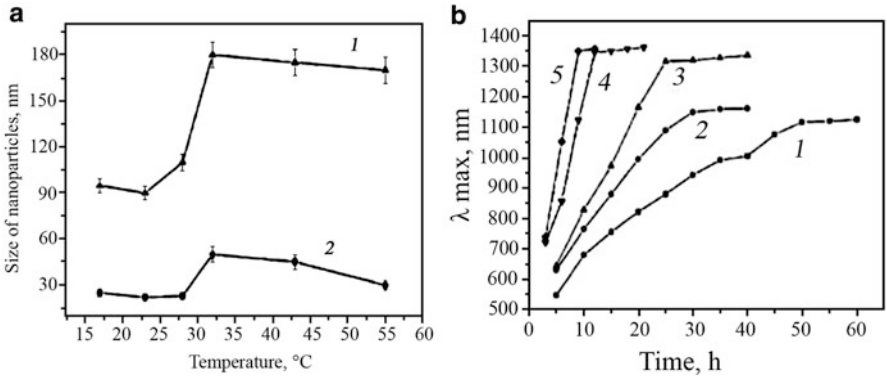

Fig. 2.17 (**a**) The average size of silver nanoplates (*1*) and nanospheres (*2*) obtained at different temperatures and (**b**) the growth rate of nanoplates *vis*. time on the λ_{max} data at temperatures 17 (*1*); 23 (*2*); 28 (*3*); 43 (*4*) and 55 °C (*5*) [140]

example is the systematic studies of chemical reduction of Ag ions in the temperature range from 0 to 55 °C [140]. The low temperatures dramatically reduce the formation and growth of nanoparticles and tens of hours are needed to complete the reaction. The shape and size of nanoparticles formed are rather not uniform. In the range temperature from 17 to 55 °C the rate of reaction as well as the size of the nanoparticles is increased (Fig. 2.17).

It is attracted attention that the increase of the size of particles occurred at 32 °C manifests an elongation of the face of nanoplates from 90 to 180 nm as well as an increase of the diameter of spherical particles from 25 to 48 nm. It was supposed that the growth of particles on this stage can follows to the mechanism of a combined fusion which differs from the Ostwald ripening at room temperature. The analogous peculiarities are characteristic for other noble metals. For example, selective deposition of platinum nanoparticles on carbon nanotubes was in the temperature range from 138 to 160 °C, while as temperature increases to 180 °C, there was aggregation of Pt nanoparticles in solution [70].

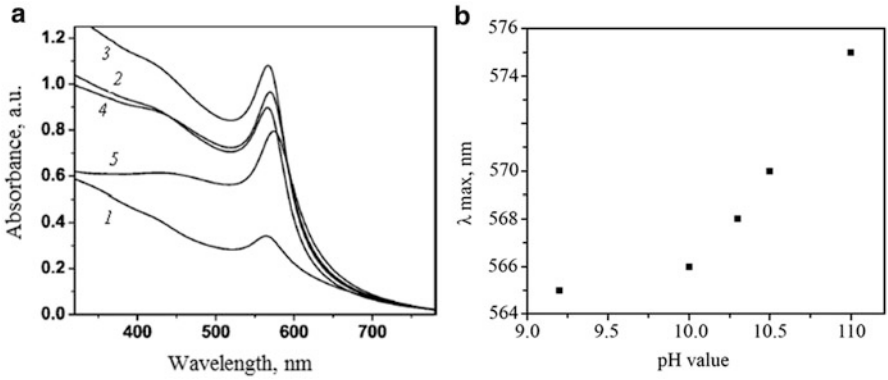

Fig. 2.18 (**a**) UV/Vis absorption spectra of copper nanoparticles synthesized in 1.0 mM aqueous PAA solution at different pH:: 9.2 (*1*), 10.0 (*2*), 10.3 (*3*), 10.5 (*4*) and 11.0 (*5*). (**b**) Absorption maximum of copper nanoparticles versus the pH value [141]

2.2.2.5 The Effect of pH

An important parameter in chemical reduction reactions is pH of a medium, which has an effect not only on sizes of formed nanoparticles, but on their shape and composition. Copper nanoparticles participate if, for example, pH of a solution is in the range 9.2–10.5. According to UV-vis spectra, intensity and position of the maximum change depending on pH (Fig. 2.18) [141].

At lower pH (9.2–10.3) peak of plasmon resonance at 565 nm is typical for copper nanoparticle [142], its intensity increases in these limits, which is the evidence of yield of nanoparticles. As pH to 10.5 and 11, the absorption peak shifts to $\lambda = 570$ nm и 575 nm, which can point to formation of metal copper nanoparticles in copper oxide shell [38, 143].

2.2.2.6 Kinetic Laws

The special features of nanoparticles is presence of so-called surface plasmon resonance (SPR), i.e. dramatic increase in intensity of absorption and spattering at some wavelength of incident light, which is in resonance with eigenfrequency of electron gas vibrations on a particle surface. Parameters of plasmon resonance are: value, spectral position, and FWHM serve for characteristics of nanoparticles and processes of their formation, which allows successful usage of the most informative method of electron spectroscopy for studies. For example, silver nanoparticles absorb light intensely with the maximum of plasmon resonance line in violet range of optical spectrum (390–450 nm). Solutions of gold nanoparticles have also maximum absorption in visible spectrum from 510 to 540 nm, copper nanoparticles have maximum at 550 nm [144].

Kinetics of formation of gold nanoparticles according to the data of UV-vis-near-IR spectroscopy at reduction of $HAuCl_4$ is shown in Fig. 2.19a [145].

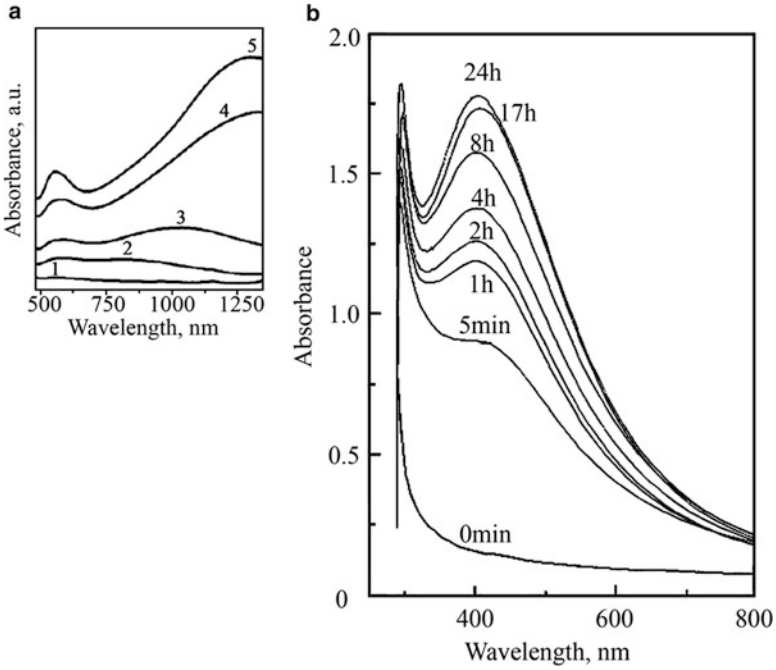

Fig. 2.19 (**a**) UV-vis-NIR absorption spectra of gold nanoparticles measured during the reduction of 10^{-3} M $HAuCl_4$ with *Aloe* V*era* extract after 5, 7.5, 8, 9, and 25 h of reaction (curves 1–5, respectively). (**b**) UV/vis spectra of composite of polymer brush and Ag nanoparticles varying the reduction time [145]

The peak of SPR at 560 nm increases monotonously during the reaction, after 7.5 h a new band appears, localized at 817 nm, as the reaction is finished, long-wave absorption undergoes additional red shift. This evolution of the spectrum can be associated with aggregated spherical nanoparticles or with anisotropic structures whose sizes change in time. For example, appearance of new plasmon peak in the long-wave range of the absorption spectrum during irradiation of $AgNO_3$-ethanol-polyvinylpyrrolidone with argon-ion laser ($\lambda = 514.5$ nm) is associated with formation of coarse quasi-ellipsoid nanoparticles and with aggregates of Ag nanoparticles with fractal dimensionality (Fig. 2.20) [146].

Amplitude of plasmon resonance at 405 nm in the polystyrene-gr-poly (methacrylic acid-block-polymethacrylate)-silver nitrate increases during reduction and reaches maximum for more than 24 h, which allowed efficient control over growth of nanoparticles (Fig. 2.19b) [147].

2.2.3 Reduction in Statu Nascendi in Polymer Matrix

Taking into account instability of nanoparticles, most preparation techniques include usage of stabilizing agents, which absorb on surface of particles. During

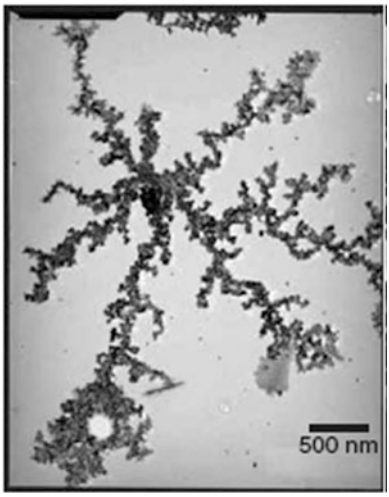

Fig. 2.20 TEM image of the aggregate formed in $AgNO_3$/ethanol/PVP-produced silver colloid [146]

steric stabilization, as was mentioned above, aggregation of the particles is prevented by absorption of large molecules (polymers or surfactants). According to some estimations, efficiency of stabilization with polymers can be expressed by their protective value [148], which for known polymers such as poly(N-vinyl-2-pyrrolidone), poly(vinylalcohol), poly(acrylamide), poly(acrylic acid), and poly (ethylene imine) is 50.0, 5.0, 1.3, 0.07, and 0.04, respectively.

Apart from steric limitations [149]

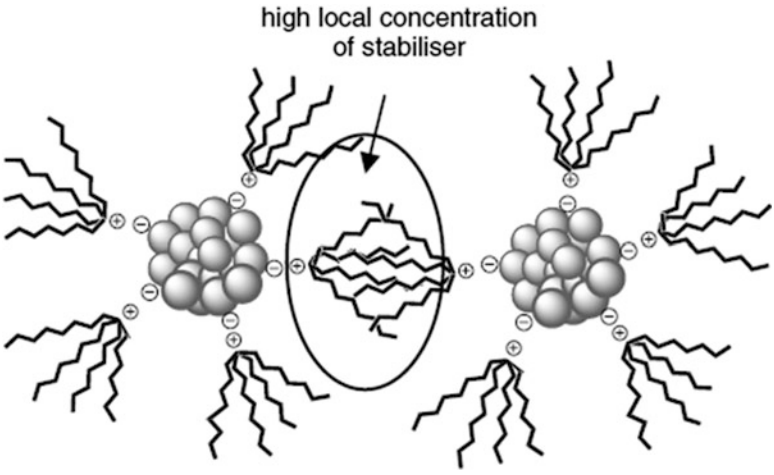

polymer molecule can weakly bound with a surface of a particle via heteroatoms acting as ligands [150].

As a rule, reduction in the medium of polymer template is preceded by formation of macromolecule complex of metal precursor with polymer molecule. The key stage in synthesis of dendrimer—template/Ag—nanocomposite is interaction of

Ag^+ ions with terminal OH-groups of the dendrimer on the basis of 3.5-dihydroxybenzyl alcohol [151] (Scheme 2.1):

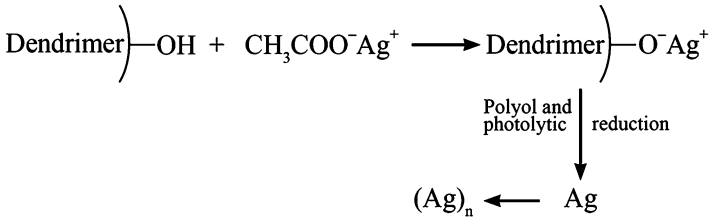

Scheme 2.1 A pathway for the dendrimer/silver nanocomposites formation

Sizes of metal nanoparticles and their size distribution increase as generation of the dendrimer increases, which correlates with increase in the dendrimer size with increase in number of generations:

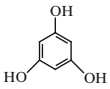

G0

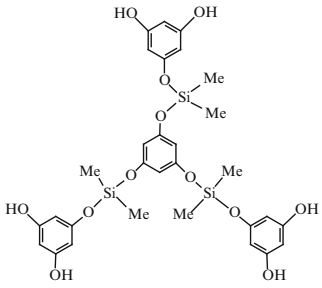

G1

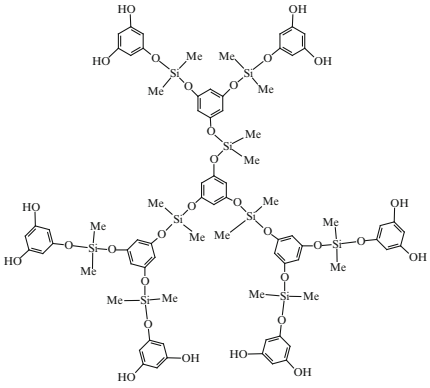

G2

It is known that as number of generations of dendrimers increases, they aggregate [152, 153], which forms template places of various sizes, in which metal nanoparticles grow.

In the case of poly(vinylpyrrolidone) most widely used stabilizing and reducing agents in chemical reactions of producing nanocomposites [154–156], the preserving effect is associated with presence of a free pair of electrons of a nitrogen and a oxygen atoms in polar PVP polar groups, which can be donated in two sp hybrid orbitals of metal ions with formation of complex ions [157] (Scheme 2.2):

Two formed types of complexes can induce various nucleation processes [158]. Moreover, it is assumed that a bond between a PVP and a metal remains after reduction of the metal [159]. The PVP molecule can prevailingly absorb on some crystal faces of a seed, inhibiting or accelerating their growth and, consequently, it advances anisotropic growth of metal nanoparticles [91, 104].

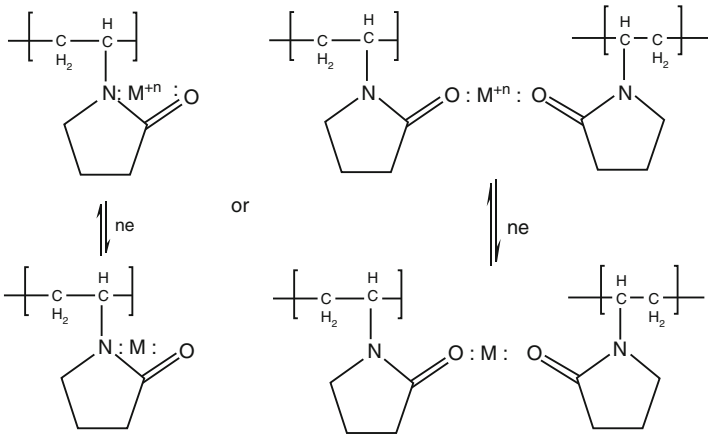

Scheme 2.2 Complexation of metal ions with poly(vinylpyrrolidone) chains

This method can be applied to fabrication of bi- and multicrystalline nanoparticles. For example, scheme of Bi_2Te_3 synthesis includes coordination of Bi(III) and Te(III) ions with polyvinylpyrrolidone, formation of a macrocomplex, and the following reduction in presence of $NaBH_4$ [160] (Scheme 2.3):

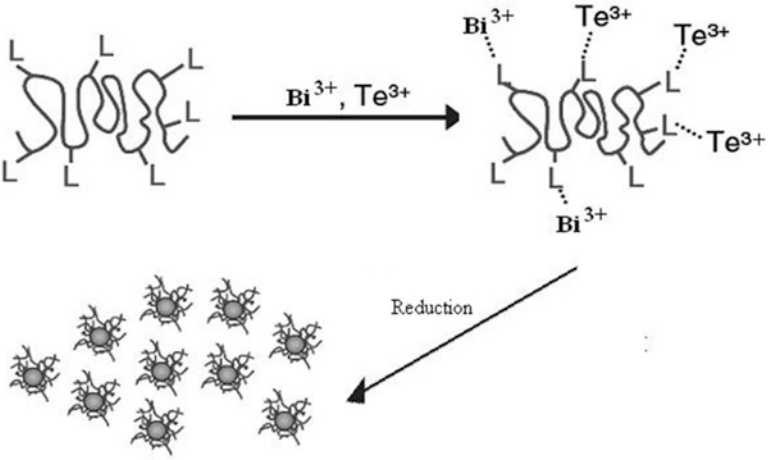

Scheme 2.3 Synthesis of bimetallic nanocomposites

Depending on a way of synthesis, a nature of the used precursors and reagents, particles with various properties, sizes and forms can be obtained. A simple example of synthesis of Ag nanoparticles during reduction of silver nitrate conducted in various media and in presence of various reducing agents [161] can demonstrate importance of all parameters and conditions of the reaction. Colloid dispersions of silver particles from 1 to 600 nm in size are obtained in water

Table 2.6 Synthesis and characterization of Ag nanocomposites (0.2 M $AgNO_3$, 0.1 M aqueous solution of stabilizing agent, ascorbic acid is a reduction agent) [161]

Stabilizing agent	The shape of particle	The size of particle
–	Rice balls consisting of rod like particles	2–4 μm, 300–600 nm
Pluronic PE PEO–PPO–PEO-block-copolymer non-ionic surfactant	Rice balls consisting of rod like particles	2–4 μm, 300–600 nm
Plurafac LF non-ionic surfactant	Rice balls consisting of rod like particles	2–4 μm, 300–600 nm
Gummi arabicum polysaccharide	Rice balls consisting of rod like particles	2–4 μm, 300–600 nm
LutensitA-ES sodium alkylphenol ether sulfate anionic surfactant	Thin large plates	–
Tamol VS vinylsulfonate, Na salt	Crystallites, leafs	From 5–6 to 20 μm
Emulphor FAS 30 alkylphenolate-free ether, Na, salt	Crystallites, leafs, hexagons, plates, spheres	From 2–4 to 3 μm
Polyvinylpyrrolidone	Hexagons, plates, spheres	From 1–3 μm to 300–500 nm

solution under action of ascorbic acid, ferric ammonium citrate, sodium borohydrate and hydroquinone. Polymers of different origins were used as stabilizing media, their variations can be efficiently used to control size and shape of colloid particles (Table 2.6).

Thus, apart from origin and structure of a polymer template, a crucial effect on characteristics of obtained nanocomposites has many parameters of the reduction reaction in polymer matrix in nascendi (concentration of a metal salt, stabilizing and reducing agents, temperature, crystal structure, and sizes of preliminary prepared or in situ grown seeds, etc.). Some of these features are considered below.

2.2.3.1 Reducing Agent

Using of strong chemical agents allows conduction of a reaction under soft conditions (at room temperature and atmospheric pressure). For example, silver nanoparticles were obtained in PMMA solution in 1,2-dichloroethane, in which ammonia solution of silver oxide was introduced (with concentration 10^{-2}–10^{-4} M) in presence of hydrate hydrazine ($2 \cdot 10^{-2}$ M) [162]. Dodecylamine as a reducing agent requires more severe conditions. CdSe nanoparticles stabilized by carbazole containing poly (benzyl ether) dendrons were obtained via reduction of cadmium oxide by dodecylamine initially during heating in vacuum (120 °C) with the following heat treatment at 270 °C in nitrogen atmosphere and fast injection of selenium and trioctylphosphine [163].

2.2.3.2 The Effect of Concentration of Polymer Ligand

It has been shown that sizes and shapes of copper nanoparticles are substantially dependent on concentration of a stabilizing ligand, polyacrylic acid (PAA) [141]. At low concentration of PAA (1.0 mM) nanoparticles were predominantly large (~80 nm) and spherical. If concentration of PAA is 1.33 mM, crystalline faced (cube-octahedron) particles formed with the size ~50 nm. At concentration of PAA 2 mM average size of nanoparticles decreased to 30 nm, and their polydispersion increased. It interesting to point out that under similar conditions, but with usage of polyvinylpyrrolidone, it is impossible to obtain metal nanoparticles of copper, their synthesis is accompanied by formation of Cu_2O nanoparticles in wide range of pH [164]. At high concentration of PVP or short chains (M_W 10000) silver ions reduce on the surface of seed particles without additional heating or other actions [165]. Under these synthetic conditions homogenous star-like, multipod nanoparticles with high yield (100 %) form (Fig. 2.21).

Using of polycrystalline golden nanoparticles (15 nm in diameter) for seeds can produce spheroid or armed Au nanoparticles at simple variation of experimental conditions of the reaction. The key feature is, probably, reduction ability of poly (vinylpyrrolidone) molecules, which has an effect on the reduction kinetics of gold and, consequently, on the deposition rate of Au atoms on the surface of Au seeds. Consequent interactions of PVP via absorption/desorption processes and high ratios

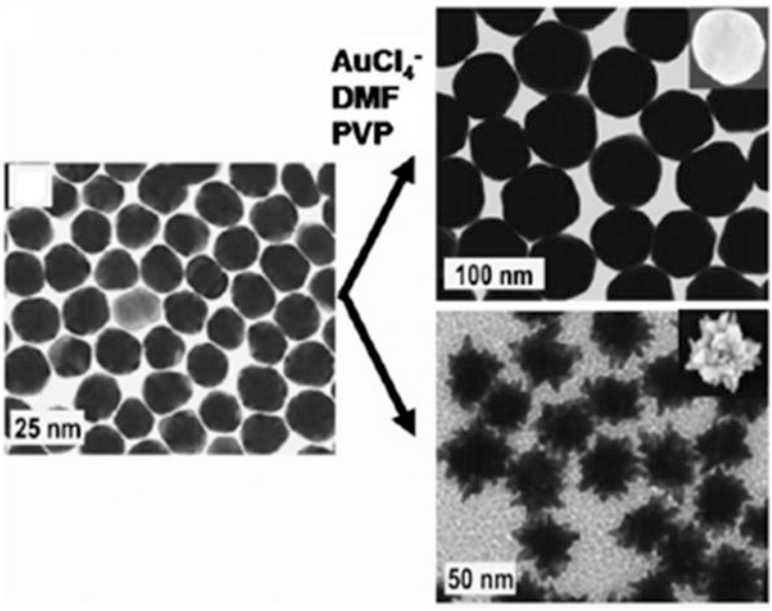

Fig. 2.21 Catalytic growth of the seeds into Au spheres or Au nanostars at high concentration of poly(vinylpyrrolidone) [165]

of poly(vinylpyrrolidone) links to Au atoms cause fast, kinetically controlled and preferable growth along certain crystallographic faces, which finally is ended by formation of star-like nanoparticles.

2.2.3.3 The Effect of Molecular Weight of a Polymer Ligand

A possibility of steric stabilization is defined by the fact that spatial dimensions of even low molecular compounds are compatible with the radius of London attracting forces or even more. If it is assumed that "diameter" of a macromolecule of a linear polymer coincides with the root-mean-square distance between its ends, then the relationship between the average geometrical size of the particle $<r^2>^{0.5}$ and molecular mass of the polymer M can be expressed as [166]

$$< r^2>^{0.5} \approx 0.06M^{0.5} \tag{2.10}$$

In the case of the polymers with $M = 10^4 < r^2 >^{0.5} = 6$ nm, and at $M = 10^5$ this value is already 20 nm. Consequently, the molecules of the polymers with $M > 10^4$ have the same sizes, which are necessary for stabilization of colloid particles. And a polymer with higher molecular weight has more efficient ability to limitation of growth and agglomeration, as it was found in the system Ni nanoparticles- poly (vinylpyrrolidone) (Fig. 2.22) [167].

Molecular weight of a polymer plays the crucial role in geometry of particles. Poly(vinylpyrrolidone) with molecular weight M_w 1300000 was used to synthesize silver decahedron with high yield [157]. As molecular weight of PVP decreases to M_w 40000, polydispersion particles formed, only 40 % of which had the shape of decahedron, and in the case of even lower molecular weights always spherical nanoparticles formed.

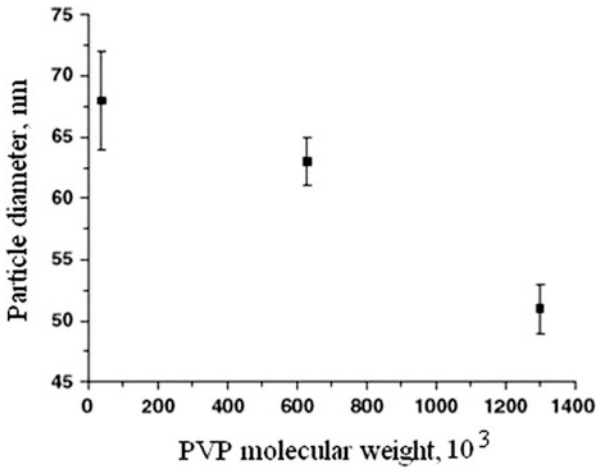

Fig. 2.22 Relationship of poly(vinylpyrrolidone) (PVP) molecular weight and synthesized Ni nanoparticles [167]

2.2.3.4 Supercritical Media

The prospective is the approach based on reduction of metal containing precursors in polymer matrices in supercritical media [168–170]. The main mechanism is diffusion of a solution of organic metal complex solved, for example, in supercritical CO_2 in polymer matrix, not soluble, but swelled. The last fact makes it possible to widely vary origin of a polymer, for example, use different dendrimers [171], natural polymers, such as chitosan [172], etc. In these systems usually H_2 is used as a reducing agent, which is well compatible with supercritical CO_2. Changing density of media can additionally help to regulate size of nanoparticles, as it was shown for Au nanoparticles synthesized in situ in pores of MCM-48 [173]. Size of formed nanoparticles was from 2 to 25 nm under pressure of CO_2 17 and 7 MPa, respectively.

In general case the stabilizing action of highly molecular compound is determined by some additional parameters, in particular, by degree of polymerization, type and number of functional groups, character of their distribution in chain, etc. Interaction of a protective polymer with a forming nanoparticle can be realized via absorption of macromolecules on a surface of the particles or their chemosorption from the solution. Physical absorption is governed by Van der Waals forces, dipole interactions, or hydrogen bonds. Non-covalent interactions of nanoparticles with a macromolecule are very weak, about 10^{-4} J/m^2. There are interactions of nanoparticles with PE, PVA, PEO, PVP, polyethylene glycol macromolecules, etc. [174]. Polymer molecules can be easily displaced from the zone of interaction during Brownian motion of particles [175]. In particular, PEO weakly interact with metal surfaces, therefore, it is a bad stabilizer of colloid gold [176]. For enhancing of stabilizing properties of polymers binary protective systems are sometimes used, as, for example, PVP dodecylamine in polyol synthesis of Ni nanoparticles [167].

Polymer chains during chemosorption can form covalent, ionic or coordination bonds with atoms of surface layers of a metal. Introduction of various functional groups in a polymer causes an increase in the role of acid-base interactions in a polymer-metal system and, respectively, to an increase in adhesion ability of a polymer. Below some polymer systems are considered, which are used as stabilizing media in chemical reactions of production of nanocomposites.

2.2.3.5 Block-Copolymers as Nanoreactors for Synthesis of Nanocomposites

Block-copolymers form micelles in diluted solutions of polar solvents, such as water, or in non-polar organic medium. Micelles of block-copolymers have a definite core-shell structure, consisting of a core of insoluble block and a shell or crown of a soluble fragment of a copolymer. The methods of obtaining of block-copolymers, characteristics of their compositions and properties are widely presented in literature, there are many monographs and reviews considering fundamental principles of their self-organization, structure, and application in synthesis of nanomaterials [177–180].

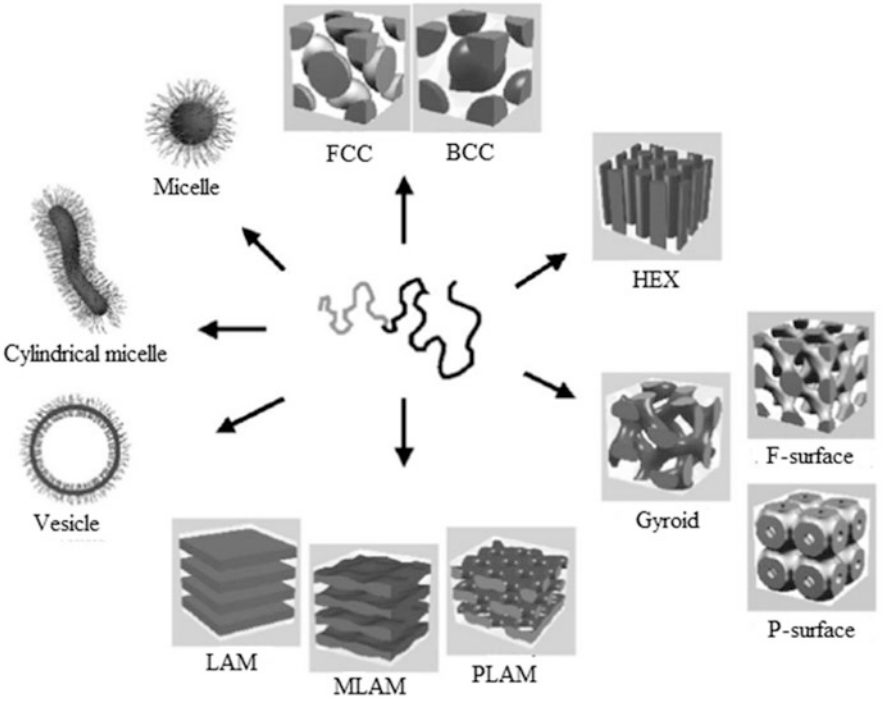

Fig. 2.23 Self-organization structures of block copolymers and surfactants: spherical micelles, cylindrical micelles, vesicles, fcc- and bcc-packed spheres (FCC, BCC), hexagonally packed cylinders (HEX), various minimal surfaces (gyroid, F-surface, P-surface), simple lamellae (LAM), as well as modulated and perforated lamellae (MLAM, PLAM) [179]

Block-copolymers in a solution and in block state (as films) have microphase separation with formation of various types of morphological structures (spheres, rods, vesicles, crew-cut structures, lamellas, cylinders, etc.) (Fig. 2.23) [179, 181, 182].

Shape of micelles can be controlled by various parameters, such as a relative block length, content of ion, composition of solvents, etc. Mainly, morphology depends on the ratio of block length f and the segregation parameter χN, where N is the total degree of polymerization $N = N_A + N_B$, χ is Huggins parameter, which characterizes the repulsive force between the polymer blocks. The value χ decreases with increase in temperature according to the dependence $\chi \sim 1/T$. Changing a degree of polymerization provides control over the superlattice unit cell parameter in wide from some nanometers to hundreds nanometers. Figure 2.24 shows this dependence for poly(butadiene-b-ethylene oxide) (PB-PEO) [179].

The initial part of the curve corresponds to short chained non-ionogenic surfactants, which confirms universality of their behavior and block-co-polymers, and, with respect with theoretical predictions, can be described by the relationship: $d \sim d_0 N^{2/3}$ ($d_0 \sim 0.9$ nm).

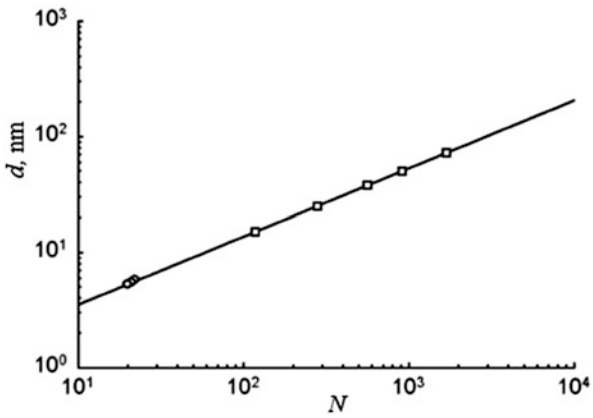

Fig. 2.24 Long period d as a function of the degree of polymerization (N) of PB-PEO (□) and non-ionogenic surfactants (O)

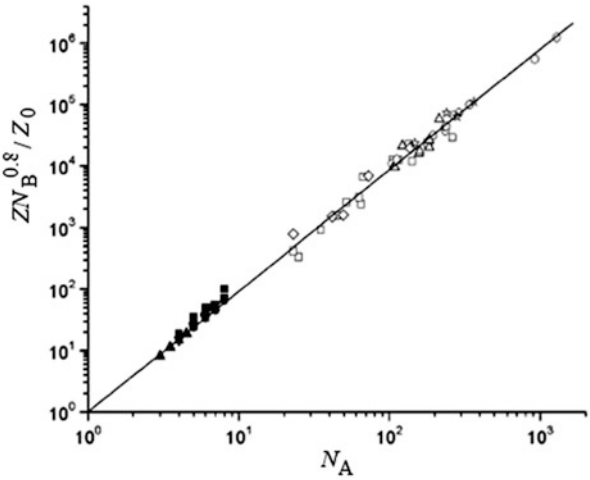

Fig. 2.25 Aggregation numbers Z as functions of the degree of polymerization N_A of the insoluble block. o, □: diblock copolymers (PS-P4VPy, PS-PMAc), Δ: triblock copolymers (PMAc-PS-PMAc), ▽: graft copolymers (PSMSA-g-PEO), *: PS-P2VPy heteroarm star polymers, ◊: PS-PAAc heteroarm star polymers, •: nonionic surfactants, ■: cationic surfactants ($RNMe_3Br$) ▲,▼: anionic surfactants ($ROSO_3Na$, RSO_3Na) [179]

The dependence of a number of aggregates Z, i.e. a number of block-polymers in a micelle on a degree of polymerization of a soluble block N_A (Fig. 2.25) can be described by equation (referred to by [179]):

$$Z = Z_0 N^{\alpha}{}_A N^{-\beta}{}_B \tag{2.11}$$

(where $\alpha = 2, \beta \sim 0.8, Z_0$ depends, mainly, on the mixing enthalpy of insoluble polymer block A and solvent), which can be applied to many bi- and tri-block

Table 2.7 Morphology of polymer particles and composites

n/n	Morphology	$\rho = R_g/R_h$
1.	Homogeneous sphere, random coil, monodisperse	0.788
	Θ-conditions	1.50
	Good solvent	1.78
2.	Random coil, polydisperse z = 1	
	Θ- conditions	1.73
	Good solvent	2.05
3.	Regular stars	
	Θ- conditions, f = 4	1.33
	Good solvent, f >> 1	1.079
4.	Rigid rod	
	Monodisperse	>2.0
	Polydisperse	>2.0

grafted and star-like co-polymers and for low molecular cation and anion surfactants, which confirms similarity of their self-assembling mechanism, and diameter of the micelles can be directly determined by a degree of polymerization of blocks, which is important for the controlled synthesis of nanocolloids.

It is known that for rigid spheres $R_g = 0.778R_h$ (R_g is gyration radius, R_h is hydrodynamic radius), and the parameter R_g/R_h changes dependently on architecture of particles and their geometry. In the Table 2.7 are shown values of parameter $\rho = R_g/R_h$ for macromolecules of various architectures [183].

On the whole, the coarser is a particle and higher its anisotropy, the higher is ρ. For example, in the PS(300)-*b*-P[2VP-Au0.5(300)] system gold nanoparticles are agglomerated with increase in R_g and parameter ρ [183], i.e. it can be assumed that the concentration at which R_g and R_h begin to increase corresponds to the critical concentration of micelle formation (CMC) of a block copolymer. Moreover, the longer a block forming a core, the lower CMC of the block-copolymer providing that length of polymer chains of the crown is approximately the same.

The theory predicts that insertion of a particle or a molecular solute in a surfactant micelle leads to perturbation in the initial structure due to the core swelling [184, 185]. However, if concentration of a solved substance is low, the structure of a surfactant micelle is predominantly determined by molecular properties of a polymer. On the contrary, arrangement of a polymer surfactant on macroscopic surface in selective solvents depends on many parameters, including relative affinity of each block of a copolymer to the surface and to the solvent, length of blocks, interphase boundary, and concentration of the polymer. These parameters have a substantial effect on thickness and regularity of the surfactant layer. A significant assumption of many theories of absorption is that curvature of a surface is small as compared to length of a polymer and thickness of a film. And, as a result, it is unclear which type of a monolayer structure is formed by a block-polymer on a strongly curved surface of a nanoparticle: absorbed layer, micelle, etc. It has been shown that curvature of a surface has effect on thickness of the absorbed

layer when the curvature radius reaches gyration radius of a polymer ($\rho/R_g \approx 1$) [186]. It is assumed that there is a range of particle sizes, beyond which polymer surfactants combine surface absorption and micelle formation [187]. In other words, block-polymers on the surface of a nanoparticle can form as a grafted layer if it is a coarse nanoparticle or a micelle, if a particle is small. For Au nanoparticles, whose size is more than 10 nm, a core-shell structure forms (Au@PS-*b*-PAA) which is well described by the general model of polymer absorption [188]. Thickness of a layer depends not on absolute concentration of a polymer or Au nanoparticles, but on their relative amount. If Au sizes are small, they dissolve as molecular factions in the core of a micelle of polystyrene-block-poly (acrylic acid) (Scheme 2.4).

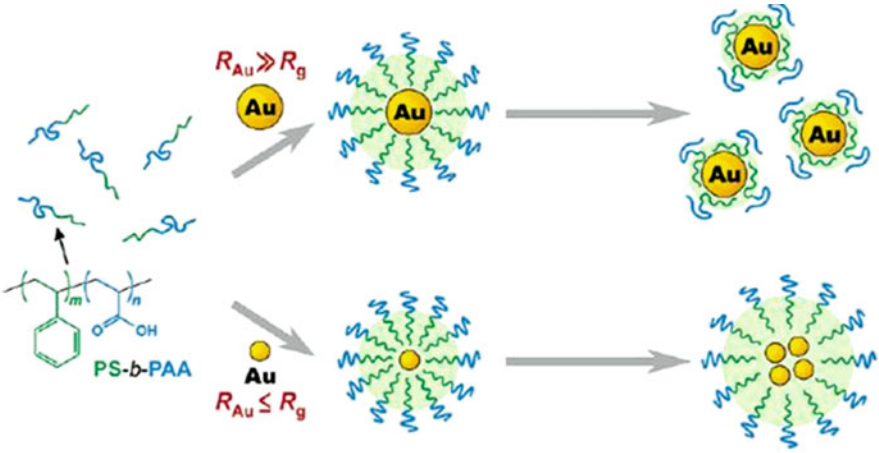

Scheme 2.4 Formation of absorption layers and micelle structures in block-copolymer nanocomposites

Relative and absolute length of the polymer blocks also has an effect on structure of absorbed polymer layer. Moderately asymmetric and symmetric copolymers (PS_{159}-*b*-PAA_{62}, PS_{49}-*b*-PAA_{54}) do not absorb on the surface of nanoparticles, while strongly asymmetric polymers (PS_{250}-*b*-PAA_{13}, PS_{160}-*b*-PAA_{13}, PS_{100}-*b*-PAA_{13}, $PMMA_{240}$-*b*-PAA_{13}) form quite well thick surfactant shell.

Various copolymers used as polymer templates are widely applied in colloid synthesis of metals: in particular, block-copolymers of styrene with poly(acrylic) acid [181], 2- and 4- vinylpyridine [183, 189–191], polyethylene oxide with 4-vinylpyridine [192], and poly(3-caprolactone) [193], etc.

Many representatives of star-like polymers $(AB)_n$, where n is a number of bi-blocked branching, which can form inverse micelles with complicated structures, relate to the block-polymers of the considered type [191, 194–196]. Micelles of this type have monomolecular structure. Thus, (PS-b-P4VPy)4 micelles with

petal structure form if toluene is added to (PS-b-PVPy)4 in CH_2Cl_2 solution [194] (Scheme 2.5):

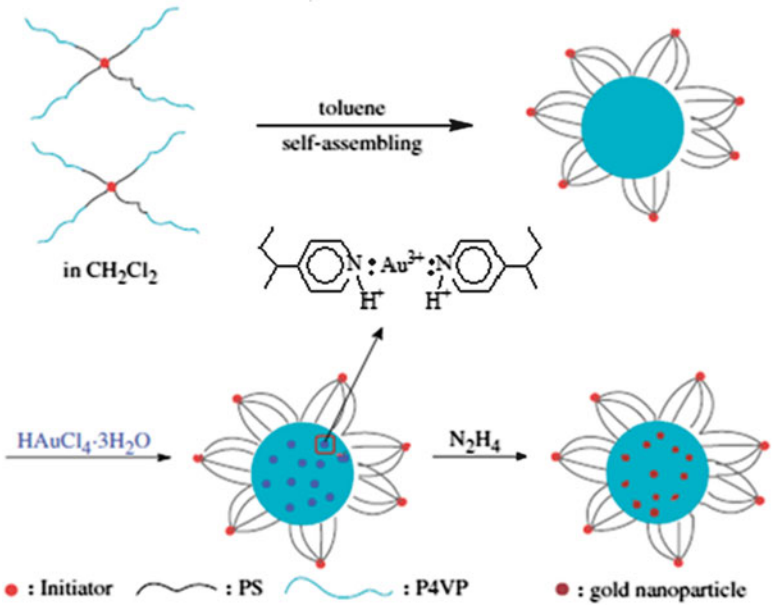

Scheme 2.5 Schematic representation for the preparation of reversed micelles and gold nanoparticles

In this case the exterior blocks (P4VPy chains) form a core and PS chains (interior blocks) serve a petal-like shell. It is interesting to note that independently on length of P4VPy chains micelles preserve spherical shape ($R_g/R_h = 0.82$, where R_g is gyration radius, R_h is hydrodynamic radius, see Table 2.8), though it is known that at high ratio R_g/R_h PS-b-P4VPy has cylindrical morphology [197].

Dense structure of petal-like formation prevents interaction of P4VPy links between two neighbor micelles, and thus prevents their aggregation. Nanoparticles formed in these templates have narrow and homogeneous size distribution in the matrix space (2.5 ± 0.2 nm, 2.4 ± 0.3 nm and 2.0 ± 0.2 nm).

The considered method of synthesis of nanocomposites is mainly based on usage for templates of already formed and well-organized block-copolymer micelles. However, there are systems in which formation of micelles proceeds also in solutions which are "good" for block polymers owing to interaction of inorganic ion with a copolymer or so called ion induced micelle formation [198–201]. Problems of influence of metal ions and nanoparticles on self-assembling processes stay in many ways unclear.

Table 2.8 The parameters of micelles of block-copolymers [194]

Block copolymers	D_h, nm	R_g, nm	R_g/R_h	D_h^{com}, nm	R_g^{com}, nm	R_g/R_h^{com}
$(PS_{25}\text{-b-}P4VP_{12})_4$	26.4	8.4	0.64	39.0	20.7	1.06
$(PS_{25}\text{-b-}P4VP_{32})_4$	44.3	13.6	0.61	51.5	21.3	0.83
$(PS_{25}\text{-b-}P4VP_{64})_4$	74.0	30.4	0.82	59.0	24.0	0.81

D_h, R_g, and R_g/R_h are data of the reverse micelles and, D_h^{com}, R_g^{com}, and R_g/R_h^{com} are data of complex micelles

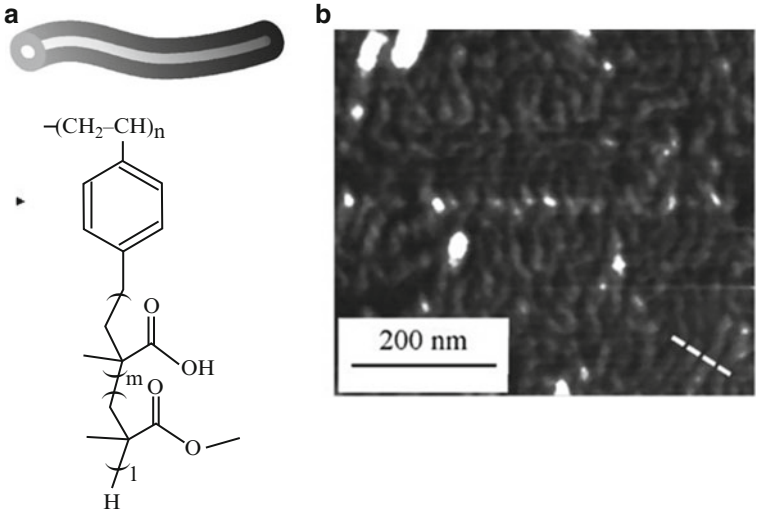

Fig. 2.26 (**a**) Schematic structure and (**b**) AFM photograph of amphiphilic copolymer PS-gr-(PMA-b-PMMA) of double-cylinder-type [147]

Soft conditions of synthesis make it possible to obtain silver nanocomposites based on polystyrene-g-(polymethacrylic acid-block-poly(methyl methacrylate) (PS-g-(PMA-b-PMMA) dissolved in organic acids [147]. Specific structure of polymer template in the shape of two-layered cylinders advances solubility (Fig. 2.26). However, formed nanoparticles have quite wide size distribution spread (7.5 ± 2.3 nm).

However, on the other hand, these systems provide a good possibility for control of particle size and their morphology during change in degree of microphase distribution via variation of a solvent type or molar ratio of hydrophilic and hydrophobic components. In the case of poly(urethane acrylate –styrene) copolymer containing (poly)propylene and poly(ethylene oxide) fragments

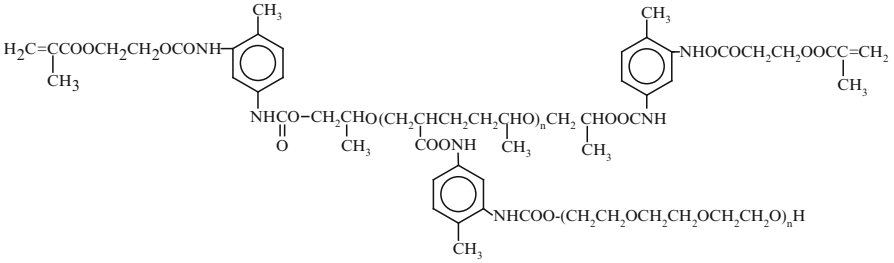

complex formation of cadmium acetate with hydrophilic poly(ethylene oxide) chain favors formation of nanodomain structure with its further fixation during copolymerization [202] on the whole, increases microphase separation.

2.2.3.6 Hydrogels

Polymer cross-linked hydrogels working as nanoreactors in synthesis of colloid metal nanoparticles attract a considerable attention due to their potential application in catalysis [203, 204], photonics [205], drug delivery [206] and biomedicine [207, 208]. In the latter case a decisive role has biocompatibility of these polymers with biomolecules and tissues (see Chapter 7).

Really, substantial free spaces in the linked polymer network in the swelled state work as nanoreactors during nucleation and growth of nanoparticles. It has been shown that size and morphology of nanoparticles can be controlled by concentration of a linking agent and functionality of a reticulate gel [209–211].

Poly(acrylamide) (PAAm) gels are very efficient for synthesis of nanoparticles [212–216]. Usually, PAAm gels are produced by polymerization of AAm in presence of bi-functional cross-linking agent, for example, *N*,*N*′-methylene *bis*-acrylamide:

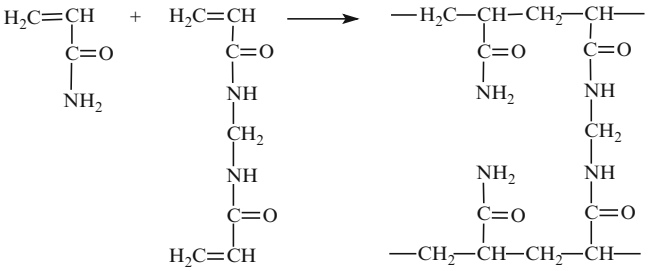

Metal ions are bound with functional groups of a cross linked polymer making monomolecular complexes, their concentration can be varied in quite wide range. In some cases metal ions are introduced already at the stage of polymerization forming in situ polymer complex, which is then subjected to reduction [217, 218].

A special interest in development of nanocomposite materials is drawn to microgels with a response to internal actions (of pH, temperature, ionic force, etc.) [219–221]. Most often used temperature sensitive component in metal/microgel

Table 2.9 Polymers with a response to temperature obtained by RAFT polymerization [222]

Polymer	The response	T °C
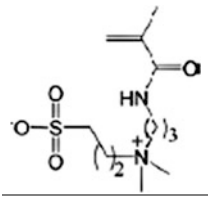	UCST	12
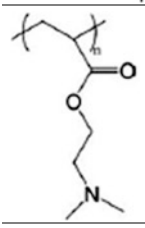	LCST	50
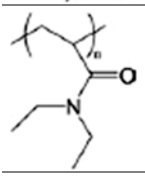	LCST	26–35
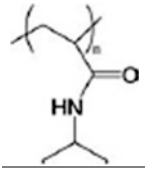	LCST	32
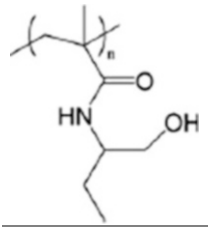	LCST	30

Note. *RAFT* is the reversible addition fragmentation chain transfer, *UCST* is upper critical solution temperature, *LCST* is low critical solution temperature

nanocomposites is poly(N-iso-propyl-acrylamide) (PNIPAAm). The temperature of phase transition, so called (the lower critical solution temperature) (LCST) of PNIPAAm is 32–34 °C, and it can be finely regulated during co-polymerization with other monomers (Table 2.9) [222]. In these microgels such monomers as acrylic acid [223], methacrylic acid [224], acrylic acid-2-hydroxy ethyl acrylate [225], 2-amino ethyl acrylate [226], etc. are used as active centers to bind metal ions. Hybrid Ag/poly[N-iso-propyl-acrylamide-(maleate carboxymethyl chitosan)] nanocomposite was obtained by reduction of silver salt with $NaBH_4$ in the microgel medium (Fig. 2.27) [227]

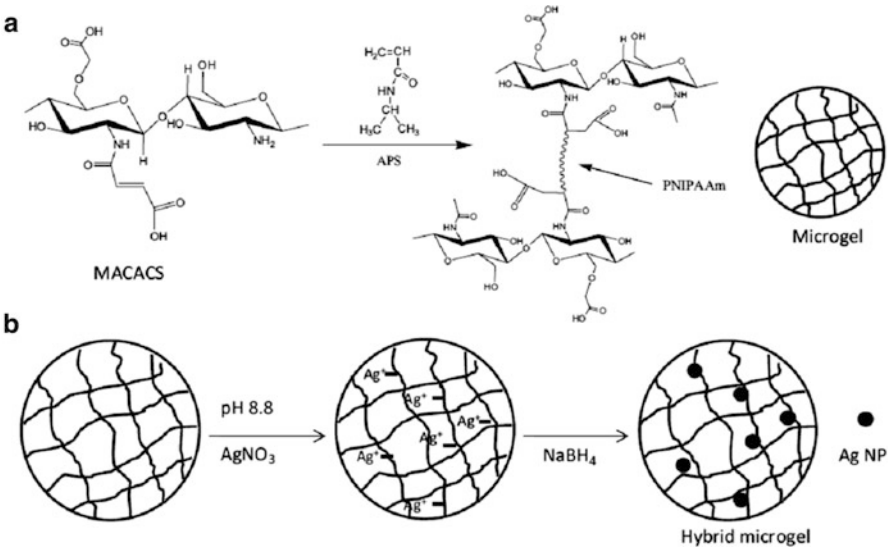

Fig. 2.27 Schematic representation of the synthesis of PNIPAAm/MACACS microgels (**a**), which were used as microreactors for the in situ preparation of Ag nanoparticles (**b**) [227]

The obtained particles are stable in wide range of pH (2–10) and temperature (15–50 °C). Hybrid nanocomposites with silver nanoparticles have the same LCST as the initial polymer microgel (Fig. 2.28).

The temperatures of phase transition of a hybrid nanocomposite were 32 and 35 °C at pH 3 и 8, respectively. For the Pt/poly[(vinylamine)-*co*-(*N*-vinylisobutyramide)] the temperature of flaking was by 0.2–1.6 °C lower than LSTC of the initial copolymer and the difference grows with increase in content of vinylamine comonomer [228]:

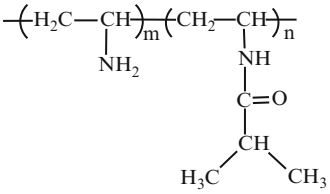

m = 4.1, 8.3, and 19.8 mol %

It should be noted that due to formation of a strong complex of Pt with the polymer chain, strong reducing agent, sodium borohydride, not alcohol, is used for its reduction:

$$H_2PtCl_6 + 6NaBH_4 + 18H_2O \rightarrow Pt_0 + 6NaCl + 6H_3BO_3 + 22H_2 \qquad (2.12)$$

Particularly, formation of the complex, not of colloid platinum was observed in the poly(ethyleneimine) and H_2PtCl_6 system in the ethanol/water mixture [229].

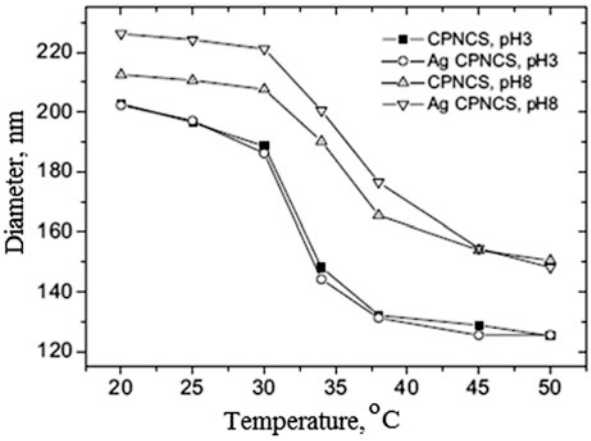

Fig. 2.28 Temperature dependence of the hydrodynamic diameters of the poly[*N*-isopropylacrylamide-(maleated carboxymethylchitosan)] microgels with and without Ag nanoparticles at pH = 3 and 8 [227]

The promising materials for template matrices used for synthesis of nanoparticles, with widespread abilities for regulation of functionality, porosity, ion-exchanging capacity, are ion-exchange resins [230, 231]. A considerable importance has their commercial availability. Usually they are produced as two physical structures: gels and microporous structures. The gels are homogeneous, have no discrete pores, whose function play channels; the microporous resins are characterized by presence of fixed pores. Strong acid resins (gels) are functioned by sulfonic acid groups, while weak acid resins (macroporous) contain carboxylic groups:

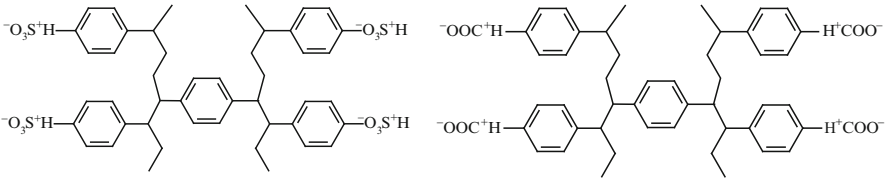

Presence of functional groups in a polymer matrix makes it possible to bind them with metal cations by ion-exchange mechanism and then reduce as, for example, during production of Ni(0)-containing nanocomposites [232] by the following scheme (Scheme 2.6):

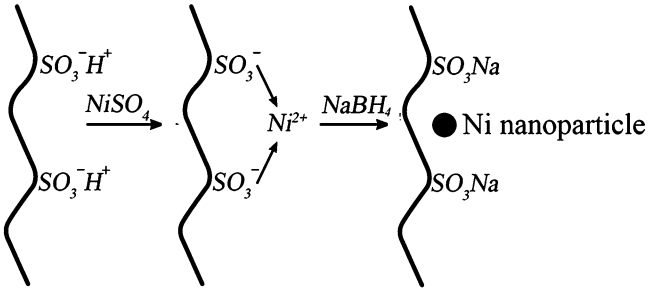

Scheme 2.6 Ion-exchange mechanism of the Ni(0)-nanoparticles formation

Table 2.10 Pd content and loading efficiency for the different prepared nanocomposites [233]

Matrix	Pd loads	Pd content, meq/g	Loading efficiency, %
Sulphonated polyethersulphone with Cardo group	1	0.31 ± 0.02	70.5 ± 0.1
Blend membranes	1	0.08 ± 0.01	30.8 ± 0.1
Blend membranes	2	0.16 ± 0.01	61.5 ± 0.1
Nafion	1	0.53 ± 0.04	48.2 ± 0.1

Redox-process can be described by the following reactions:

$$2Ni^{2+} + 4BH^{4-} + 9\,H_2O \rightarrow\ Ni_2B + 12\,H_2 + 3B\,(OH)_3 \qquad (2.13)$$

$$4Ni_2B + 3O_2\ \rightarrow\ 8Ni + 2B_2O_3 \qquad (2.14)$$

It should be noted that average sizes (19 nm) of nickel nanoparticles in strong acid gels are smaller than in the respective macroporous resins (about 40 nm), probably, it is caused by agglomeration of nanoparticles in pores, whose sizes vary in the range 60–70 nm. Repeated loading and reduction cycles provide achievement of content of magnetic active phase in a nanocomposite up to 21 % (gel) and 16 % (microporous resin). The fact that the origin of a polymer membrane plays a crucial role in the loading-reduction cycles is confirmed by the data on concentration of Pd nanoparticles in catalytic membranes (Table 2.10) [233].

2.2.3.7 Polyelectrolites (Polymeric "Brushes")

In the recent years a great interest is attracted to the polymer systems called polymeric brushes [234]. The polymeric brush is a monolayer of polymeric chains bound to some surface by end groups. There are several ways of fabrication of polymeric brushes: chemical, when the end groups are grafted to a surface by a chemical bond, another one is based on ability of polymer molecules to self-organization due to in- and intermolecular interactions [235]. Covalent bonding can be realized in two ways: "grafting to" and "grafting from" technique. In the first case the end functional group of a polymer chain under some conditions settles on the grafted surface. However, this way has some limitations caused by low density of grafting and thickness of the formed polymeric film, through which the polymer molecules should diffuse to reaction places of setting. Therefore the "grafting from" way is preferable. This approach is based on development of a surface-immobilized layer of initializing agent and the following in situ polymerization with generation of the polymeric brush. Thick polymeric films form which are bound by covalent bonds to a substrate with high density of grafting. In this method a convenient way of polymerization is atom-transfer radical polymerization (ATRP) [236–240]. The main advance of the controlled radical polymerization for creation of polymeric

brushes is a possibility of a brush thickness control, narrow molecular –weight distribution, and a possibility of synthesis of block-copolymers during re-inducing of the end sleeping chains, etc.

Two-component copolymers of this structure can serve as polymeric carriers for metal nanoparticles. For example, core-shell polymeric brushes of cylindrical or spherical structure are used in synthesis of Ag [147], Au [241, 242], CdS [243], Pd and Pt [242], Au and Pt [244] nanoparticles. The general scheme of production of nanoparticles looks as follows (Scheme 2.7):

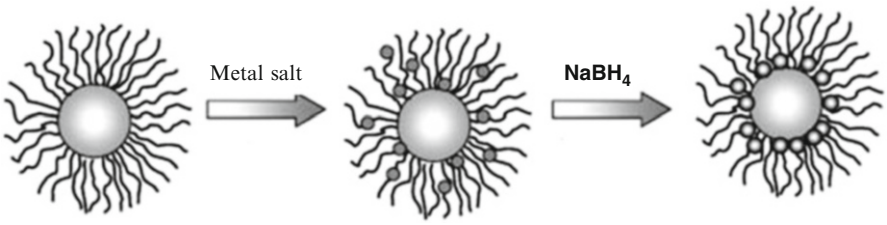

Scheme 2.7 A general scheme of template synthesis of nanoparticles in polymer brushes

As a rule, polymer "brushes" form close-packed grafted chains on a surface of a polymer core, so that the total contour length of the grafted chain far exceeds average distance between them on the surface, as it is, for example, typical of a polyelectrolytic copolymer poly(styrene)-g- poly(2-methylpropenoxyethyl trimethyl ammonium chloride) [242]:

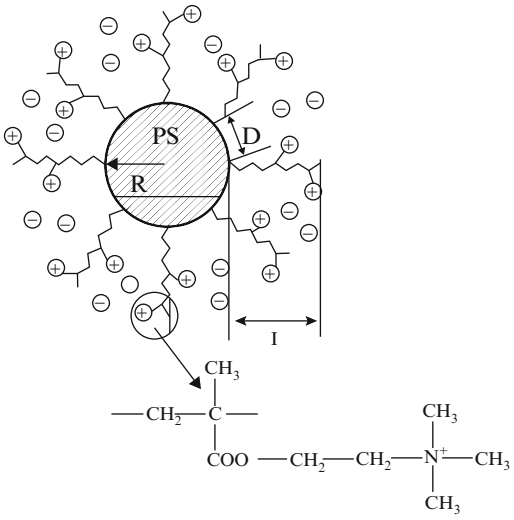

Advantage of this approach is that reduction of a precursor and formation of nanoparticles take place in the polymeric layer.

Multilayer thin films of polyelectrolytes are widely used as nanoreactors in synthesis of metal (Ag, Ni, Pd, Cu) and semiconductor (PbS) nanoparticles [225, 245–248]. A special interest is in polyelectrolytic polymeric brushes shaped as films with response to external actions, so called "smart surface coatings" [249]. Hybrid inorganic/polyelectrolytic brush complexes Si/SiO_2//PS-*b*-PAA-(Ag^+) и Si/SiO2//PS-*b*-PAA(Pd^{2+}) are obtained by the Scheme 2.8 with fixation of the initializing agent on a silicon surface at the first stage with the following synthesis of Si/SiO_2/polystyrene of the polymeric brush with settling by ATRP method of the second bi-block component, *tert*-butyl acrylate, which is subjected to acid hydrolysis with transformation into acrylic acid functional group. Interaction of the obtained polyelectrolytic brush with a metal salt causes condensation of the latter in the layer of blocked polyacrylic acid and formation of the required complex, which is reduced to metal nanoparticles in presence of H_2 (2 atm) at 120 °C during 48 h [250]. It is interesting that content of silver in the nanocomposite was 4.9 %, which corresponded to 87 % of the loaded block of polyacrylic acid (PAA).

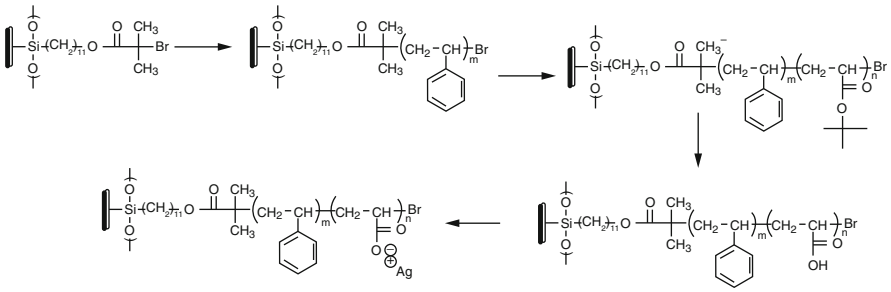

Scheme 2.8 Synthesis of the Si/SiO_2//PS-*b*-PAA(Ag+) brush on a silicon substrate [250]

Polymeric brushes of the considered type response to stimulating external action, i.e. pH of a matter and low molecular electrolyte (NaCl, $CaCl_2$) (Fig. 2.29).

As pH increases from 2 to 10, thickness of a polymeric brush increases from 16 to 26 nm. Increase in size of the polymeric brush at addition of a base is appearance of well-known polyelectrolyte effect. As far as the acid groups along the polymeric chain become deprotonated like carriers causing Coulomb repulsion and, therefore, compelling the polymer to take extended conformation, which causes increase in the brush thickness. On the contrary, with addition of electrolyte, as was expected, thickness of the polymeric layer decreases from 22 to 17 nm with increase in [NaCl] concentration, and increases from 24 to 20 nm with increasing of [$CaCl_2$] concentration.

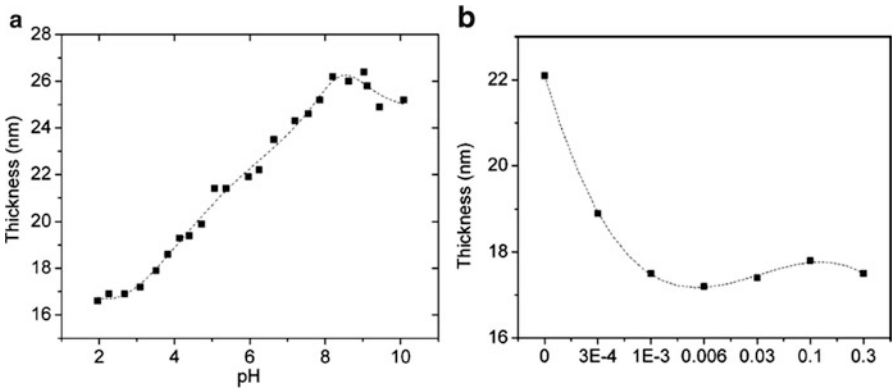

Fig. 2.29 The dependence of the polymer brush thickness of a Si/SiO2//poly(acrylic acid) brush on the solution pH (**a**) and on the concentration of NaCl (**b**) [250]

2.2.3.8 Polyethylene Glycols

Polyethylene glycols are widely used in synthesis of nanocomposites, especially for obtaining of water-solved and biocompatible systems due to complex of valuable properties, such as resistance to oxidation, effect of acids, and bases, moderate thermal stability, etc. Polyethylene glycols have good solvating characteristics and complex forming with respect to many metals [251]. In the literature also special term "PEGylation" is used, which means absorption or coating of the surface of nanoparticle with polyethylene glycol molecules via surface absorption, covalent bond, capture, etc. [252, 253]. It is important preserved by PEG or its copolymers gain not only water-soluble or biocompatible properties, they also become "invisible" for protective systems of organism, thus widening capacities of biomedical application of the nanocomposites [253–255].

Polyethylene glycols are widely used as structurally-oriented templates in synthesis of inorganic nanoparticles with various morphology and sizes [256, 257]. In the PEG media nanoparticles of gold, silver [258] and antimony [259] are obtained. Functional possibilities of polyethylene glycols can be considerably broadened in the case of grafted copolymers based on PEG, such as polyethylene imines [260], PMMA [261], polyamidoamines (PAMAM) [262]. PEGylated nanostructures and their biomedical application (see Chap. 7) are described in detail in the recent review [252].

2.2.3.9 Organo-element Polymers

Element-organic polymers are rarely used as stabilizing ligands in synthesis of nanoparticles. It has been shown that though poly(vinylene arsine) and the

polymers obtained via radical co-polymerization of phenyl acetylene with hexaphenyl-cyclohexa-arsine by the Scheme 2.9:

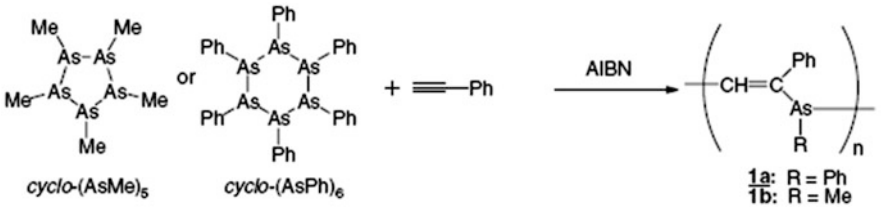

Scheme 2.9 Synthesis of organo-element polymers based on arsenium

favors formation of colloid silver particles, but to the end of several hours there is increase in particle size and its aggregation, the weaker stabilizing agent is phenyl derivative, probably, due to spatial limitations [263].

Combination of simultaneous reduction of a metal ion and formation of a cross-linked polymer in situ under UV irradiation and the following heat treatment at 120 °C of epoxy resin containing silver tri-fluorine acetate provides production of one-, two- and three-dimensional nanostructures [264].

2.2.3.10 Polymeric Microspheres

One of the interests in polymer microspheres is caused by a possibility of metal nanoparticles settling on their surface, which provides substantial accessibility of active centers in the nanoparticles to reagents, for example, in catalytic reactions and, thus, it enhances efficiency of catalysts based on them. Nanoparticles, as a rule, are strongly bound to a microsphere surface and cannot be removed either during severe mixing, or during ultrasonic treatment. Various types of polymers are used as such carriers, for example, microspheres of amino-functioned polystyrene [265], polystyrene-co-poly(N-iso-propylacrylamide) [266], poly(styrene-co-4- vinylpyridine) [267], microspheres with a grafted layer of polyelectrolyte [220, 268, 269]. To immobilize nanoparticles also polymeric ion liquids are applied, first of all, due to their high ability to ion exchange [270, 271] (Fig. 2.30).

Formation of highly dense and well-dispersed Pt nanoparticles [272] (diameter about 2 nm) is defined by low values of interphase tension of imidazole groups on the surface of a microsphere, which causes efficient nucleation in parallel with low rates of Ostwald ripening [273].

2.2.4 Polymers as Reducing Agents and Templates

Very attractive are the methods when a stabilizing polymeric ligand is simultaneously a reducing agent. The advantages of this method are obvious. This is displacement of

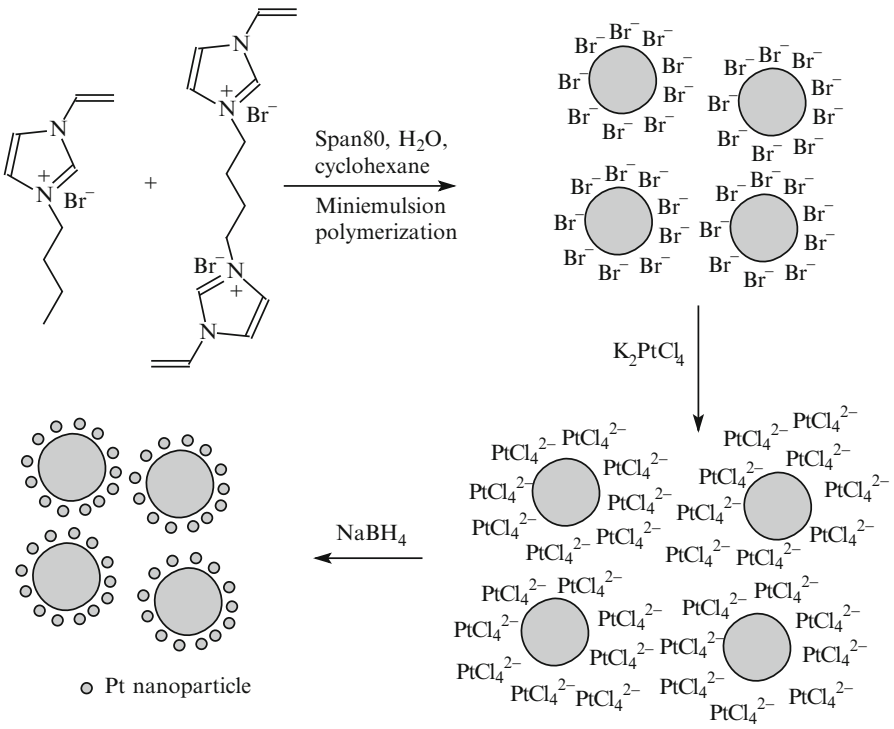

Fig. 2.30 Reaction scheme for the preparation of Pt/poly(1-butyl-3-vinylimidazolium bromide) microspheres [271]

toxic reducing agents, lower expenses, higher efficiency, etc. Most often for these purposes are used polymers whose molecules contain a great number of different functional groups (polysaccharides [274], humic substances, peptides, etc.).

2.2.4.1 Oxygen-Containing Reducing Centers

Representative in this view are cellulose derivatives [275, 276], methyl hydroxyethylcellulose (MHEC), hydroxymethylpropylcellulose, carboxymethylcellulose (CMC). Studies of the mechanism of these process in the system gold-chloride-hydrogen acid- MHEC or its anion derivative CMC [277] point to participation of primary hydroxyl groups in reduction of gold ions, and the formed carboxylic groups interact in some way with the surface of formed microparticles, thus stabilizing them. Dual origin of CMC is demonstrated also for in situ production of Au nanoribbons [278]. It should be noted that formation of intermediate alcohol molecules is associated with self-regulated reduction properties of long chained acryl sulfates [278]:

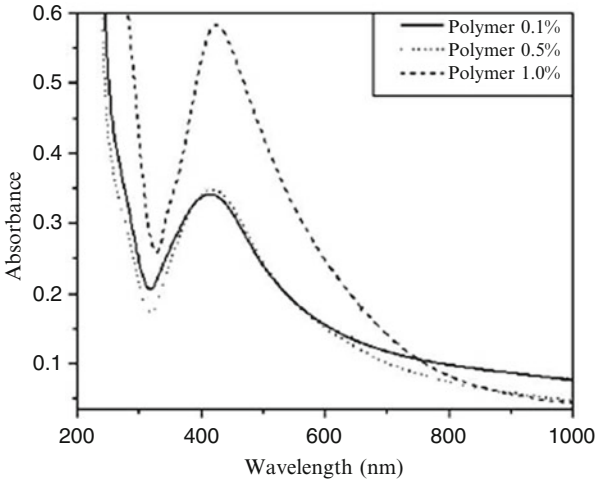

Fig. 2.31 UV-vis spectra of colloidal Ag nanoparticles at a varying concentration of PVM/MA. $[AgNO_3] = 10^{-4}$ M [279]

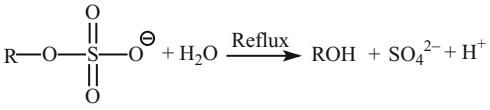

$$R_nOH + M^{2+} + H_2O \rightarrow R_{n-1}COOH + M^0 + 2H^+$$

Reduction ability in the system changes in the range C8 > C10 > C12 > C14 and diameter of the particles decreases as the length of alkyl chain increases.

Reducing character of action of the polymer in the reaction mixture poly(methyl vinylic ether-co-maleic anhydride) (PVM-MA)-$AgNO_3$ points to accumulation of Ag nanoparticles with increase in the copolymer concentration (Fig. 2.31), whereas average diameter stays unchanged [279].

Role of the reducing agent in these systems plays -OCH_3 groups of PVM/MA [280] (Scheme 2.10):

Amphiphilic polyethers are products of polycondensation of sebacic acid and polyethyleneglycol (Mw = 9,200 g/mol and 22,600 g/mol) consisting of alternative hydrophilic and hydrophobic links:

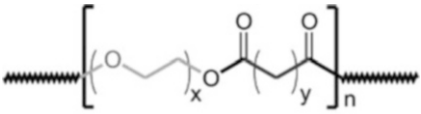

were used as nanoreactors and reducing agents for synthesis of Ag, Au, Pd nanoparticles in benzene or water media [281, 282]. It is known that pseudo-crown-etheric structures PEG can bind and reduce metal ions [258, 283]. In principle, formation of amphiphilic copolymer and metal nanoparticles can be performed simultaneously. Thus, reaction of co-polymerization of urethane

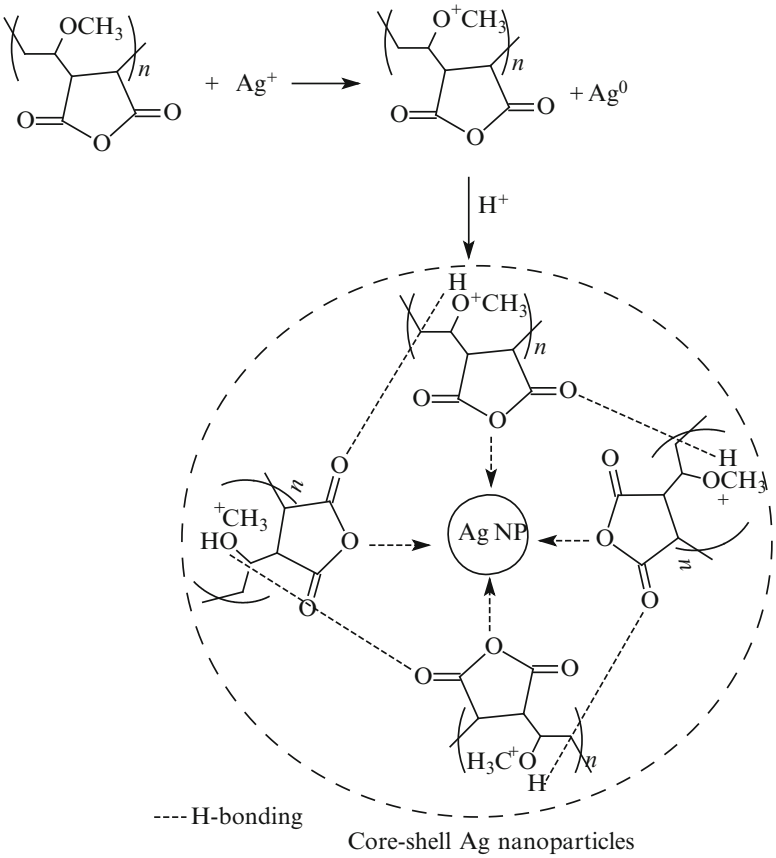

Scheme 2.10 Reduction of Ag^+ by CH_3O-groups of copolymer chain

acrylate oligomer based on poly(propylenoxide)triole, 2,4-toluene-di-iso-cianite, 2-hydroxyethylmethacrylate and polyethylene glycol with styrene in presence of silver nitrate causes formation of polymer nanocomposite film, containing silver nanoparticles [284]. Reduction of metal ion goes with participation of primary or growing radicals in polymerizing system by the scheme:

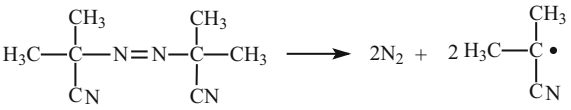

(2.15)

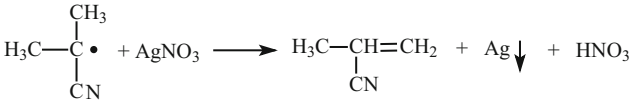

(2.16)

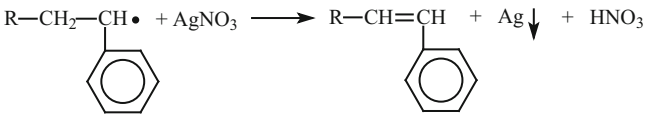

(2.17)

It should noted that similar reactions take place in oxidizing-reducing initializing or radical reduction of metal ions [285, 286], including reactions of intermolecular chain breakage [287, 288]:

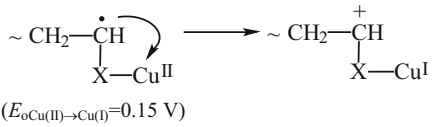

($E_{oCu(II)\rightarrow Cu(I)}$=0.15 V) (2.18)

Mechanism of one-electron reduction is realized in many systems [289, 290]. In general form it can include (i) interaction of cations of metals with labile hydrogen atom with formation of a macroradical; (ii) generation of proton; (iii) reduction of metal ions. In this case protonation of acrylamide with $HAuCl_4$ causes formation of a complex and facilitates electron transport to the amino-group and reduction of the metal ion in the polymerizing acrylamide and N, N-methylene-bis-acryl-amide system [291]. Usually hydroxyl or carbonyl groups form as a result of one-electron oxidation of a polymer chain.

A polymer cross linked hydro gel poly(acrylamide)/poly(N-hydroxymethyl) acrylamide (PAAm-PHMAAm) contains hydroxymethyl fragment –CH_2–OH with labile hydrogen atom, which can be easily removed with formation of macroradicals and the following reduction of a metal ion in the PAAm-PHMAAm/$[Ag(NH_3)_2]NO_3$ [292]:

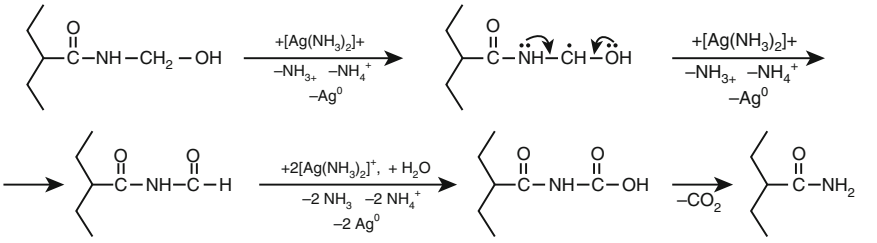

(2.19)

Due to ammonia molecules the reaction medium remains alkaline, Ag^+ cations gain electron from the macroradical and reduces to silver atom. The macroradical generates H^+ proton and two oxygen electrons form C=O double bond (aldehyde group), then aldehyde groups oxidize to carboxyl group.

2.2.4.2 Nitrogen-Containing Reduction Centers

Double function of the reducing agent and stabilizing ligand is typical of many amino compounds. Simple amines, amino acids, polymers with functional amino groups are widely used, for example, in production of Au nanoparticles [293–297], the oleylamine-paraffin hydrocarbon is efficient in synthesis of monodisperse silver particles [298].

Usage of dendrimer polymers with functional amino groups allows avoiding side products. Their structure and chemical properties can be controlled by modification of a core, type and a number of branching, and by terminal functional groups (Scheme 2.11) [149, 299, 300]:

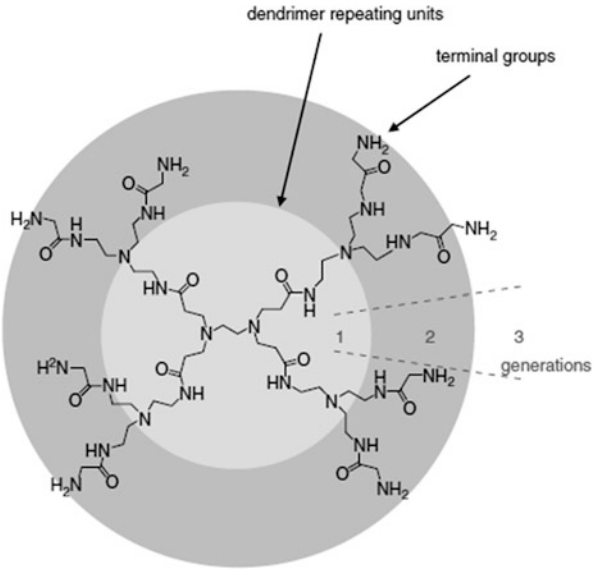

Scheme 2.11 Representation of generational structure PAMAM dendrimer

It is assumed that under conditions of UV radiation during reduction of $AgNO_3$ solution with poly(amidoamine) (PAMAM) electrons transfer from the primary amino groups to metal ions encapsulated in the dendrimer cavity [301]. At the same time mechanistic studies of similar systems confirm that, first of all, tertiary amines of dendrimers, rather than primary or secondary aminogroups play the role of the reducing agents, despite their lower basicity (pKa of the primary and tertiary amines is 9.23 and 6.30, respectively, for the PAMAM dendrimers [302]). A tendency of dendrimer molecules to association is very important [303–306]. Owing to ability of terminal PAMAM amino groups to formation of great aggregates as compared to dendrimer molecules with end COOH-groups, in the first case a polymer molecule contains inner homogeneous in shape cavities, which appears in spherical or nanoprismatic or nanohexagonal silver nanoparticles, respectively [307] (Scheme 2.12):

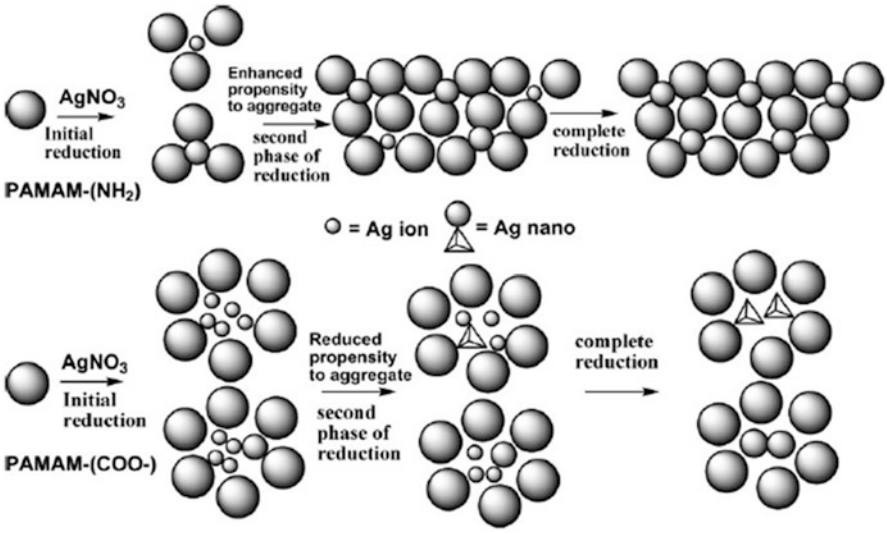

Scheme 2.12 The effect of the peripheral groups in PAMAM dendrimers on the size and shape of the metal nanoparticle

This behavior reflects in kinetic growth of nanoparticles (Fig. 2.32).

It should be noted that under comparable conditions sizes of nanoparticles and Pt clusters reduced by poly(N-vinyl-2-pyrrolidone) are lower than when using additional reducing agent HCHO formaldehyde [308]. It is assumed that metal ions bound in complex with a polymer chain are subjected to reduction, in this case size of a nanoparticle is limited by space confined to local PVP chain containing metal ion (Scheme 2.13):

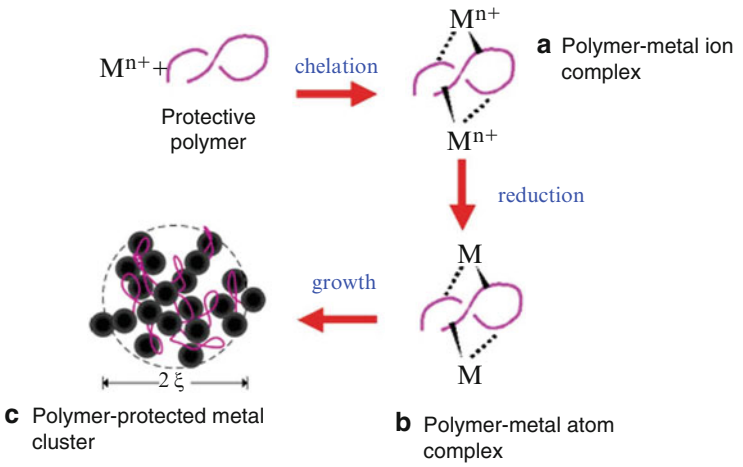

Scheme 2.13 A route for the formation of the polymer–metal complex and nanocomposite

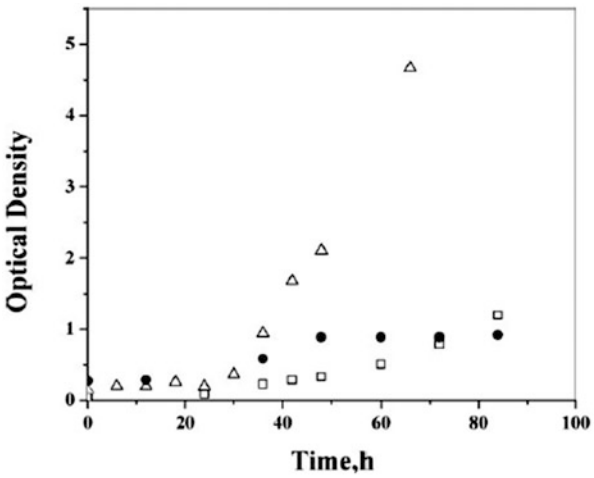

Fig. 2.32 Optical density versus time plot for the formation of silver nanoparticles in amine (Δ)-, hydroxy (•)-, and carboxylate (□) terminated PAMAM dendrimers. ($AgNO_3$ $15 \cdot 10^{-3}$ M, PAMAM $0.20 \cdot 10^{-3}$ M) [307]

It is assumed that particularly electrons of pyrrolidone nitrogen are responsible for reduction of metal ion, which points to appearance of a new C-N band near 1,667 cm^{-1} in FTIR spectrum of Ag^0-poly(N-vinyl-pyrrolidone) [309]. The examples of usage of poly(N-vinyl-pyrrolidone) simultaneously as reducing and stabilizing agent are not uncommon [79, 310–312].

An interesting is the approach in which low molecular reducing agent is chemically bound with polymer via polymer-analogous reaction. This technique is used for metallization of granules of the ternary copolymer of glycidyl methacrylate, methyl methacrylate, and divinylbenzene [313]. At the first stage polymer-fixed hydrazine with concentration of the functional group 2.3 mmol/g is obtained, at the second stage metal ions are reduced from their salt solutions:

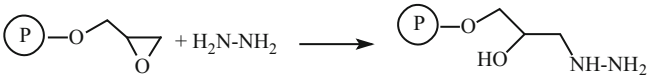

(2.20)

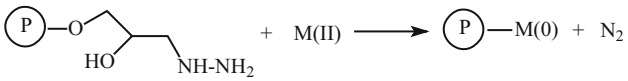

(2.21)

M = Ni, Cu, Ag

These examples can be shown also for inorganic polymer matrices. For example, surface of silica gel can be especially chemically modified by functional groups having reduction properties. Thus, silica gel with grafted silicon-hydride groups occurred very efficient at production of Au- and Ag- [314] or Pd- [315] containing nanocomposites:

$$\equiv \mathrm{SiH} + \mathrm{Pd}^{2+} + \mathrm{H_2O} \rightarrow \equiv \mathrm{SiOH} + \mathrm{Pd}^0 + 2\mathrm{H}^+ \qquad (2.22)$$

It may be assumed that many conducting polymers can serve as efficient reducing agents, due to presence in their molecules of potentially easily oxidized centers [316, 317]. Low oxidizing potential of poly(2,5-dimethoxyaniline) (PDMA) [318, 319]:

$$\begin{aligned} &\mathrm{PDMA} \rightleftharpoons \mathrm{PDMA}^{n+} + n\mathrm{e}^-, E_{\mathrm{PDMA}} < 0.4\,\mathrm{V} \\ &\mathrm{Ag}^+ + \mathrm{e}^- \rightarrow \mathrm{Ag}, E_0 = 0.791\,\mathrm{V}\,vs\,\mathrm{NHE} \end{aligned} \tag{2.23}$$

favors reduction of silver ions in PDMA matrix forming in situ in presence of poly (styrene sulfonic acid) [320] by the scheme (Scheme 2.14):

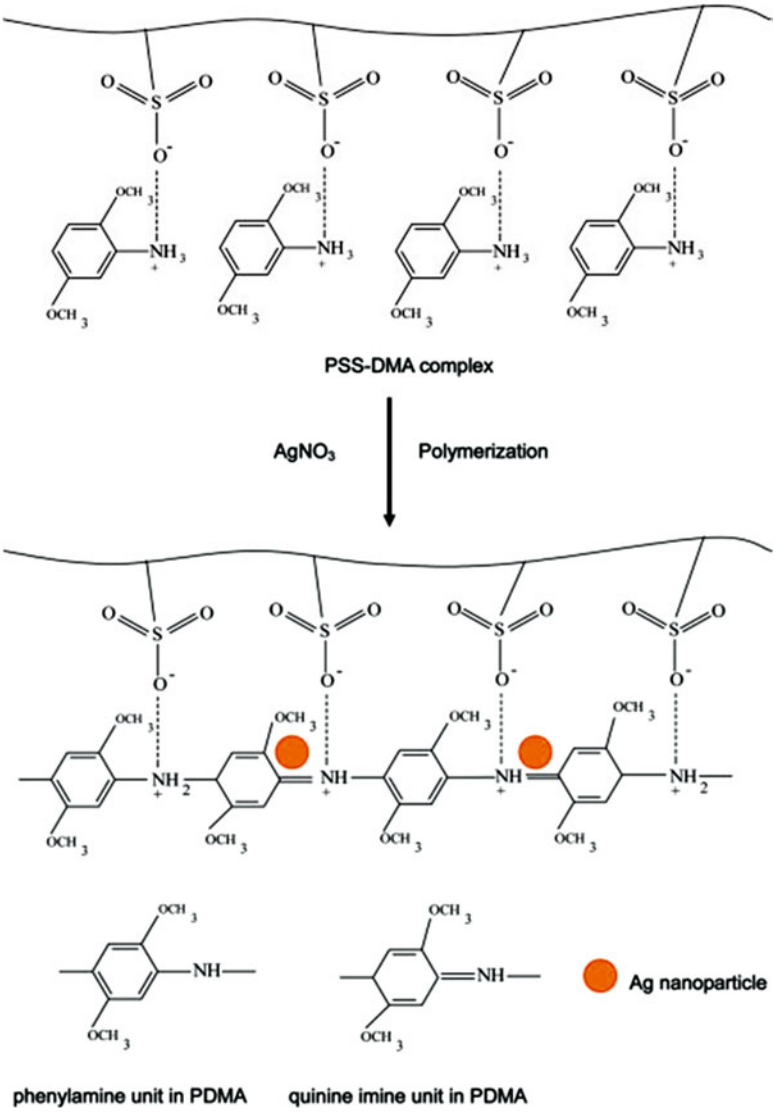

Scheme 2.14 Reduction of metal ions in a matrix of conducting polymer

Ag^+ ions modulate oxidization of DMA with formation of cation-radicals and, respectively, polymerization of molecules of a monomer bound to PSS. The formed PDMA in combination with PSS molecules form a nanoreactor cavity, in which Ag^0 particles localize. Probably, appearance of imine cross-links in the polymer chain is caused by participance of PDMA groups in reduction.

2.2.5 Co-reduction (Bi-metal Nanocomposites)

As shows analysis of soluble synthetic methods, in the case of monometallic systems the process of nucleation and growth can be easily controlled by the reaction conditions: concentration of reagents, molar ratios of precursors and surfactants, temperature, etc. However, in the case of bimetal nanoparticles this becomes a complicated problem, since their kinetic and thermodynamic parameters differ under the same conditions of reactions. In order to avoid separation of the nucleation processes for two metals, it is necessary to choose a suitable reducing agent and reagents.

2.2.5.1 Reduction Agents

Though usage of strong reduction agents, as was repeatedly mentioned, causes an increase in nucleation rates, on the other hand, because of the same reasons, it is more difficult to separate nucleation and growth processes in the case of bimetal substances. For example, co-reduction of $Cu(CH_3COO_2)_2$ и $HAuCl_4$ in presence of $NaBH_4$ at the initial stage causes just formation of Au/Cu aggregates of nanoparticles, and only the following annealing can bring to production of AuCu and $AuCu_3$ intermetallic nanoparticles [321]. Therefore, in these systems also surfactants and polymeric ligands play an important role [322–324]. Poly(vinylpyrrolidone) and poly(2-ethyl-2-oxazoline) are used in these purposes for production of some intermetallic nanocrystals ($FeSn_2$, $CoSn_3$, $NiSn_3$, PdSn) in presence of $NaBH_4$ [325], and for gold intermetallic compounds (Au_3Fe_{1x}, Au_3Co_{1x}, Au_3Ni_{1x}) there is another strong compound *n*-BuLi [326].

However, relatively often to obtain bimetal nanoparticles, weaker reduction agents are used, which provides more efficient control over the nucleation and growth processes [322–324, 327–330]. In some cases a mixture of reduction agents is used, for example, borane tert-butylamine and hexadecanediol in synthesis of Pt_3N nanoparticles [331].

A character of reduction makes it possible to kinetically control the reaction of co-reduction. For example, due to weak reducing ability of poly(vinylpyrrolidone) (PVP), generation and absorption of metal atoms during synthesis of Pd-Pt bimetal nanoparticles is slow, and the formed clusters coalesce easily, which can cause generation of star-like decahedrons and triangle nanoplates [327]. When ethylene glycol is used instead of PVP, the reduction rate increases significantly, fast

reduction causes abrupt increase in supersaturation degree and, consequently, fast growth of seed with formation of a single crystal with distorted octahedral shape. Examples of these reactions can be found in the recent review [332].

2.2.5.2 Redox-Potentials of Reagents

It is known that metals with higher redox-potentials are reduced in the first turn. Just chemical behavior of the second metal after completion of its reduction defines a final structure of an article. If the second metal deposits homogeneously on a surface of a preliminary formed seed, the core-shell structure forms; if a metal deposits on some specific face, heterostructures can be obtained. In the case when atom of the second metal diffuses in the lattice of the first metal, with formation of a metal-metal bond, intermetallic compounds or alloys form. Depending on conditions, dynamically more stable state is preferable. If, for example, two different metals A and B are reduced, and redox-potential of A is higher than that of B, the core-shell structure (A)-(B) forms. However, in presence of a surfactant or a stabilizing ligand, which can bind strongly with A, the inverse type of particles with B core and A shell are more stable.

The effective way of approaching of a relative content of reduced metals in alloy and the respective ions in solution is choice of ligands, providing the closest approach of redox-potentials of complexes containing ions of co-deposited metals. However, equality of redox-potentials of the complexes of various metals does not mean that their ions will be reduced at equal rate. A significant role play kinetic factors, which determine a rate of discharge of different ions under specific conditions, providing co-deposition of metals [51].

An interesting synthetic strategy of production of hollow nanostructures is based on interaction of solution of some metal salt with a solid template of more electrochemically active metal. Typical examples include salts of Au^{3+}, Pt^{2+} и Pd^{2+} and silver nanoparticles or nanowires [333]. The schematic illustration of the experimental procedure of this process is shown in Fig. 2.33.

Due to higher redox-potential of the pair $AuCl_4^-/Au$ (0.99 V, vs SHE) as compared to the pair Ag^+/Ag (0.80 V, vs SHE) silver nanostructures suspended in the solution can be oxidized by $HAuCl_4$ according to the following substitution reaction:

$$3Ag_{(s)} + AuCl_4^-{}_{(aq)} \rightarrow Au_{(s)} + 3Ag^+{}_{(aq)} + 4Cl^-{}_{(aq)} \qquad (2.24)$$

The elemental gold formed in this reaction is localized in immediate vicinity of the template surface. Here its nucleation and growth to small particles goes, and in the end, a thin shell forms around the Ag template. At the initial stage the shell has open structure, because $HAuCl_4$ and AgCl diffuse continuously through a layer until the silver template is consumed completely. At the temperature of reaction 100 °C the Au shell develops crystal structure via the processes of Ostwald ripening. This

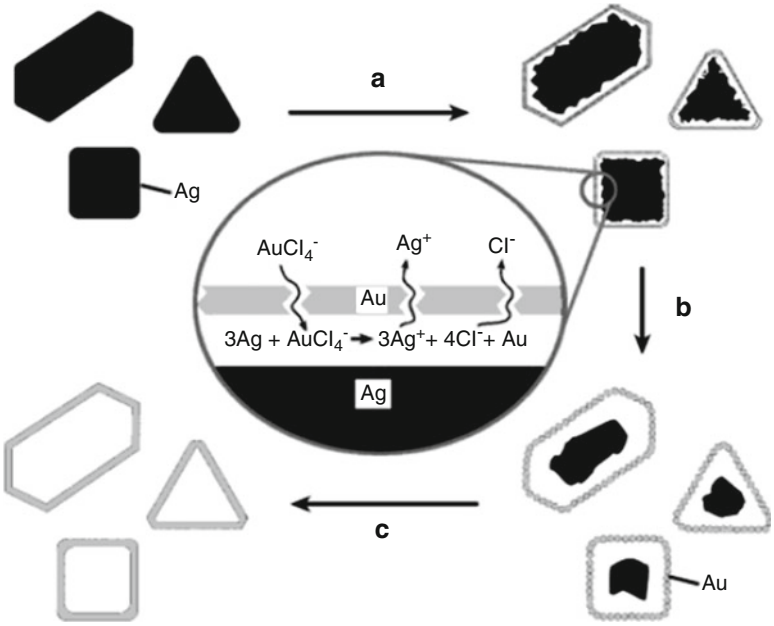

Fig. 2.33 Schematic illustration of production of hollow nanostructures. (**a**, **b**) Addition of $HAuCl_4$ to a dispersion of silver nanoparticles and the replacement reaction; (**c**) Total depletion of a template metal and annealing of the resultant shells [333]

method is used to obtain hollow structures with definite cavity sizes and homogenous high-crystal walls. The main characteristics of these nanostructures are determined by parameters of a template particle. Higher redox-potentials of Pd^{2+}/Pd (0.83 V, vs SHE) и Pt^{2+}/Pt (1.2 V, vs. SHE) pairs make it possible to generate also Pd and Pt hollow nanostructures via interaction of their salts with Ag template:

$$Pd(NO_3)_{2(aq)} + 2Ag_{(s)} \rightarrow Pd_{(s)} + 2AgNO_{3(aq)} \quad (2.25)$$

$$Pt(CH_3COO)_{2(aq)} + 2Ag_{(s)} \rightarrow Pt_{(s)} + 2Ag(CH_3COO)_{(aq)} \quad (2.26)$$

2.2.5.3 Molar Relationship of Metal Precursors

For bimetal nanostructures the couple: content-controlled synthesis is especially important for the dependence of their physical and chemical properties on content. Thus, the surface plasmon resonance of AuAg alloy is finely regulated by molar ratio Au:Ag in the block-copolymer based on 4-VPy and styrene (PS-PVPy) (Fig. 2.34) [334].

As Au content decreases, SPR peak is blue-shifted to the SPR of Ag nanoparticles. Due to the lower reduction rate of Ag^+ as compared to Au^+, fraction of silver can be increased by increase in the reaction time or in concentration of a precursor. $Au_{0.52}Ag_{0.48}$ и $Au_{0.39}Ag_{0.61}$ nanoparticles of the alloys were synthesized

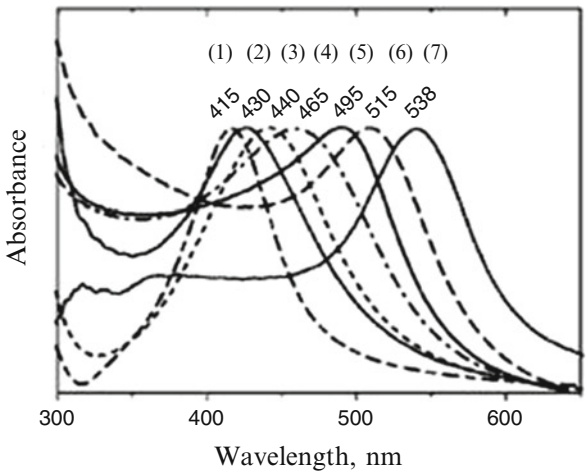

Fig. 2.34 UV-vis absorption spectra of nanocomposites PS-b-PVPy/Ag (1), PS-b-PVPy/AuAg in molar ratio Au:Ag: 1:3(2), 1:2 (3), 1:1(4), 2:1 (5), 3:1(6) and PS-b-PVPy/Au (7) [334]

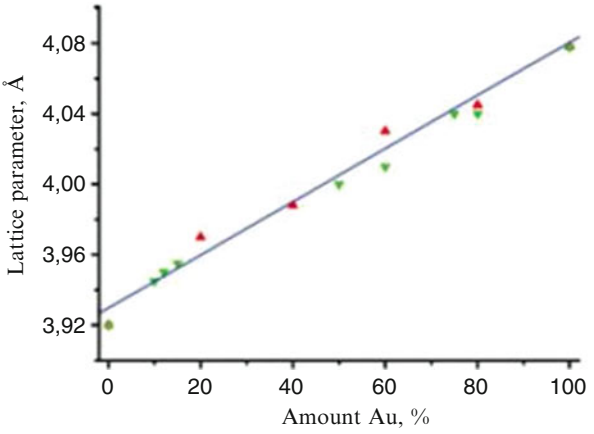

Fig. 2.35 Plot of the lattice parameter dependence on the composition of the alloy particle [244]

during co-reduction of $AgNO_3$ и $HAuCl_4$ (molar ratio 20:1) at 120 °C during 1 and 2 h, respectively [335]. Formation of homogeneous solid solutions was found for the binary system of Au-Pt nanoparticles in the surface polyelectrolyte layer of the polymeric brushes consisting of poly(2-aminoethylmethacrylate hydrochloride) chain [244], which was confirmed by linear dependence of the unit cell parameter of the crystal lattice on Au concentration in the nanocomposite (Fig. 2.35).

Thus, the chemical reduction of metal ions in aqueous and non-aqueous medium in the presence of polymers which can serve both as a stabilizing matrix and/or a reducing agent is one of the preferred synthetic condensation strategies for preparing a wide variety of nanocomposites. According to the classical scheme, reduction of metal-containing precursors (metal salts, monomer and polymer complexes, organometallic compounds, etc.) includes a number of successive transformations: metal atoms → cluster → colloid particle. Usage of strong reduction agents such as borohydrides, aminoboranes, etc. results in the formation of fine, and to a certain degree,

monodisperse particles. Meanwhile, more weak reduction agents (citrates, ascorbic acid, alcohols, etc.) are responsible to the lower reduction rates and more narrow particle size distribution. Namely, solution methods of chemical reduction allow using the multiple parameters to control the composition and size of nanoparticles, their shape and dispersity as well as their stability. A crucial point is to reveal the interconnection between main physicochemical parameters: size/shape-function. Systematic studies in this direction are very wide [336–340]. Thus, monodisperse Rh nanocrystals with different shapes were obtained by one-step polyol synthesis owing to adjusting the reaction conditions as temperature, $Rh(acac)_3$ precursor concentration, inert or oxidizing atmosphere, and reaction time (Scheme 2.15) [341]:

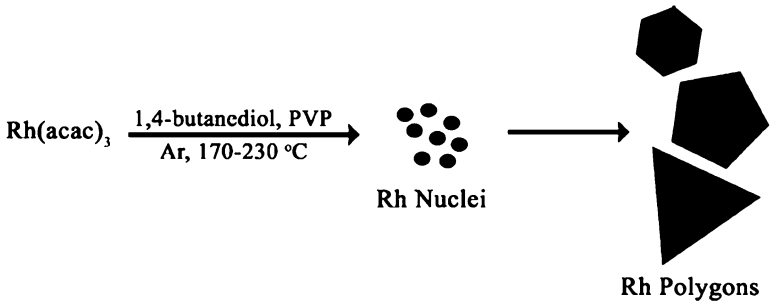

Scheme 2.15 Schematic illustration of one-step polyol synthesis of monodisperse well-shaped Rh nanocrystals

Two-dimensional projects of the nanocrystals are polygons, dominated by hexagons, pentagons (>45 %), and triangles with catalytically active (111) surfaces.

Some characteristics of reaction conditions, composition and sizes of dispersive phases of nanocomposites synthesized by chemical reduction are given in Table 2.11.

2.3 Electrochemical Reduction

Advantages of the electrochemical method of production of nanostructural materials are relative simplicity of the method, high reaction yields, as a rule, absence of side products of reaction. Several approaches to production of these materials are known.

2.3.1 Electrochemical Deposition

This method is based on the reactions of electrochemical deposition of nanoparticles on various surfaces, including polymer templates [342], graphite or carbon substrates, [343, 344], etc. Nanoporous materials used for templates are etched polymers, anodized aluminum oxide, etc. [345–347]. Electrochemical

Table 2.11 Synthesis and characterization of nanocomposites obtained by chemical reduction in polymer matrices

Nanoparticles	Diameter, nm	Reduction agent	Stabilizing agent	The reaction conditions	References
Reduction in polymer matrix in statu nascendi					
Cu, $Cu@Cu_2O$	48.2 ± 7.8	Hydrazine hydrate (0.1 M)	PVPdn (MW 360 000)	60 °C, DMF, $Cu(OAc)_2 \cdot H_2O$	[38]
Cu	30–50	$N_2H_4 \cdot H_2O$ solution; 78–82 %	(PAA; Mw = 1,800)	60 °C, water, pH = 9.2–11, $CuSO_4$	[141]
Ag	20–25	NaOH, 5 wt.%	Poly(AAm-*co*-N,N-methylene-bis-acrylamide)	Water, room temperature	[217]
Pd	2.4 ± 0.7–5.2 ± 1.1	H_2 (0.4 MPa)	Dendrite polymers with perfluorine-, perfluorineoligoether-, polysiloxane-, alkyl- and oligoethylene glycole groups	Pd acetylacetonate, CO_2 100 °C, 90 min	[171]
Au	1.25	$NaBH_4$	Polystyrene-gr-poly(2-methylpropeonyloxyethyl)trimethylammonium chloride	$AuCl_4^{2-}$	[242]
Pt	2.1	The same	The same	$PtCl_6^{2-}$	[242]
Pd	2.4	The same	The same	$PdCl_4^{2-}$	[242]
Ag	7.5	$NaBH_4$	PS- N,N-diethyldithiocarbamate-gr-(polymethacrylic acid-b-PMMA)	([$AgNO_3$]/[COO] - 1.2 mol/mol), ([$NaBH_4$]/[Ag]- 2.0 mol/mol), THF, 258 °C	[147]
Pt	2.1 ± 0.2	$NaBH_4$	Poly(1-butyl-3-vinylimidazolium bromide), poly(N-vinyl-2-pyrrolidone) (PVP, Mn =55,000)	K_2PtCl_4, room temperature, 1 h	[271]
Ag	1–3	H_2, 60 °C, 2 MPa	Chitosan Mv = 140 kDa, deacetylation degree 98 %	Silver 1,5-cyclooctadiene -, 1,1,5,5,5-hexafluoroacetylacetonate, CO_2	[172]
Cu	1–40	H_2, 125 °C, 2 MPa	Chitosan Mv = 140 kDa, deacetylation degree 98 %	Cu 1,1,1,5,5,5- hexafluoroacetylacetonate hydrate, CO_2	[172]

Ag		Hydrazine hydrate ($2 \cdot 10^{-2}$ M)	PMMA	Silver oxide ammonium solution ($10^{-2} - 10^{-4}$ M), 1,2-dichloroethane	[162]
Ag	5–35	UV ($\lambda = 320$ nm)	PHEMA	Silver oxide ammonium solution ($10^{-2} - 10^{-4}$ M), 11,2-dichloroethane, 2-hydroxyethylmethacrylate	[162]
Ag	~20	Ethanol	Poly(vinylpyrrolidone)	$AgNO_3$, 76–79 °C	[146]
Au	2.5 ± 0.2,	Non-aqueous N_2H_4 (0.02 vol.%)	$(PS_{25}$-b-$P4VP_{17})_4$	0.5 eq. $HAuCl_4 \cdot 3H_2O$	[194]
	2.4 ± 0.3		$(PS_{25}$- b -$P4VP_{37})_4$	24 h	
	2.0 ± 0.2		$(ПС_{25}$- block -$P4VP_{63})_4$	0.2 mg/mL micelle solution	
Polymer as reducing agent					
Au	~ 5	Acrylamide, sodium sulphite	Copolymer of acrylamide, N,N-methylene-bisacrylamide, sodium sulphite	$HAuCl_4$, 0.25 мМ в воде pH 7.0, 70 °C	[291]
Ag	10–40	Poly(methylvinylether-co-maleic anhydride)	Poly(methylvinylether-co-maleic anhydride)	$AgNO_3$ (10^{-4}–10^{-3} M), water, pH 8–9, NaOH	[279]
Ag	12	Poly(2,5-dimethoxyaniline)	Poly(styrenesulphonic acid)	$AgNO_3$, [Ag]: [monomer] = 2:1 (mol), pH 1.4	[320]
Au	18–40	Carboxymethylcellulose, methylhydroxyethylcellulose	Carboxymethylcellulose, methylhydroxyethylcellulose	$HAuCl_3$ $3H_2O$, pH – 5.7–9.0	[277]
Pt	2	Poly(N-vinyl-2-pyrrolidone), HCHO	Poly(N-vinyl-2-pyrrolidone), (PVP, Mw = 10 000)	$PtCl_4$, pH 12, NaOH	[308]
Ag	8.7–15.4	Poly(acrylo-uretane-*co*-styrene)	Poly(acrylo-uretane-*co*-styrene)	$AgNO_3$ (0.5 wt.-%), 65 °C, 3–4 h	[284]

deposition is performed by deposition of a metal film on one surface of the membrane, which acts as a cathode for galvanic coating. The respective metal ions are then electrochemically reduced and precipitate in pores of a template membrane [348–350]. Sizes and morphology of nanoparticles can be varied by changing parameters of electric precipitation, such as voltage, temperature, precipitating time, and origin of surfactants and polymers [348, 349, 351]. Nanoparticles are extracted from a template by physical-chemical means [352].

Electrochemical synthesis in the etched templates is efficient method of obtaining of multi-segmented nanowires of various metals [351, 353]. Sometimes the processes of chemical reduction in solution and electrochemical deposition are combined. Thus, for example, highly oriented triangle golden nanoparticles on conducting glass surfaces are used [354].

2.3.2 *Direct Electric Reduction of Metal Ions in Electrolyte Solution*

The essence of the method is in direct electric reduction of metal ions in aqua electrolytes [355]. The main difficulty with which one encounters in this case is competition between two opposite processes. On the one hand, it is formation of metal nanoparticles, on the other hand, it is electric precipitation of metal on the cathode surface [356], and the second process usually dominates.

Under conditions of the controlled potential, electric plating of Pt nanoparticles from H_2PtCl_6 water solutions takes place. It is necessary to use a stabilizer (tetraalkylammonium salts) to prevent deposition of particles on the cathode surface [8].

2.3.3 *The Method of Anode Oxidizing Electrolysis*

Reduction is conducted in electrolytic cell, with solution of anode as a metal source. Tetraalkylammonium salts are most often used as electrolyte and stabilizing surfactant. The general scheme of the process includes oxidization of a block metal of anode with formation of metal cations, which migrate to the cathode, where they are reduced to atomic metal. The clusters formed captured by a surfactant form stable colloids [357, 358] (Scheme 2.16).

Scheme 2.16
Electrochemical synthesis of transition metal colloids

$$\text{Anode: } M_{bulk} \rightarrow M^{n+} + ne^-$$

$$\text{Cathode: } M^{n+} + ne^- + \text{stabilizer} \rightarrow M_{colloid}/\text{stabilizer}$$

$$M_{bulk} + \text{stabilizer} \rightarrow M_{colloid}/\text{stabilizer}$$

Growth of the particles is predominantly by the coalescence mechanism of the formed colloid particle with ensembles of the reacting atoms [138].

The main parameters, which allow control over particle size in the electrochemical process, are polarity of medium, current density, space between electrodes, temperature.

2.3.3.1 The Effect of Current Density

It is known that the critical size r_{crit} of a cluster during formation of metal powder on the cathode is found by the equation [359]

$$r_{\text{crit}} = \frac{2M\gamma}{nF\eta\rho} \tag{2.27}$$

where M is molecular weight, γ is surface tension, F is Faraday constant, η is overtension, ρ is density of the cluster, n is valence.

As is seen, r_{crit} in inverse dependence on overtension, and it is directly related to current density: the higher current density, the smaller particles. This tendency was found during production of Pd nanoparticles under action of current 2.16 and 5.41 mA/cm^2, while particle sizes were 2.56 and 1.39 nm, respectively [138]. Moreover, at longer time of electrolysis and lower current density nanoparticles had bimodal distribution, while at high current density the size distribution of particles was narrow. As the current density increases, the reaction yield also increases [360].

2.3.3.2 The Effect of Space Between Electrodes

The effect of space between electrodes is one of the important factors of control over dispersion of particles. Though the reasons are not quite clear, if the space between electrodes was, for example, 5 mm, small particles of constant size formed independently on time of electrolysis, while at the distance 0.75 mm particle sizes were greater and they increased during the reaction (Fig. 2.36) [138].

Probably, the crucial role in this case play transport velocities, and electrophoretic mobility in a system, i.e. parameters which depend directly of a field strength.

Thus, chemical reactions of reduction are the most widespread and available methods of production of nanocomposite materials. A wide range of reducing agents (from vapor compounds such as H_2, CO, etc., hydrides and salts, such as borohydride and sodium citrate, to oxidized solvents such as alcohols and polymer molecules), vast variety of synthetic and natural polymers and surfactants used as matrix and stabilizing media, multivariate control over conditions of the reactions (temperature, molar ratios of reagents, pH of a medium, etc.) provide development of materials with given structures and properties. Kinetic and mechanical studies [361] show that formation of monodisperse nanoparticles conforms with classical mechanisms of nucleation and growth of nanoparticles including fast nucleation

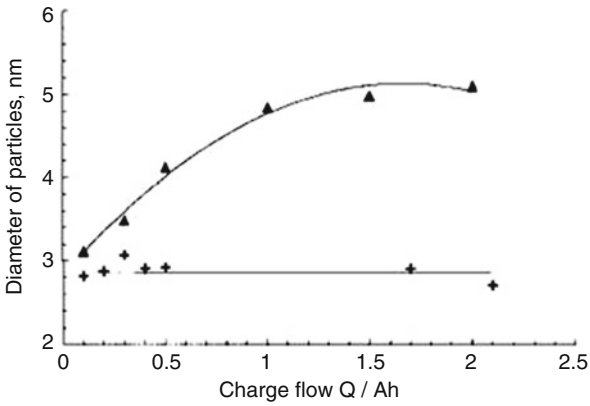

Fig. 2.36 Dependency of particle size of electrochemically prepared $(n\text{-}C_8H_{17})_4N^+Br^-$-stabilized Pd colloids on electrode distance (D_E) at different charge flow Q: $D_E = 0.75$ mm (×), $D_E = 5.0$ mm (▲) ($T = 20$ °C, $I_E = 5.41$ mA cm^{-2}, THF) [138]

with formation of a great amount of nuclei and their growth due to molecular incorporation [362–364]. The problem in the case of aggregation of fine nanocrystallites is described by alternative models, according to which the initial nucleation and growth origin from nanocrystalline aggregates of critical sizes. Growth of nanoparticles is achieved by coalescence of these aggregates, and the formed particles are characterized by polycrystalline structure, bimodal size distribution at the early stages and sigmoid growth kinetics [365–367]. Synthesis of anisotropic particles in solutions often demands deviation from thermodynamically controlled paths of reaction towards kinetically controlled, for example, by decrease in the rate of precursor decomposition or use of a weaker reducing agent, etc. A typical approach to synthesis of anisotropic particles is "seed" method, incorporation of a small amount of earlier prepared seed grains of nanoparticles into solution [368]. It should be noted that though chemical methods allow production of nanoparticles with controlled composition, sizes and homogeneous size distribution, use of organic solvents and hazardous chemical reagents are dangerous for environment. Moreover, target products are often contaminated by traces of reducing agent or intermediate products of reactions. Some of these problems are successfully solved with use of physical-chemical methods of production of nanocomposites.

References

1. M. Niederberger, G. Garnweitner, Chem. Eur. J. **12**, 7282 (2006)
2. S. Iijima, Nature **354**, 56 (1991)
3. C.B. Murray, D.J. Norris, M.G. Bawendi, J. Am. Chem. Soc. **115**, 8706 (1993)
4. X.G. Peng, L. Manna, W.D. Yang, J. Wickham, E. Scher, A. Kadavanich, A.P. Alivisatos, Nature **404**, 59 (2000)
5. C. Burda, X. Chen, R. Narayanan, M.A. El-Sayed, Chem. Rev. **105**, 1025 (2005)
6. Z.R. Dai, Z.W. Pan, Z.L. Wang, Adv. Funct. Mater. **13**, 9 (2003)
7. Y.N. Xia, P.D. Yang, Y.G. Sun, Y.Y. Wu, B. Mayers, B. Gates, Y.D. Yin, F. Kim, Y.Q. Yan, Adv. Mater. **15**, 353 (2003)

8. B.L. Cushing, V.L. Kolesnichenko, C.J. OSConnor, Chem. Rev. **104**, 3893 (2004)
9. T. Dwars, E. Paetzold, G. Oehme, Angew. Chem. Int. Ed. **44**, 7174 (2005)
10. U. Jeong, Y. Wang, M. Ibisate, Y. Xia, Adv. Funct. Mater. **15**, 1907 (2005)
11. J. Park, J. Joo, S.G. Kwon, Y. Jang, T. Hyeon, Angew. Chem. Int. Ed. **46**, 4630 (2007)
12. N. Pinna, M. Niederberger, N. Pinna, M. Niederberger, Angew. Chem. Int. Ed. **47**, 5292 (2008)
13. C. Feldmann, H. Goesmann, Nanoparticulate functional materials. Angew. Chem. Int. Ed. **49**, 1362 (2010)
14. Y. Yin, R.M. Rioux, C.K. Erdonmez, S. Hughes, G.A. Somerjai, A.P. Alivisatos, Science **304**, 711 (2004)
15. P.R. Selvakannan, M. Sastry, Chem. Commun. **1684** (2005)
16. Y.W. Jun, J.S. Choi, J. Cheon, Angew. Chem. Int. Ed. **45**, 3414 (2006)
17. S.E. Skrabalak, J. Chen, L. Au, X. Liu, X. Li, Y. Xia, Adv. Mater. **19**, 3177 (2007)
18. D. Kim, J. Park, K. An, N.K. Yang, J.G. Park, T. Hyeon, J. Am. Chem. Soc. **129**, 5812 (2007)
19. X. Wang, H. Fu, A. Peng, T. Zhai, Y. Ma, F. Yuan, J. Yao, Adv. Mater. **21**, 1636 (2009)
20. A.D. Pomogailo, V.N. Kestelman, *Metallopolymer Nanocomposites* (Springer, Berlin, 2005)
21. C.H. Kuo, M.H. Huang, Langmuir **21**, 2012 (2005)
22. S. Chen, Z.L. Wang, J. Ballato, S.H. Foulger, D.L. Carroll, J. Am. Chem. Soc. **125**, 16186 (2003)
23. J. Turkevich, P.C. Stevenson, P.C.J. Hiller, Discuss. Faraday Soc. **11**, 55 (1951)
24. B.J. Hornstein, R.G. Finke, Chem. Mater. **16**, 139 (2004)
25. A. Cacciuto, S. Auer, D. Frenkel, Nature **428**, 404 (2004)
26. U. Gasser, E.R. Weeks, A. Schofield, P.N. Pusey, D.A. Weitz, Science **292**, 258 (2001)
27. V.K. LaMer, R.H. Dinegar, J. Am. Chem. Soc. **72**, 4847 (1950)
28. Y. Yin, A.P. Alivisatos, Nature (London) **437**, 664 (2005)
29. X. Peng, J. Wickham, A.P. Alivisatos, J. Am. Chem. Soc. **120**, 5343 (1998)
30. Z.A. Peng, X. Peng, J. Am. Chem. Soc. **124**, 3343 (2002)
31. L.C. Ciacchi, M. Mertig, W. Pompe, S. Meriani, A. De Vita, Platin. Met. Rev. **47**, 98 (2003)
32. L.C. Ciacchi, W. Pompe, A. De Vita, J. Am. Chem. Soc. **123**, 7371 (2001)
33. L.C. Ciacchi, W. Pompe, A. De Vita, J. Phys. Chem. B **107**, 1755 (2003)
34. L.C. Ciacchi, M. Mertig, R. Seidel, W. Pompe, A. De Vita, Nanotechnology **14**, 840 (2003)
35. E.E. Finney, R.G. Finke, J. Colloid Interface Sci. **317**, 351 (2008)
36. S. Kinge, M. Crego-Calama, D.N. Chem, Phys. Chem. **9**, 20 (2008)
37. I. Haas, S. Shanmugam, A. Gedanken, J. Phys. Chem. B **110**, 16947 (2006)
38. I. Pastoriza-Santos, A. Sánchez-Iglesias, B. Rodríguez-González, L.M. Liz-Marzán, Small **5**(4), 440 (2009)
39. B.G. Ershov, Ros. Khim. Kh. (Zh. Ros. Khim. Obshch. D.I. Mendeleev) **45**, 21 (2001)
40. S. Kéki, L. Nagy, G. Deák, M. Zsuga, L. Somogyi, A. Lévai, J. Am. Soc. Mass Spectrom. **15**, 879 (2004)
41. J.A. McLean, K.A. Stumpo, D.H. Russell, J. Am. Chem. Soc. **127**, 5304 (2005)
42. X. Li, A.E. Kuznetsov, H.F. Zhang, A.I. Boldyrev, L.S. Wang, Science **291**, 859 (2001)
43. L.A. Peyser, A.E. Vinson, A.P. Bartko, R.M. Dickson, Science **291**, 103 (2001)
44. J. Zheng, R.M. Dickson, J. Am. Chem. Soc. **124**, 13982 (2002)
45. J.T. Petty, J. Zheng, N.V. Hud, R.M. Dickson, J. Am. Chem. Soc. **126**, 5207 (2004)
46. A. Henglein, Chem. Phys. Lett. **154**, 473 (1989)
47. T. Linnert, P. Mulvaney, A. Henglein, H. Weller, J. Am. Chem. Soc. **112**, 4657 (1990)
48. B.G. Ershov, E. Janata, A. Henglein, J. Phys. Chem. **97**, 339 (1993)
49. B.G. Ershov, N.L. Sukhov, D.A. Troitskii, Radiat. Phys. Chem. **39**, 127 (1992)
50. E. Janata, A. Henglein, B.G. Ershov, J. Phys. Chem. **98**(42), 10888 (1994)
51. V.V. Sviridov, T.N. Vorob'eva, T.V. Gaevskaya, L.I. Stepanova, in *Khimicheskoi osazhdenie metallov iz vodnykh rastvorov*, ed. by V.V. Sviridov (Izd. Universitetskoe, Minsk, 1987), p. 270
52. Z. Wu, J. Chen, R. Jin, Adv. Funct. Mater. **21**, 177 (2011)

53. D.V. Talapin, A.L. Rogach, M. Haase, H. Weller, J. Phys. Chem. B **105**, 21278 (2001)
54. D.V. Talapin, A.L. Rogach, E.V. Shevchenko, A. Kornowski, M. Haase, H. Weller, J. Am. Chem. Soc. **124**, 5782 (2002)
55. Q. Zhang, J. Xie, J. Liang, J.Y. Lee, Adv. Funct. Mater. **19**, 1387 (2009)
56. D.K. Lee, S.I. Park, J.K. Lee, N.M. Hwang, Acta Mater. **55**, 5281 (2007)
57. A.C.S. Samia, J.A. Schlueter, J.S. Jiang, S.D. Bader, C.J. Qin, X.M. Lin, Chem. Mater. **18**, 5203 (2006)
58. N.R. Jana, L. Gearheart, C.J. Murphy, Chem. Mater. **13**, 2313 (2001)
59. J. Park, E. Lee, N.M. Hwang, M. Kang, S.C. Kim, Y. Hwang, J.G. Park, H.J. Noh, J.Y. Kim, J.H. Park, T. Hyeon, Angew. Chem. **117**, 2932 (2005)
60. C.J. Murphy, N.R. Jana, Adv. Mater. **14**, 80 (2002)
61. H. Yu, P.C. Gibbons, K.F. Kelton, W.E. Buhro, J. Am. Chem. Soc. **123**, 9198 (2001)
62. J.P. Wilcoxon, P.P. Provencio, J. Am. Chem. Soc. **126**, 6402 (2004)
63. D.V. Talapin, A.L. Rogach, A. Kornowski, M. Haase, H. Weller, Nano Lett. **1**, 207 (2001)
64. J. Hambrock, R. Becker, A. Birkner, J. Weiss, R.A. Fischer, Chem. Commun. 68 (2002)
65. N.R. Jana, X. Peng, J. Am. Chem. Soc. **125**, 14280 (2003)
66. C. de Mello Doneg, P. Liljeroth, D. Vanmaekelbergh, Small **1**, 1152 (2005)
67. J. van Embden, P. Mulvaney, Langmuir **21**, 10226 (2005)
68. T.F. Tadros, *Applied Surfactants* (Wiley-VCH, Weinheim, 2005)
69. C.S.S.R. Kumar, *Biofunctionalization of Nanomaterials* (Wiley-VCH, Weinheim, 2005)
70. Y. Wang, X. Xu, Z. Tian, Y. Zong, H. Cheng, C. Lin, Chem. Eur. J. **12**, 2542 (2006)
71. Y. Song, J. Hormes, C.S.S.R. Kumar, Small **4**, 698 (2008)
72. Z. Wu, J. Suhan, R. Jin, J. Mater. Chem. **19**, 622 (2009)
73. Z. Wu, E. Lanni, W. Chen, M.E. Bier, D. Ly, R. Jin, J. Am. Chem. Soc. **131**, 16672 (2009)
74. Z. Wu, D. Jiang, E. Lanni, M.E. Bier, R. Jin, J. Phys. Chem. Lett. **1**, 1423 (2010)
75. T.K. Sau, A.L. Rogach, Adv. Mater. **22**, 1781 (2010)
76. Y. Xia, Y. Xiong, B. Lim, S.E. Skrabalak, Angew. Chem. Int. Ed. **48**, 60 (2009)
77. P.-F. Ho, K.-M. Chi, Nanotechnology **15**, 1059 (2004)
78. Y. Xiong, A.R. Siekkinen, J. Wang, Y. Yin, M.J. Kim, Y. Xia, J. Mater. Chem. **17**, 2600 (2007)
79. I. Washio, Y. Xiong, Y. Yin, Y. Xia, Adv. Mater. **18**, 1745 (2007)
80. Y. Xiong, I. Washio, J. Chen, H. Cai, Z.-Y. Li, Y. Xia, Langmuir **22**, 8563 (2006)
81. B. Lim, P.H.C. Camargo, Y. Xia, Langmuir **24**, 10437 (2008)
82. Y. Xiong, J.M. McLellan, J. Chen, Y. Yin, Z.-Y. Li, Y. Xia, J. Am. Chem. Soc. **127**, 17118 (2005)
83. Y. Sun, Y. Xia, Adv. Mater. **15**, 695 (2003)
84. Y. Sun, B. Mayers, Y. Xia, Nano Lett. **3**, 675 (2003)
85. H. Partridge, C.W. Bauschlicher Jr., S.R. Langhoff, Chem. Phys. Lett. **175**, 531 (1990)
86. T. Leisner, S. Vajda, S. Wolf, L. Woste, J. Chem. Phys. **111**, 1017 (1999)
87. Y. Xiong, I. Washio, J. Chen, M. Sadilek, Y. Xia, Angew. Chem. Int. Ed. **46**, 4917 (2007)
88. M.-P. Pileni, Nat. Mater. **2**, 145 (2003)
89. S. Brown, M. Sarikaya, E. Johnson, J. Mol. Biol. **299**, 725 (2000)
90. S.S. Shankar, A. Rai, A. Ahmad, M. Sastry, Chem. Mater. **17**, 566 (2005)
91. Y. Sun, B. Mayers, T. Herricks, Y. Xia, Nano Lett. **3**, 955 (2003)
92. Z.S. Pillai, P.V. Kamat, J. Phys. Chem. B **108**, 945 (2004)
93. M.H. Rashid, R.R. Bhattacharjee, A. Kotal, T.K. Mandal, Langmuir **22**, 7141 (2006)
94. M.H. Rashid, T.K. Mandal, J. Phys. Chem. C **111**, 16750 (2007)
95. H. Rashid, T.K. Mandal, Adv. Funct. Mater. **18**, 2261 (2008)
96. M. Liu, P. Guyot-Sionnest, J. Phys. Chem. B **109**, 22192 (2005)
97. T.K. Sau, C.J. Murphy, J. Am. Chem. Soc. **126**, 8648 (2004)
98. M. Faraday, Philos. Trans. R. Soc. Lond. **151**, 183 (1857)
99. B.V. Enüstün, J. Turkevich, J. Am. Chem. Soc. **85**, 3317 (1963)
100. J. Turkevich, G. Kim, Science **169**, 873 (1970)

101. Y. Wang, J. Ren, K. Deng, L. Gui, Y. Tang, Chem. Mater. **12**, 1622 (2000)
102. B.K. Park, S. Jeong, D. Kim, J. Moon, S. Lim, J.S. Kim, J. Colloid Interface Sci. **311**, 417 (2007)
103. B. Wiley, Y. Sun, B. Mayers, Y. Xia, Chem. Eur. J. **11**, 454 (2005)
104. F. Kim, S. Connor, H. Song, T. Kuykendall, P. Yang, Angew. Chem. Int. Ed. **43**, 3673 (2004)
105. S.I. Cha, C.B. Mo, K.T. Kim, Y.J. Jeong, S.H. Hong, J. Mater. Res. **21**, 2371 (2006)
106. E.I. Suvorova, V.V. Klechkovskaya, V.V. Kopeikin, P.A. Buffat, J. Cryst. Growth **275**, e2351 (2005)
107. H. Bonnemann, R. Richards, Eur. J. Inorg. Chem. 2455 (2001)
108. S. Kinge, H. Bonnemann, Appl. Organomet. Chem. **19**, 750 (2005)
109. H. Bonnemann, K.S. Nagabhushana, *Encyclopedia of Nanoscience and Nanotechnology* (Marcel Dekker, New York, 2004), pp. 739–760
110. Y. Yang, Y. Yan, W. Wang, J.R. Li, Nanotechnology **19**, 175603 (2008)
111. R.B. Vasil'ev, D.N. Darin, A.M. Gas'kov, Uspekhi Khimii **80**, 1190 (2011)
112. S. Komarneni, D. Li, B. Newalkar, H. Katsuki, A.S. Bhalla, Langmuir **18**, 5959 (2002)
113. J. Yang, T.C. Deivaraj, H.-P. Too, J.Y. Lee, Langmuir **20**, 4241 (2004)
114. R.O. Hutchins, K. Learn, B. Nazer, D. Pytlewski, A. Pelter, Org. Prep. Proced. Int. **16**, 335 (1984)
115. S.B. Kalidindi, U. Sanyal, B.R. Jagirdar, ChemSusChem **4**, 317 (2011)
116. D.V. Goia, J. Mater. Chem. **14**, 451 (2004)
117. M.T. Reetz, M. Maase, Adv. Mater. **11**, 773 (1999)
118. C.M. Welch, R.G. Comp, Anal. Bioanal. Chem. **384**, 601 (2006)
119. A. Troupis, T. Triantis, A. Hiskia, E. Papaconstantinou, Eur. J. Inorg. Chem. 5579 (2008)
120. Y. Ma, J. Zeng, W. Li, M. McKiernan, Z. Xie, Y. Xia, Adv. Mater. **22**, 1930 (2010)
121. T.K. Sau, C.J. Murphy, Philos. Mag. **87**, 2143 (2007); X. Jiang, Q. Zeng, A. Yu, Nanotechnology **17**, 4929 (2006)
122. N.R. Jana, Small **1**(8–9), 875 (2005)
123. P. Qiu, C. Mao, J. Nanopart. Res. **11**, 885 (2009)
124. I. Lisiecki, M.P. Pileni, J. Am. Chem. Soc. **115**, 3887 (1993)
125. I. Lisiecki, F. Billoudet, M.P. Pileni, J. Phys. Chem. **100**, 4160 (1996)
126. J. Tanori, M.P. Pileni, Adv. Mater. **7**, 862 (1995)
127. N. Pinna, K. Weiss, H. Sack-Kongehl, W. Vogel, J. Urban, M.P. Pileni, Langmuir **17**, 7982 (2001)
128. M. Maillard, S. Giorgio, M.P. Pileni, J. Phys. Chem. B **107**, 2466 (2003)
129. V. Germain, J. Li, D. Ingert, Z.L. Wang, M.P. Pilen, J. Phys. Chem. B **107**(34), 8717 (2003)
130. C. Salzemann, I. Lisiecki, J. Urban, M.P. Pileni, Langmuir **20**, 11772 (2004)
131. C. Salzemann, I. Lisiecki, J. Urban, M.P. Pileni, Adv. Funct. Mater. **15**, 1277 (2005)
132. X. Ji, X. Song, J. Li, Y. Bai, W. Yang, X. Peng, J. Am. Chem. Soc. **129**, 13939 (2007)
133. X. Liu, R. Huang, J. Zhu, Chem. Mater. **20**, 192 (2008)
134. D.O. Yener, J. Sindel, C.A. Randall, J.H. Adair, Langmuir **18**, 8692 (2002)
135. G. Wei, H. Zhou, Z. Liu, Y. Song, L. Wang, L. Sun, Z. Li, J. Phys. Chem. B **109**, 8738 (2005)
136. J. Zhang, H. Liu, Z. Wang, N. Ming, Adv. Funct. Mater. **17**, 3295 (2007)
137. S.A. Tikhomirov, M.A. Alymov, I.V. Tregubova, V.S. Shustov, Ross. Nanotekhn. **6**(3-4), 105 (2011)
138. M.T. Reetz, M. Winter, R. Breinbauer, T. Thurn-Albrecht, W. Vogel, Chem. Eur. J. **7**(5), 1084 (2001)
139. A. Miyazaki, Y. Nakano, Langmuir **16**, 7109 (2000)
140. X.C. Jiang, W.M. Chen, C.Y. Chen, S.X. Xiong, A.B. Yu, Nanoscale Res. Lett. **6**, 32 (2011)
141. Y. Wang, A.V. Biradar, G. Wang, K.K. Sharma, C.T. Duncan, S. Rangan, T. Asefa, Chem. Eur. J. **16**, 10735 (2010)
142. C. Salzemann, A. Brioude, M.P. Pileni, J. Phys. Chem. B **110**, 7208 (2006)
143. D.B. Pedersen, S. Wang, S.H. Liang, J. Phys. Chem. C **112**, 8819 (2008)
144. V.V. Klimov, *Nanoplazmonika* (Fizmatlit, Moscow, 2009)

145. S.P. Chandran, M. Chaudhary, R. Pasricha, A. Ahmad, M. Sastry, Biotechnol. Prog. **22**, 577 (2006)
146. A.K. Popov, J. Brummer, R.S. Tanke, G. Taft, M. Loth, R. Langlois, A. Wruck, R. Schmitz, Laser Phys. Lett. **3**(11), 546 (2006)
147. K. Ishizu, H. Kakinuma, K. Ochi, S. Uchida, M. Hayashi, Polym. Adv. Technol. **16**, 834 (2005)
148. H. Hirai, N. Yakura, Polym. Adv. Technol. **12**, 174 (2001)
149. L. Durán Pachón, G. Rothenberg, Appl. Organomet. Chem. **22**, 288 (2008)
150. L.S. Ott, B.J. Hornstein, R.G. Finke, Langmuir **22**, 9357 (2006)
151. A. Sutton, G. Franc, A. Kakkar, J. Polym. Sci. Part A Polym. Chem. **47**, 4482 (2009)
152. R. Hourani, M.A. Whitehead, A.K. Kakkar, Macromolecules **41**, 508 (2008)
153. R. Hourani, M.A. Whitehead, A.K. Kakkar, J. Mater. Chem. **15**, 2106 (2005)
154. H. Tsunoyama, H. Sakurai, Y. Negishi, T. Tsukuda, J. Am. Chem. Soc. **127**, 9374 (2005)
155. J.A. Widegren, R.G. Finke, J. Mol. Catal. A Chem. **191**, 187 (2003)
156. X. Mu, D.G. Evans, Y. Kou, Catal. Lett. **97**, 151 (2004)
157. I. Pastoriza-Santos, L.M. Liz-Marzán, Adv. Funct. Mater. **19**, 679 (2009)
158. P. Jiang, S.-Y. Li, S.-S. Xie, Y. Gao, L. Song, Chem. Eur. J. **10**, 4817 (2004)
159. J.L. Elechiguerra, L. Larios-Lopez, C. Liu, D. Garcia-Gutierrez, A. Camacho-Bragado, M.J. Yacaman, Chem. Mater. **17**, 6042 (2005)
160. N. Toshima, Macromol. Symp. **235**, 1 (2006)
161. J. Widoniak, S. Eiden-Assmann, G. Maret, Coll Surf A Physicochem. Eng. Asp. **270–271**, 340 (2005)
162. P.A. Muzalev, I.D. Kosobudskii, N.M. Ushakov, L.G. Panova, Perspect. Mater. **3**, 84 (2011)
163. Y. Park, P. Taranekar, J.Y. Park, A. Baba, T. Fulghum, R. Ponnapati, R.C. Advincula, Adv. Funct. Mater. **18**, 2071 (2008)
164. W. Wang, G. Wang, X. Wang, Y. Zhan, Y. Liu, C. Zheng, Adv. Mater. **14**, 67 (2002)
165. P.S. Kumar, I. Pastoriza-Santos, B. Rodríguez-González, F.J. García de Abajo, L.M. Liz-Marzán, Nanotechnology **19**, 015606(1–5) (2008)
166. D. Cabane, R. Duplessix, J. Physique **48**, 651 (1987)
167. D. Li, S. Komarneni, J. Am. Ceram. Soc. **89**(5), 1510 (2006)
168. E.N. Sobol, V.N. Bagratishvili, S.M. Khoudl, Dokl. AN **356**(6), 777 (1997)
169. J. Watkins, T. McCarthy, Chem. Mater. **7**, 1991 (1995)
170. A. Kameo, T. Yoshimura, K. Esumi, Colloids Surf. A **215**, 181 (2003)
171. S. Moisan, V. Martinez, P. Weisbecker, F. Cansell, S. Mecking, C. Aymonier, J. Am. Chem. Soc. **129**, 10602 (2007)
172. E. Said-Galiev, A.I. Gamzadze, T.E. Grigor'ev, A.R. Khokhlov, N.P. Bakuleva, I.G. Lyutova, E.V. Shtykova, K.A. Dembo, V.V. Volkov, Ross. Nanotekhn. **6**(5–6), 94 (2011)
173. M. Chatterjee, Y. Ikushima, Y. Hakuta, H. Kawanami, Adv. Synth. Catal. **348**, 1580 (2006)
174. A.D. Pomogailo, A.S. Rozenberg, I.E. Uflyand, *Metal Nanoparticles in Polymers* (Khimiya, Moscow, 2000)
175. T. Hasell, J. Yang, W. Wang, P.D. Brown, S.M. Howdle, Mater. Lett. **61**, 4906 (2007)
176. V. Sankaran, J. Yue, R.E. Cohen, R.R. Schrock, R.J. Silbey, Chem. Mater. **5**, 1133 (1993)
177. K. Holmberg, *Surfactants and Polymers in Aqueous Solution*, 2nd edn. (Wiley, Chichester, 2003)
178. R. Savic, L. Luo, A. Eisenberg, D. Maysinger, Science **300**, 615 (2003)
179. S. Főrster, M. Konrad, J. Mater. Chem. **13**, 2671 (2003)
180. S. Sun, C.B. Murray, D. Weller, L. Folks, A. Moser, Science **287**, 1989 (2000)
181. L. Luo, A. Eisenberg, Langmuir **17**, 6804 (2001)
182. L. Luo, A. Eisenberg, J. Am. Chem. Soc. **123**, 1012 (2001)
183. S. Mossmer, J.P. Spatz, M. Moller, T. Aberle, J. Schmidt, W. Burchard, Macromolecules **33**, 4791 (2000)
184. J.X. Zhao, C. Allen, A. Eisenberg, Macromolecules **30**, 7143 (1997)

185. R. Nagarajan, K. Ganesh, J. Colloid Interface Sci. **184**, 489 (1996)
186. N. Singh, A. Karim, F.S. Bates, M. Tirrell, K. Furusawa, Macromolecules **27**, 2586 (1994)
187. X. Qiu, Z.-G. Wang, J. Colloid Interface Sci. **167**, 294 (1994)
188. Y. Kang, T.A. Taton, Macromolecules **38**, 6115 (2005)
189. P. Spatz, S. Mőssmer, C. Hartmann, M. Mőller, Langmuir **16**, 407 (2000)
190. L.M. Bronstein, D.M. Chernyshov, I.O. Volkov, M.G. Ezernitskaya, P.M. Valetsky, V.G. Matveeva, E.M. Sulman, J. Catal. **196**, 302 (2000)
191. Y.J. Ho, M.K. Park, J. Locklin, R. Advincula, J.H. Yang, J. Mays, Langmuir **18**, 2457 (2002)
192. S.N. Sidorov, L.M. Bronstein, Y.A. Kabachii, P.M. Valetsky, P.L. Soo, D. Maysinger, A. Eisenberg, Langmuir **20**, 3543 (2004)
193. M. Filali, M.A.R. Meier, U.S. Schubert, J.F. Gohy, Langmuir **21**, 7995 (2005)
194. J. Li, L. Shi, Y. An, Y. Li, X. Chen, H. Dong, Polymer **47**, 8480 (2006)
195. M. Gauthier, J.M. Li, J. Dockendorff, Macromolecules **36**, 2642 (2003)
196. R. Zhang, J. Liu, B. Han, B. Wang, D. Sun, J. He, Polymer **46**, 3936 (2005)
197. F. Calderara, G. Riess, Macromol. Chem. Phys. **197**, 2115 (1996)
198. M. Moffitt, L. McMahon, V. Pessel, A. Eisenberg, Chem. Mater. **7**, 1185 (1995)
199. C.W. Wang, M.G. Moffitt, Langmuir **20**, 11784 (2004)
200. N. Duxin, F. Liu, H. Vali, A. Eisenberg, J. Am. Chem. Soc. **127**, 10063 (2005)
201. K. Gatsouli, S. Pispas, E.I. Kamitsos, J. Phys. Chem. C **111**, 15201 (2007)
202. J.-Y. Kim, D.-H. Shin, K.-J. Ihn, J. Appl. Polym. Sci. **97**, 2357 (2005)
203. A. Biffis, N. Orlandi, B. Corain, Adv. Mater. **15**, 1551 (2003)
204. C. Aymonier, D. Bortzmeyer, R. Thomann, R. Mulhaupt, Chem. Mater. **15**, 4874 (2003)
205. S. Xu, J. Zhang, C. Paquet, Y. Lin, E. Kumacheva, Adv. Funct. Mater. **13**, 468 (2003)
206. Y.Y. Li, F. Cunin, J.R. Link, T. Gao, R.E. Betts, S.H. Reiver, V. Chin, S.N. Bhatia, M.J. Sailor, Science **299**, 2045 (2003)
207. M. Han, X. Gao, J.Z. Su, S. Nie, Nat. Biotechnol. **19**, 631 (2001)
208. A.N. Shipway, I. Willner, Chem. Commun. 2035 (2001)
209. Y. Lu, P. Spyra, Y. Mei, M. Ballauff, A. Pich, Macromol. Chem. Phys. **208**, 254 (2007)
210. Y.M. Mohan, K.J. Lee, T. Premkumar, K.E. Geckeler, Polymer **48**, 158 (2007)
211. C. Wang, N.T. Flynn, R. Langer, Mater. Res. Soc. Symp. Proc. **820**, R2. 2. 1. (2004)
212. V. Thomas, M.M. Yallapu, B. Sreedhar, S.K. Bajpai, J. Colloid Interface Sci. **315**, 389 (2007)
213. A.N. Shipway, I. Willner, Chem. Commun. **20**, 35 (2001)
214. V. Pardo-Yissar, R. Gabai, A.N. Shipway, T. Bourenko, I. Willner, Adv. Mater. **13**, 1320 (2001)
215. P. Saravanan, M. Padmanabha Raju, S. Alam, Mater. Chem. Phys. **103**, 278 (2007)
216. Y. Murali Mohan, T. Premkumar, K.J. Lee, K.E. Geckeler, Macromol. Rapid Commun. **27**, 1346 (2006)
217. E.M. Ahmed, F.S. Aggor, J. Appl. Polym. Sci. **117**, 2168 (2010)
218. C. Wang, N.T. Flynn, R. Langer, Adv. Mater. **16**, 1074 (2004)
219. D. Suzuki, H. Kawaguchi, Langmuir **21**, 12016 (2005)
220. Y. Mei, Y. Lu, F. Polzer, M. Ballauff, M. Drechsler, Chem. Mater. **19**, 1062 (2007)
221. S.H. Anastasiadis, M. Vamvakaki, Int. J. Nanotechnol. **6**, 46 (2009)
222. C. Boyer, M.H. Stenzel, T.P. Davis, J. Polym. Sci. Part A Polym. Chem. **49**, 551 (2011)
223. Y. Dong, Y. Ma, T. Zhai, F. Shen, Y. Zeng, H. Fu, J. Yao, Macromol. Rapid Commun. **28**, 2339 (2007)
224. J.G. Zhang, N. Coombs, E. Kumacheva, J. Am. Chem. Soc. **124**, 14512 (2002)
225. J. Zhang, S. Xu, E. Kumacheva, J. Am. Chem. Soc. **126**, 7908 (2004)
226. D. Palioura, S.P. Armes, S.H. Anastasiadis, M. Vamvakaki, Langmuir **23**, 5761 (2007)
227. J.-T. Zhang, G. Wei, T.F. Keller, H. Gallagher, C. Stőtzel, F.A. Műller, M. Gottschaldt, U.S. Schubert, K.D. Jandt, Macromol. Mater. Eng. **295**, 1049 (2010)
228. C.-W. Chen, K. Arai, K. Yamamoto, T. Serizawa, M. Akashi, Macromol. Chem. Phys. **201**, 2811 (2000)

229. H. Hirai, N. Toshima, Polymer-attached catalysts, in *Tailored Metal Catalyst*, ed. by Y. Iwasawa (D. Deidel Publishing Company, Dordrecht, 1986), p. 87
230. M.L. Wang, C.H. Wang, W. Wang, Mater. Chem. Phys. **104**, 162 (2007)
231. K.A. Malini, M.R. Anantharaman, S. Sindhu, C.N. Chinnasamy, N. Ponpandian, A. Narayanasamy, B. Balachandran, V.N. Shivasankarapillai, J. Mater. Sci. **36**, 821 (2001)
232. E. Veena Gopalan, K.A. Malini, G. Santhoshkumar, T.N. Narayanan, P.A. Joy, I.A. Al-Omari, D. Sakthi Kumar, Y. Yoshida, M.R. Anantharaman, Nanoscale Res. Lett. **5**, 889 (2010)
233. B. Domènech, M. Muñoz, D.N. Muraviev, J. Macanás, Catal. Today **193**(1), 158 (2012)
234. R.C. Advincula, W.J. Brittain, K.C. Caster, J. Ruhe, in *PolymerBrushes: Synthesis, Characterization, Applications*, ed. by R. Advincula, W.J. Brittain, K.C. Caster, J. Ruhe (Wiley, Weinheim, 2004)
235. T.M. Birshtein, Soros. Obrazov. Kh. **5**, 42 (1999)
236. S.G. Boyes, W.J. Brittain, X. Weng, S.Z.D. Cheng, Macromolecules **35**, 4960 (2002)
237. A.M. Granville, S.G. Boyes, B. Akgun, M.D. Foster, W.J. Brittain, Macromolecules **37**, 2790 (2004)
238. B. Zhao, W.J. Brittain, W. Zhou, S.Z.D. Cheng, J. Am. Chem. Soc. **122**, 2407 (2000)
239. R. Iwata, H. Li, H. Zhang, Y. Xu, K. Zhang, P. Ai, X. Jin, J. Wang, Mater. Chem. Phys. **90**, 90 (2005)
240. K. Ohno, T. Morinaga, K. Koh, Y. Tsujii, T. Fukuda, Macromolecules **38**, 2137 (2005)
241. R. Djalali, S.Y. Li, M. Schmidt, Macromolecules **35**, 4282 (2002)
242. M. Yu, Y. Lu, M. Schrinner, F. Polzer, M. Ballauff, Macromol. Symp. **254**, 42 (2007)
243. M. Zhang, M. Drechsler, A.H.E. Müller, Chem. Mater. **16**, 537 (2004)
244. M. Schrinner, S. Proch, Y. Mei, R. Kempe, N. Miyajima, M. Ballauff, Adv. Mater. **20**, 1928 (2008)
245. D.G. Shchukin, G.B. Sukhorukov, Adv. Mater. **16**, 671 (2004)
246. T.C. Wang, M.F. Rubner, R.E. Cohen, Langmuir **18**, 3370 (2002)
247. M. Fang, P.S. Grant, M.J. McShane, G.B. Sukhorukov, V.O. Golub, Y.M. Lvov, Langmuir **18**, 6338 (2002)
248. T.C. Wang, B. Chen, M.F. Rubner, R.E. Cohen, Langmuir **17**, 6610 (2001)
249. S. Moya, O. Azzaroni, T. Farhan, V.L. Osborne, W.T.S. Huck, Angew. Chem. Int. Ed. **44**, 4578 (2005)
250. N. Ayres, S.G. Boyes, W.J. Brittain, Langmuir **23**, 182 (2007)
251. J. Chen, S.K. Spear, J.G. Huddleston, R.D. Rogers, Green Chem. **7**, 64 (2005)
252. A.S. Karakoti, S. Das, S. Thevuthasan, S. Seal, Angew. Chem. Int. Ed. **50**, 1980 (2011)
253. M.D. Howard, M. Jay, T.D. Dziublal, X.L. Lu, J. Biomed. Nanotechnol. **4**, 133 (2008)
254. M.J. Joralemon, S. McRae, T. Emrick, Chem. Commun. **46**, 1377 (2010)
255. P.K. Sudeep, Z. Page, T. Emrick, Chem. Commun. 6126 (2008)
256. N. Uekawa, M. Endo, K. Kakegawa, Y. Sasaki, Phys. Chem. Chem. Phys. **2**, 5485 (2000)
257. S. Kuchibhatla, A.S. Karakoti, S. Seal, Nanotechnology **18**, 075303 (2007)
258. M. Popa, T. Pradell, D. Crespo, J.M. Calderon-Moreno, Colloids Surf. A **303**, 184 (2007)
259. M. Zhang, Z.H. Wang, G.C. Xi, D.K. Ma, R. Zhang, Y.T. Qian, J. Cryst. Growth **268**, 215 (2004)
260. U.I. Tromsdorf, N.C. Bigall, M.G. Kaul, O.T. Bruns, M.S. Nikolic, B. Mollwitz, R.A. Sperling, R. Reimer, H. Hohenberg, W.J. Parak, S. Forster, U. Beisiegel, G. Adam, H. Weller, Nano Lett. **7**, 2422 (2007)
261. L. Gu, Z. Shen, C. Feng, Y.G. Li, G.L. Lu, X.Y. Huang, G.W. Wang, J.L. Huang, J. Mater. Chem. **18**, 4332 (2008)
262. M.L. Ji, W.L. Yang, Q.G. Ren, D.R. Lu, Nanotechnology **20**, 075101 (2009)
263. K. Naka, A. Nakahashi, M. Bravo, Y. Chujo, Appl. Organomet. Chem. **24**, 573 (2010)
264. J.-J. Park, X. Bulliard, J.M. Lee, J. Hur, K. Im, J.-M. Kim, P. Prabhakaran, N. Cho, K.-S. Lee, S.-Y. Min, T.-W. Lee, S. Yong, D.-Y. Yang, Adv. Funct. Mater. **20**, 2296 (2010)

265. A. Dokoutchaev, J.T. James, S.C. Koene, S. Pathak, G.K.S. Prakash, M.E. Thompson, Chem. Mater. **11**, 2389 (1999)
266. C.W. Chen, T. Serizawa, M. Akashi, Chem. Mater. **14**, 2232 (2002)
267. F. Wen, W. Zhang, G. Wei, Y. Wang, J. Zhang, M. Zhang, L. Shi, Chem. Mater. **20**, 2144 (2008)
268. Y. Mei, G. Sharma, Y. Lu, M. Ballauf, M. Drechsler, T. Irrgang, R. Kempe, Langmuir **21**, 12229 (2005)
269. Y. Lu, Y. Mei, M. Drechsler, M. Ballauf, Angew. Chem. Int. Ed. **45**, 813 (2006)
270. S. Li, J. Wang, Y. Kou, S. Zhang, Chem. Eur. J. **16**, 1812 (2010)
271. J. Yang, L. Qiu, B. Liu, Y. Peng, F. Yan, S. Shang, J. Polym. Sci. Part A Polym. Chem. **49**, 4531 (2011)
272. Y.S. Gu, X.M. Hou, H.Y. Hua, B. Yu, L.X. Wang, F. Zhou, Mater. Chem. Phys. **116**, 284 (2009)
273. S.F. Zheng, J.S. Hu, L.S. Zhong, L.J. Wan, W.G. Song, J. Phys. Chem. C **111**, 11174 (2007)
274. C.J. Murphy, J. Mater. Chem. **18**, 2173 (2008)
275. A.I. Loskutov, O.Ya. Uryupina, V.V. Vysotskii, M.P. Kiselev, Nanotekhnika 39 (2010)
276. O.Ya. Uryupina, V.V. Vysotskii, A.I. Loskutov, V.V. Matveev, A.V. Cherkasova, V.I. Roldugin, Kh. Prikl. Khim. **86**. P. 1268 (2013)
277. A.I. Loskutov, O.Y. Uryupina, V.V. Vysotskii, A.V. Gusel'nikov, Nanotekhnika **1**, 62 (2011)
278. R.R. Bhattacharjee, M.H. Rashid, T.K. Mandal, J. Nanosci. Nanotechnol. **8**, 3610 (2008)
279. D. Maity, M.K. Bain, B. Bhowmick, J. Sarkar, S. Saha, K. Acharya, M. Chakraborty, D. Chattopadhyay, J. Appl. Polym. Sci. **122**, 2189 (2011)
280. Z. Shervani, Y. Ikushima, M. Sato, H. Kawanami, Y. Hakuta, T. Yokoyama, T. Nagase, H. Kuneida, K. Aramaki, Colloid Polym. Sci. **286**, 403 (2008)
281. A. Kohut, A. Voronov, V. Samaryk, W. Peukert, Macromol. Rapid Commun. **28**, 1410 (2007)
282. A. Voronov, A. Kohut, W. Peukert, Langmuir **23**, 360 (2007)
283. T. Sakai, P. Alexandridis, Chem. Mater. **18**, 2577 (2006); T. Sakai, P. Alexandridis, Nanotechnology **16**, 8019 (2005)
284. J.-Y. Kim, D.-H. Shin, K.-J. Ihn, Macromol. Chem. Phys. **206**, 794 (2005)
285. C.H. Bamford, *Encyclopedia of Polymer Science and Engineering* (Wiley-Interscience, New York, 1988), p. 763
286. G.G. Odian, *Principles of Polymerization*, 3rd edn. (Wiley, New York, 1991), p. 220
287. Y.M. Shulga, O.S. Roshchupkina, G.I. Dzhardimalieva, A.D. Pomogailo, Izv. AN, Ser. Khim. **9**, 1565 (1993)
288. G.I. Dzhardimalieva, A.D. Pomogailo, Uspekhi Khimii **77**, 270 (2008)
289. A.A. Berlin, V.N. Kislenko, Prog. Polym. Sci. **17**, 765 (1992)
290. V.I. Kurlyankina, V.N. Shadrin, E.N. Kazbekov, V.A. Molotkov, M.K. Bukina, Zh. Obsch. Khim. **44**, 1593 (1974)
291. Y. Song, Z. Li, L. Wang, Y. Yao, C. Chen, K. Cui, Microsc. Res. Tech. **71**, 409 (2008)
292. I. Tarnavchyk, A. Voronov, A. Kohut, N. Nosova, S. Varvarenko, V. Samaryk, S. Voronov, Macromol. Rapid Commun. **30**, 1564 (2009)
293. J.D.S. Newman, G.J. Blanchard, Langmuir **22**, 5882 (2006)
294. C. Subramaniam, R.T. Tom, T. Pradeep, J. Nanopart. Res. **7**, 209 (2005)
295. M. Aslam, L. Fu, M. Su, K. Vijayamohanan, V.P. Dravid, J. Mater. Chem. **14**, 1795 (2004)
296. P.R. Selvakannan, A. Swami, D. Srisathiyanarayanan, P.S. Shirdue, R. Pasricha, A.B. Mandale, M. Sastry, Langmuir **20**, 7825 (2004)
297. J. Keilitz, M.R. Radowski, J.-D. Marty, R. Haag, F. Gauffre, C. Mingotaud, Chem. Mater. **20**, 2423 (2008)
298. M. Chen, Y.-G. Feng, X. Wang, T.-C. Li, J.-Y. Zhang, D.-J. Qian, Langmuir **23**, 5296 (2007)
299. K. Esumi, Top. Curr. Chem. **227**, 31 (2003)
300. I. Gitsov, C. Lin, Curr. Org. Chem. **9**, 1025 (2005)
301. S. Keki, J. Tőrők, G. Deák, L. Daróczi, M. Zsuga, J. Colloid Interface Sci. **229**, 550 (2000)
302. Y. Niu, L. Sun, R.M. Crooks, Macromolecules **36**, 5725 (2003)

303. M.J. Jasmine, M. Kavitha, E. Prasad, J. Lumin. **129**, 506 (2009)
304. X. Luo, T. Imae, J. Mater. Chem. **17**, 567 (2007)
305. F. Grőhn, Macromol. Chem. Phys. **209**, 2295 (2008)
306. I. Willerich, F. Grőhn, Chem. Eur. J. **14**, 9112 (2008)
307. M. Kavitha, M.R. Parida, E. Prasad, C. Vijayan, P.C. Deshmukh, Macromol. Chem. Phys. **210**, 1310 (2009)
308. J.-M. Lin, T.-L. Lin, U.-S. Jeng, Y.-J. Zhong, C.-T. Yeh, T.-Y. Chena, J. Appl. Cryst. **40**, s540 (2007)
309. D. Debnath, C. Kim, S.H. Kim, K.E. Geckeler, Macromol. Rapid Commun. **31**, 549 (2010)
310. M.L.C.E. Hoppe, I. Pardiñas-Blanco, M.A. López-Quintela, Langmuir **22**, 7027 (2006)
311. H.H. Huang, X.P. Ni, G.L. Loy, C.H. Chew, K.L. Tan, F.C. Loh, J.F. Deng, G.Q. Xu, Langmuir **12**, 909 (1996)
312. Y. Gao, P. Jiang, L. Song, J.X. Wang, L.F. Liu, D.F. Liu, Y.J. Xiang, Z.X. Zhang, X.W. Zhao, X.Y. Dou, S.D. Luo, W.Y. Zhou, S.S. Xie, J. Cryst. Growth **298**, 376 (2006)
313. N. Bicak, S. Sungur, N. Tan, F. Bensebaa, Y. Deslandes, J. Polym, Sci. Part A Polym. Chem. **40**, 748 (2002)
314. V.A. Tertykh, K.V. Katok, V.V. Yanishpolskii, Russ. J. Phys. Chem. **82**, 1438 (2008)
315. N. Ivashchenko, V. Tertykh, V. Yanishpolskii, S. Khainakov, A. Dikhtiarenko, Mater. Werkst. **42**, 64 (2011)
316. K.G. Neoh, T.T. Yong, N.T. Looi, E.T. Kang, Chem. Mater. **9**, 2906 (1997)
317. E.T. Kang, Y.P. Ting, K.L. Tan, J. Appl. Polym. Sci. **53**, 1539 (1994)
318. L.M. Huang, T.C. Wen, A. Gopalan, Thin Solid Films **473**, 300 (2005)
319. L.M. Huang, T.C. Wen, A. Gopalan, Mater. Lett. **57**, 1765 (2003)
320. L.-M. Huang, C.-C. Tsai, T.-C. Wen, A. Gopalan, J. Polym. Sci. Part A Polym. Chem. **44**, 3843 (2006)
321. A.K. Sra, R.E. Schaak, J. Am. Chem. Soc. **126**, 6667 (2004)
322. B.M. Leonard, N.S.P. Bhuvanesh, R.E. Schaak, J. Am. Chem. Soc. **127**, 7326 (2005)
323. Y. Vasquez, A.K. Sra, R.E. Schaak, J. Am. Chem. Soc. **127**, 12504 (2005)
324. Y. Vasquez, Z. Luo, R.E. Schaak, J. Am. Chem. Soc. **130**, 11866 (2008)
325. N.H. Chou, R.E. Schaak, J. Am. Chem. Soc. **129**, 7339 (2007)
326. J.F. Bondi, R. Misra, X. Ke, I.T. Sine, P. Schiffer, R.E. Schaak, Chem. Mater. **22**, 3988 (2010)
327. B. Lim, J. Wang, P.H.C. Camargo, C.M. Cobley, M.J. Kim, Y. Xia, Angew. Chem. Int. Ed. **48**, 6304 (2009)
328. K.E. Elkins, T.S. Vedantam, J.P. Liu, H. Zeng, S. Sun, Y. Ding, Z.L. Wang, Nano Lett. **3**, 1647 (2003)
329. S. Sun, S. Anders, T. Thomson, J.E.E. Baglin, M.F. Toney, H.F. Hamann, C.B. Murray, B.D. Terris, J. Phys. Chem. B **107**, 5419 (2003)
330. X. Huang, H. Zhang, C. Guo, Z. Zhou, N. Zheng, Angew. Chem. Int. Ed. **48**, 4808 (2009)
331. J.B. Wu, J.L. Zhang, Z.M. Peng, S.C. Yang, F.T. Wagner, H. Yang, J. Am. Chem. Soc. **132**, 4984 (2010)
332. D. Wang, Y. Li, Adv. Mater. **23**, 1044 (2011)
333. Y. Sun, B.T. Mayers, Y. Xia, Nano Lett. **2**, 481 (2002)
334. W.G. Menezes, V. Zielasek, G.I. Dzhardimalieva, S.I. Pomogailo, K. Thiel, D. Wohrle, A. Hartwig, M. Baumer, Nanoscale **4**, 1658 (2012)
335. C. Wang, H. Yin, R. Chan, S. Peng, S. Dai, S. Sun, Chem. Mater. **21**, 433 (2009)
336. H. Song, F. Kim, S. Connor, G.A. Somorjai, P. Yang, J. Phys. Chem. B **109**, 188 (2005)
337. S.M. Humphrey, M.E. Grass, S.E. Habas, K. Niesz, G.A. Somorjai, T.D. Tilley, Nano Lett. **7**, 785 (2007)
338. N. Zettsu, J.M. McLellan, B. Wiley, Y. Yin, Z.-Y. Li, Y. Xia, Angew. Chem. Int. Ed. **45**, 1288 (2006)
339. Y. Xiong, J. Chen, B. Wiley, Y. Xia, S. Aloni, Y. Yin, J. Am. Chem. Soc. **127**, 7332 (2005)
340. D. Seo, J.C. Park, H. Song, J. Am. Chem. Soc. **128**, 14863 (2006)

341. Y. Zhang, M.E. Grass, S.E. Habas, F. Tao, T. Zhang, P. Yang, G.A. Somorjai, J. Phys. Chem. C **111**, 12243 (2007)
342. T.M. Whitney, J.S. Jiang, P.C. Searson, C.L. Chien, Science **261**, 1316 (1993)
343. S. Dominguez-Dominguez, J. Arias-Pardilla, A. Berenguer-Murcia, E. Morallon, D. Cazorla-Amoros, J. Appl. Electrochem. **38**, 259 (2008)
344. S. Kim, Y. Jung, Y.S. Lee, S.J. Park, Diffus. Defect Data Pt. B **124–126**, 1821 (2007)
345. C.R. Martin, Chem. Mater. **8**, 1739 (1996)
346. J.-S. Yu, J.Y. Kim, S. Lee, J.K.N. Mbindyo, B.R. Martin, T.E. Mallouk, Chem. Commun. 2445 (2000)
347. C.K. Preston, M. Moskovits, J. Phys. Chem. **97**, 8495 (1993)
348. M. Wirtz, C.R. Martin, Adv. Mater. **15**, 455 (2003)
349. E.K. Payne, K.L. Shuford, S. Park, G.C. Schatz, C.A. Mirkin, J. Phys. Chem. B **110**, 2150 (2006)
350. J. Wang, J. Mater. Chem. **18**, 4017 (2008)
351. J.-G. Wang, M.-L. Tian, T.E. Mallouk, M.H.W. Chan, Nano Lett. **4**, 1313 (2004)
352. S.J. Lee, J.M. Baik, M. Moskovits, Nano Lett. **8**, 3244 (2008)
353. J.J. Mock, S.J. Oldenburg, D.R. Smith, D.A. Schultz, S. Schultz, Nano Lett. **2**, 465 (2002)
354. P.R. Sajanlal, T. Pradeep, Adv. Mater. **20**, 980 (2008)
355. L. Delplancke, J. Dille, J. Reisse, G.J. Long, A. Mohan, F. Grandjean, Chem. Mater. **12**, 946 (2000)
356. L. Rodrigues-Sanchez, M.C. Blanco, M.A. Lopez-Quintela, J. Phys. Chem. B **104**, 9683 (2000)
357. M.T. Reetz, W. Helbig, J. Am. Chem. Soc. **116**, 7401 (1994)
358. J. Becker, R. Schäfer, R. Festag, W. Ruland, J.H. Wendorff, J. Pebler, S.A. Quaiser, W. Helbig, M.T. Reetz, J. Chem. Phys. **103**, 2520 (1995)
359. Southampton Electrochemistry Group, *Instrumental Methods in Electrochemistry* (Ellis Horwood, Chichester, 1990)
360. A.B. Isaev, N.A. Zakargalieva, Z.M. Aliev, Ross. Nanotekhnol. **6**, 88 (2011)
361. T.S. Sabir, D. Yan, J.R. Milligan, A.W. Aruni, K.E. Nick, R.H. Ramon, J.A. Hughes, Q. Chen, R.S. Kurti, C.C. Perry, J. Phys. Chem. C **116**, 4431 (2012)
362. A.E. Saunders, M.B. Sigman, B.A. Korgel, J. Phys. Chem. B **108**, 193 (2003)
363. D.T. Robb, V. Privman, Langmuir **24**, 26 (2007)
364. H. Zheng, R.K. Smith, Y.-W. Jun, C. Kisielowski, U. Dahmen, A.P. Alivisatos, Science **324**, 1309 (2009)
365. S.P. Shields, V.N. Richards, W.E. Buhro, Chem. Mater. **22**, 3212 (2010)
366. T.O. Drews, M.A. Katsoulakis, M. Tsapatsis, J. Phys. Chem. B **109**, 23879 (2005)
367. V.N. Richards, N.P. Rath, W.E. Buhro, Chem. Mater. **22**, 3556 (2010)
368. J. Millstone, G. Métraux, C. Mirkin, Adv. Funct. Mater. **16**, 1209 (2006)

http://www.springer.com/978-90-481-2564-7

Nanostructured Materials Preparation via Condensation Ways

Pomogailo, A.D.; Dzhardimalieva, G.I.

2014, XIX, 460 p. 320 illus., 40 illus. in color., Hardcover
ISBN: 978-90-481-2564-7